



UNIVERSITY
OF
JOHANNESBURG

COPYRIGHT AND CITATION CONSIDERATIONS FOR THIS THESIS/ DISSERTATION

This copy has been supplied on the understanding that it is copyrighted and that no quotation from the thesis may be published without proper acknowledgement.



Please include the following information in your citation:

Name of author

Year of publication, in brackets

Title of thesis, in italics

Type of degree (e.g. D. Phil.; Ph.D.; M.Sc.; M.A. or M.Ed. ...etc.)

Name of the University

Website

Date, accessed

Example

Surname, Initial(s). (2012) Title of the thesis or dissertation. PhD. (Chemistry), M.Sc. (Physics), M.A. (Philosophy), M.Com. (Finance) etc. [Unpublished]: University of Johannesburg. Retrieved from: <https://ujdigispace.uj.ac.za> (Accessed: Date).



**EFFECTIVENESS OF ZINC-PHTHALOCYANINE AND
HYPERICIN IN INDUCING CELL DEATH IN HUMAN BREAST
CANCER CELLS (MCF-7) USING LOW INTENSITY LASER
IRRADIATION (LILI)**

A dissertation submitted to the Faculty of Health Sciences, University of
Johannesburg, Johannesburg, in fulfillment of the requirements for the
Degree of Master of Technology, Biomedical Technology

By

Ivan Sosthene Mfouo-Tynga
(Student number: 200504361)

Supervisor: _____
Prof. Heidi Abrahamse Date

Co-supervisor: _____
Dr. Nicolette Houreld Date

Johannesburg, 2013

DECLARATION

I, **Ivan Mfouo-Tynga**, declare that this dissertation is my own, unaided work. It is being submitted for the Degree of Master of Technology, Biomedical Technology, at the University of Johannesburg, Johannesburg. This work has not been submitted before for any qualification at any other institution.



UNIVERSITY
OF
JOHANNESBURG

Signature of Candidate

_____ day of _____ 2013.



OUTCOMES OF THE STUDY

Part of this work was presented at the following conferences and workshops

- The 4th (poster, 2010) and 5th (oral, 2011) African Laser Centre Student Workshops, University of Stellenbosch, South Africa.
- The Cross Faculty Symposium (poster, 2010), University of Johannesburg, South Africa.
- Laboratory Medicine Congress (oral, 2011), Sandton Conference Centre, South Africa.
- The 57th Annual Conference of South African Institute of Physics Conference (oral, 2012), University of Pretoria, South Africa.
- PDT As Minimal Invasive Therapy Conference (oral, 2012), University of Johannesburg, South Africa.

The following publications emanated from this study

- I.M Tynga and H. Abrahamse, Caspase-8 properties, functions and regulation during Photodynamic Therapy In Advances in Genetics Research, K.V. Urbano ed., Nova Sciences Publishers, Inc (2012), ISBN: 998-1-62081-466-6, volume 9, chapter 4, pp.107-119.
- I.M. Tynga, N.N. Houreld and H. Abrahamse (2012), Ability of ZnPcSmix phthalocyanine in inducing cellular death in human breast cancer cells (MCF-7) using laser irradiation. Proceedings of the 57th Annual Conference of the South African Institute of Physics (SAIP), *submitted*.
- I. M. Tynga, N. N. Houreld and H. Abrahamse (2013), The primary subcellular localization of Zinc phthalocyanine and its cellular impact on viability, proliferation and structure of breast cancer cells (MCF-7), Journal of Photochemistry and Photobiology B: Biology, *in Press*.
- I.M Tynga, N. Houreld and H. Abrahamse (2013), The effectiveness of activated ZnPcS_{mix} in inducing cell death in malignant breast cancer (MCF-7) cells, *in draft*.

ABSTRACT

The uncontrolled growth of cells in the body is often associated with cancer. It constitutes a major health problem and is one of the leading causes of death in the world. Cancers of the lung, breast, colon/rectum and prostate are no longer only associated with developed countries but are the most common occurring cancers worldwide. Breast cancer is the leading cancer faced by women in South Africa as well as in the world. Conventional cancer therapies often result in uncertain outcomes with numerous side effects and may be associated with limited therapeutic advantage. This has led to the development of safer and better treatment regimes with improved therapeutic outcomes. Photodynamic therapy (PDT) is a treatment used for a wide range of conditions, including cancer. This treatment utilises a photosensitiser (PS), a light activated chemotherapeutic agent, and light of a specific wavelength and power density. It is based on the selective tumour localisation of the PS and the ability to generate high levels of reactive oxygen species (ROS) in the presence of light. The generation of ROS causes permanent damage to the tumour cells resulting in cancer cell death. The distinctive criteria when comparing different PDT modalities is the choice of PS as the treatment outcomes are greatly influenced by the light dependent properties of the chemotherapeutic agent. Phthalocyanines are second generation PSs used in PDT. Effects of members of this PS family have been studied and they exhibited good photosensitising properties including lack of cytotoxicity in the absence of light, extended retention times in the tumour and high triplet lifetime of singlet oxygen species.

This study investigated the phototoxic effectiveness of ZnPcS_{mix}, a novel Zinc metallated phthalocyanine mix, on human breast MCF-7 cancer cells. A commercially available and established PS, Hypericin, was also used in this study. The MCF-7 cell line is estrogen positive and a suitable cell line for in

vitro studies. The cell line mimics the problems seen with tumour resistance to therapy well. Cells were cultured in supplemented Dulbecco's Modified Eagle's Medium (DMEM) in an 85% humidified atmosphere at 37°C and 5% CO₂. A mixed isomer of sulfophthalocyanines (ZnPcS_{mix}), that has a peak absorbance at 680 nm, was used to treat the cells. A 680 nm diode laser with an output power of 52 mW and power density of 5.73 mW/cm² was used to irradiate the cells at fluencies of 5, 10 and 15 J/cm². Cells treated with Hypericin were irradiated with a 594 nm diode laser, which delivered an output power of 99 mW and a power density of 11.58 mW/cm². Cell cultures were divided into 4 study groups. Group 1 received no ZnPcS_{mix} and was not irradiated, Group 2 contained ZnPcS_{mix} but was not irradiated and Group 3 was irradiated but no ZnPcS_{mix} was added. Group 4 was treated with ZnPcS_{mix} and was irradiated. A similar cell culture grouping was performed where Hypericin was used. Twenty four hours post treatment, cellular responses were determined and dose responses using both ZnPcS_{mix} and Hypericin mediated PDT were performed to determine the treatment parameters that led to a decrease in cell viability of 50% (IC₅₀).

Due to the relatively low effectiveness of Hypericin after the dose response assay (the Trypan blue exclusion assay), and the significant decrease in cell viability demonstrated by the phthalocyanine PS, only the ZnPcS_{mix} was used for the rest of the study. Fluorescent microscopy was employed to determine ZnPcS_{mix} localisation, visualising the nuclei, mitochondria and lysosomes. Cell damage due to ZnPcS_{mix} mediated PDT was assessed by inverted light microscopy for morphology, the Trypan blue exclusion assay for viability, adenosine triphosphate (ATP) luminescence assay and alamarBlue[®] for proliferation, and Lactate Dehydrogenase (LDH) membrane integrity assay for cytotoxicity. Then, flow cytometric analysis using Annexin V-FITC, Hoechst staining, cell death immunoassay and gene expression using a

Human Cell Death PathwayFinder™ PCR Array were performed post PDT using the treatment parameters that led to 50% decreased cell viability to identify the mode of cell death.

Fluorescent microscopy revealed that the ZnPcS_{mix} localised in mitochondria, lysosomes and around the nuclear envelopes, which correspond to the Golgi apparatus. Laser irradiation alone as well as the inactive form of the PS did not cause cell damage. Morphological change was seen with PDT treated cells with 0.5 and 1 µM ZnPcS_{mix} and included cell rounding up, anoikis and cell permeabilisation as confirmed with the Trypan Blue exclusion and LDH membrane integrity assays. A decrease in cell viability and cell proliferation, as well as an increase in cytotoxicity, were observed 24 h post PDT. A combination of 0.5 µM ZnPcS_{mix} with irradiation at 10 J/cm² was identified as the PDT dose that led to a 50% decrease in cell viability and was used for the cell death study. ZnPcS_{mix} is an effective inducer of ROS and was 8 times more efficient than Hypericin in inducing a 50% decrease in cell viability. Although being able to induce a decrease in cell viability at higher concentrations, the light activated Hypericin was found to be less effective than the new synthesised ZnPcS_{mix} and was not used for the rest of the study.


The effectiveness of ZnPcS_{mix} was found to correlate with both its concentration and laser fluence used; an increase in either concentration of PS or laser fluence led to a subsequent decrease in both cell viability, proliferation and a concomitant increase in cytotoxicity. Apoptotic cells predominated over necrotic and normal cells after Annexin V-FITC flow cytometric analysis. Signs of nuclear fragmentation and condensation were noted using Hoechst staining and the cell death immunoassay. Finally, three

genes (BCL-2, DFFA-1 and CASP-2) involved in apoptotic cell death pathways were found to be up-regulated. Taken together, the predominant apoptotic cell population, nuclear degradation and gene expression post PDT suggested that an apoptotic pathway was the mode of cell death. ZnPcS_{mix} displayed toxic effects on breast cancer cells at a relatively low concentration. In its natural form prior to irradiation and activation, the PS did not induce cell damage. After PDT, evidence of apoptotic cell death was demonstrated. This study identified the positive attributes of ZnPcS_{mix} as a novel PS with extensive potential as a future therapeutic application.



DEDICATION

I dedicate this dissertation to my twin brother Jeremy Talys. A great feeling of appreciation to my adorable mother for her wisdom and encouraging words, emotional support, all have enabled me to complete this study and move one step closer to the accomplishment of my mission on earth.



If patience is a path of gold therefore I strongly believe that perseverance is a path of excellence.

UNIVERSITY
OF
JOHANNESBURG

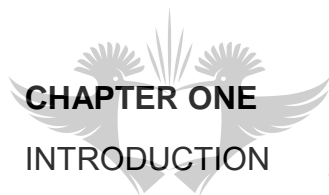
ACKNOWLEDGEMENTS

- First and foremost, I would like to give my deepest appreciation to the Lord, the Alpha and Omega, for always being with me and taking me victoriously through the hard and good times of this journey.
- Prof Heidi Abrahamse, head of the Laser Research Centre and her supervision, leadership, assistance, guidance and support throughout this study.
- Dr N.N. Houreld for mentorship, patience, availability, proof reading my work and all the support throughout this study.
- Dr M. Snymann and Dr H.A. Byth Illing for guidance and advice through the flow cytometric analysis of this study.
- Dr Sarah Taylor for guidance and support through the PCR-Array data analysis of this project.
- Prof T. Nyokong from Rhodes University for synthesising the PS (ZnPcS_{mix}), which was used in the study.
- The University of Johannesburg, African Laser Centre, National Research Foundation and National Laser Centre for the facilities, equipment at the Laser Research Centre and financial support.
- Ms C. Robertson and Ms J. de Villiers for their support and mentorship at the beginning of this project.
- Dr A. Hussein, Mr S. Manoto and Ms P.R Sekhajane for their help with the live imaging microscope and advice throughout the project.
- My fellow research colleagues, Sandra, Roland, Anine, Louis, Bernard, Ahmed, Sello and Palesa for support and creating a good friendly environment for research.
- Ms D.G. Yamba, my fiancée for her comfort and support during this project.
- To my team mates (AEGAS) for good times and helping me dealing effectively with stressful issues.

- Dr P. Voua Otomo, my cousin for being a model, encouraging words and for his brotherhood.
- To the Talys, Tynga and Mfouo families for their continuous support, love, appreciation and for believing in me.



TABLE OF CONTENTS	PAGE
TITLE	
DECLARATION	ii
AFFIDAVIT OF MASTRES STUDENT	iii
OUTCOMES OF THE STUDY	iv
ABSTRACT	v
DEDICATION	ix
ACKNOWLEDGEMENTS	x
TABLE OF CONTENTS	xii
LIST OF FIGURES	xvii
LIST OF TABLES	xxvi
LIST OF SYMBOLS AND ACRONYMS	xxix



UNIVERSITY
OF
JOHANNESBURG

1.1 Foreword	1
1.2 Problem Statement	2
1.3 Aims and Objectives	3
 CHAPTER TWO 	
LITERATURE REVIEW	
2.1 Cancer	4
2.2 Types of Cancers	5
2.3 Carcinogenesis	7
2.4 Breast Cancer	8
2.4.1 Types of breast cancer	9
2.4.2 Symptoms of breast cancer	10
2.4.3 Etiology of breast cancer	11

2.4.4	Incidence and mortality	13
2.5	Cancer Therapy	16
2.5.1	Conventional therapies	16
2.5.2	Photodynamic therapy (PDT)	18
2.5.2.1	PDT seen as a photochemical and photophysical process	19
2.5.2.2	Mechanisms of PDT	21
2.5.2.3	Properties of photosensitizer (PS)	21
2.5.2.4	Properties of light	25
2.5.2.5	Properties of molecular oxygen	27
2.6	Mechanisms of Cell Death	28
2.6.1	Apoptosis	28
2.6.2	Autophagy	30
2.6.3	Necrosis	32
2.6.4	Mitochondria as a critical regulator of cell death	33
2.6.5	Caspase family	34
2.6.6	BCL-2 family	36
2.7	Effects of PDT <i>in Vivo</i>	38

CHAPTER THREE

MATERIALS AND METHODS

3.1	Experimental Design	40
3.2	Human Breast Cancer Cells (MCF-7)	41
3.2.1	Cell culture	42
3.2.2	Cell stock preparation	43
3.2.3	Preparation of cells for experimentation	44
3.3	Photosensitisers	44
3.4	Laser Irradiation	45
3.5	Biological Responses	46
3.5.1	ZnPcS _{mix} localisation study	46

3.5.2	Dose response study	47
3.5.2.1	Cellular morphology	49
3.5.2.2	Cellular viability: Trypan blue exclusion assay	49
3.5.2.3	Cellular proliferation	50
	ATP luminescence	50
	alamarBlue®	51
3.5.2.4	Cytotoxicity	52
3.5.3	Cell death study	52
3.5.3.1	Flow cytometry	53
3.5.3.2	Hoechst staining	54
3.5.3.3	Cell death Enzyme Linked Immunosorbent Assay (ELISA)	55
3.5.3.4	Real-time Reverse Transcriptase Polymerase Chain Reaction	56
	Extraction of ribonucleic acid (RNA)	57
	RNA quantification	57
	RNA purity	58
	Complementary DNA (cDNA) synthesis	58
	cDNA purity	59
	Gene expression	60
	Real-time PCR array data analysis	64
3.6	Statistical Analysis	65

CHAPTER FOUR

RESULTS

4.1	Cell Culture	67
4.2	Biological Responses	68
4.2.1	ZnPcS _{mix} localisation study	68
4.2.2	Dose response study	68
4.2.2.1	Cellular morphology	69

4.2.2.2	Cellular viability	73
	Trypan blue exclusion assay for Hypericin	73
	Trypan blue exclusion assay for ZnPcS _{mix}	78
4.2.2.3	Cellular proliferation	79
	ATP luminescence	79
	alamarBlue [®]	82
4.2.2.4	Cytotoxicity	83
4.2.3	Cell death study	85
4.2.3.1	Flow cytometry	85
4.2.3.2	Hoechst staining	86
4.2.3.3	Cell death ELISA	87
4.2.3.4	Real time RT-PCR	88
	Real time PCR data analysis	89
	Gene expression profiles of ZnPcS _{mix} treated MCF-7 cells	89
	Gene expression profiles of PDT treated MCF-7 cells	90
CHAPTER FIVE		
DISCUSSION AND CONCLUSION		91
REFERENCES		105
APPENDICES		
APPENDIX A		
LIST OF CONSUMABLES		129
APPENDIX B		
LIST OF CHEMICALS, SOLUTIONS, AND MEDIA		132
APPENDIX C		
CALCULATIONS		134

C1. Calculation of cell viability	134
C2. Calculation of cell seeding culturing of cell in flaks	135
C3. Calculation of cell seeding for cryopreservation	135
C4. Calculation for seeding of cell culture plates	136
C5. Calculation of working concentration of 0.5 μ M Hypericin	138
C6. Calculation of average laser irradiation times for the diode lasers cell viability	139
C7. Purity of nucleic acid	140
APPENDIX D	
ETHICAL APPROVAL	141
APPENDIX E	
RT-PCR RESULTS	142
Gene expression profiling (p-values)	142
APPENDIX F	
LIST OF PUBLICATIONS	145
Article	145
Chapter in Book	151
Review	166



LIST OF FIGURES

- Figure 1** Cancers are caused by a sequence of changes; each change alters the behaviour of the cell in a certain manner (National Cancer Institute, 2004). 8
- Figure 2** Anatomy of the breast, updated from Atossa Genetics (2010). 9
- Figure 3** Age standardised incidence and mortality rates for breast cancer (Boyle and Levin, 2008). 15
- Figure 4** Modified Jablonski energy diagram. Energy level diagram of photon excited PS. S_0 , S_1 and S_n indicate ground or zero, first and n order of the singlet electronic state of PS while T_1 and T_2 represent the first and second triplet state of the excited PS. The molecule relaxes back to the ground state S_0 from S_1 or T_1 radiatively or nonradiatively. K_{nr} , K_{isc} , K_f and K_p are rate constants for nonradiative decay, intersystem crossing, fluorescence and phosphorescence respectively (Josefsen and Boyle, 2007). 19
- Figure 5** Mechanism of PDT, adapted from Ho *et al.*, (2008). 20
- Figure 6** Porphyrin structure (Chemistry About, 2009). 22
- Figure 7** Structure of metallated phthalocyanine (O'Malley *et al.*, 2007). 24

Figure 8 The electromagnetic spectrum with different wavelengths and the frequencies. As the wavelength of light decreases, the frequency increases in frequency. The visible spectrum of light is around a wavelength of 10^{-6} (adapted from Zebu.uoregon.edu. 2010). 26

Figure 9 Apoptosis includes cellular shrinking, chromatin condensation and margination at the nuclear periphery with the eventual formation of membrane-bound apoptotic bodies that contain organelles, cytosol and nuclear fragments and are phagocytised without triggering inflammatory processes. The necrotic cell swells, becomes leaky and is finally disrupted and releases its contents into the surrounding tissue resulting in inflammation (Gewies, 2003). 29

Figure 10 Apoptosis signalling pathways. Death receptor pathway is stimulated by the binding of death receptor ligand (CD95/TNFR/ TRAIL ligands) to death receptors (CD95/TNFR/ TRAILRs). The ligation triggers receptor trimerisation, recruitment of the adaptor Fas associated death domain protein (FADD) and procaspase-8 to form the death inducing signalling complex (DISC) and activation of caspase-8 through induced proximity at this complex. The cross talk between extrinsic and intrinsic pathway is initiated by a proapoptotic truncated Bid (tBid), processed by caspase-8. tBid translocates to mitochondria and favours Smac, AIF and cytochrome C release from

mitochondria into the cytosol. Cytochrome C together with caspase-9 and Apaf-1 forms the apoptosome, triggers caspase-3 activation, while AIF and Smac promote apoptosis, the latter by neutralising “Inhibitor of Apoptosis Proteins” (IAPs) (Tynga and Abrahamse, 2012).

36

Figure 11 Domain structure of Bcl-2 family proteins, depending on subfamily proteins, Bcl-2 can inhibit (antiapoptotic members) or induce (proapoptotic members) apoptosis. Bcl-2 subfamily (antiapoptotic): Bcl-2, Bcl-XL, Bcl-w, Mcl-1 and A1; the multidomain (proapoptotic): Bax, Bak and Bok; and BH3 only proteins (proapoptotic): Bad, Bid, Bik, Blk, Hrk, BNIP3 and BimL (Gustafsson and Gottlieb, 2007).

37

Figure 12 Flow diagram of ZnPcS_{mix} mediated PDT. The project comprised of localisation, dose response and cell death studies. MCF-7 cell cultures were divided into 4 study groups. Group 1 was an untreated control, group 2 received PS but was not irradiated and group 3 was irradiated with a 594 or 680 nm diode laser for Hypericin and ZnPcS_{mix} respectively but received no PS. Group 4 was irradiated and received PS. All samples were incubated for 24 h (except for PCR array, 3 h) and thereafter localisation, dose response and then cell death studies were performed.

40

Figure 13 The 680 nm diode laser used to irradiate the human breast cancer cells.

45

Figure 14 Layout of the catalogued 96-well PCR Array. Wells A1 through G12 contain individual qPCR assays for the 84 genes relevant to the human cell death pathway. Wells H1 through H5 contain a panel of housekeeping genes (HK1-HK5) used for normalising the PCR array data. Well H6 to H12 contain controls naming genomic DNA contamination (GDC), Reverse Transcription Controls (RTC), and Positive PCR Control (PPC). 62

Figure 15 Microscopic representation of confluent breast cancer cells. Cells were grown as a flat monolayer sheet. 67

Figure 16 Subcellular localisation of ZnPcS_{mix} in MCF-7 cells. DAPI stained the nuclei (blue a, e and i), Mito- and Lyso-tracker stained mitochondria (green, d) and lysosomes (green, h), respectively. ZnPcS_{mix} (red, b, f, j) localised in both the mitochondria and lysosomes as the red and green fluorescence merged and coincided to a slight yellow fluorescence (g and k). Distinct red and blue fluorescence were seen (merged) as ZnPcS_{mix} does not localise in the nuclei and ZnPcS_{mix} localised in the perinuclear area (c). 69

Figure 17 Morphology of MCF-7 cells treated with either laser irradiation or ZnPcS_{mix}. The untreated control (a) received no PS and was not irradiated. Cells were irradiated at 5 (b), 10 (c) and 15 J/cm² (d). ZnPcS_{mix} treated cells received 0.05 (e), 0.1 (f), 0.5 (g) and 1 µM (h) of the PS. No morphological change was noted when cells were treated with either laser alone (b, c

and d) or ZnPcS_{mix} alone (e, f, g and h) and compared to the untreated control (200 x magnifications).

70

Figure 18 Morphology of PDT treated MCF-7 cells with 0.05 μM ZnPcS_{mix}. The untreated control (a) received no PS and was not irradiated. Three hours after receiving the PS, cells were irradiated at 5 (b), 10 (c) and 15 J/cm^2 (d) using a 680 nm diode laser. At this concentration of ZnPcS_{mix}, PDT treated cells showed no morphological changes when compared to the untreated control cells (200 x magnifications).

71

Figure 19 Morphology of PDT treated MCF-7 cells with 0.1 μM ZnPcS_{mix}. The untreated control (a) received no PS and was not irradiated. Three hours after receiving the PS, cells were irradiated at 5 (b), 10 (c) and 15 J/cm^2 (d) using a 680 nm diode laser. When compared to the untreated control, all PDT treated cells showed a slight decrease in cell density and cell morphology started to change as cells became elongated (200 x magnifications).

72

Figure 20 Morphology of PDT treated MCF-7 cells with 0.5 μM ZnPcS_{mix}. The untreated control (a) received no PS and was not irradiated. Three hours after receiving the PS, cells were irradiated at 5 (b), 10 (c) and 15 J/cm^2 (d) using a 680 nm diode laser. Morphological change was observed in a fluence dependent manner; the longer the cells were irradiated, the more cell changes were noted when compared to the untreated control.

These changes included elongated cells with few rounded cells (b), decrease in number of attached cells to the culture surface (c) and cells rounded off as they detached from the culture surface (d) (200 x magnifications).

73

Figure 21 Morphology of PDT treated MCF-7 cells with 1 μM $\text{ZnPcS}_{\text{mix}}$. The untreated control (a) received no PS and was not irradiated. Three hours after receiving the PS, cells were irradiated at 5 (b), 10 (c) and 15 J/cm^2 (d) using a 680 nm diode laser. Morphological features of PDT treated cells had totally changed when compared to the untreated control. Most cells have already rounded off as they detached from the culture surface (200 x magnifications).

74

Figure 22 ATP luminescence cell proliferation assay in MCF-7 cells. When compared to untreated control cells, the relative light units (RLU) of both laser irradiated and $\text{ZnPcS}_{\text{mix}}$ treated cells did not present any major change in cell proliferation and no significant change in ATP levels was noted.

80

Figure 23 ATP luminescence cell proliferation assay in PDT treated MCF-7 cells. Activated $\text{ZnPcS}_{\text{mix}}$ during PDT caused a decreased in cell proliferation. A decrease in ATP levels was observed with most of PDT cells when compared to the untreated control and significant differences ($p < 0.05^*$) ($p < 0.01^{**}$) ($p < 0.001^{***}$) were noted.

81

- Figure 24** alamarBlue[®] cell proliferation in MCF-7 cells. Both irradiated alone and ZnPcSmixtreated cells did not show any significant proliferation change. 82
- Figure 25** alamarBlue[®] cell proliferation in PDT treated MCF-7 cells. PDT treated cells had slow proliferation rates and significant differences ($p < 0.05^*$) and ($p < 0.01^{**}$) were noted when compared to the untreated control cells only. 83
- Figure 26** The CytoTox96[®] nonradioactive cytotoxicity assay in MCF-7 cells. Irradiated cells and ZnPcS_{mix} treated cells alone showed no significant change in LDH levels when compared to the untreated control cells only. 84
- Figure 27** The CytoTox96[®] nonradioactive cytotoxicity assay in PDT treated MCF-7 cells. The cell damages were significant with all PDT cells and significant levels of LDH were noted. Significant differences ($p < 0.05^*$) and ($p < 0.01^{**}$) were noted when compared to the untreated control cells only. 85
- Figure 28** Hoechst immunofluorescence staining in MCF-7 cells. Intense fluorescence was seen when the nuclei of the untreated control (a) and unirradiated ZnPcS_{mix} treated (b) were analysed. After 3 h incubation post PDT, the nuclei appeared smaller in size with smears seen around them, an indication of nuclear condensation (damage). The smear cleared up and smaller distinct

nuclear fluorescence was seen 9 and 15 h after irradiation (d and e respectively) (200x magnification). 87

Figure 29 Evaluation of nuclear degradation using the Cell Death Detection ELISA assay. Untreated control cells (MCF-7) and both treated laser irradiated and ZnPcS_{mix} treated MFC-7 cells showed low amounts of DNA fragmentation. After PDT, the amount of DNA fragmentation significantly increased ($p < 0.01^{**}$). Significant difference was noted when compared to the untreated control cells. 88

Figure 30 Gene expression profile of ZnPcS_{mix} treated cells was analysed using the Human Cell Death PathwayFinder Profiler™ PCR Array System. Treatment did not have an effect on the gene expression and none of the genes were significantly regulated as represented with the 3D Profile (fold-difference, a) and volcano plot (b). In the volcano plot, the horizontal line designates the target threshold ($p = 0.05$) and vertical lines, the fold change (central) and target fold change threshold (peripheral) in gene expression. 89

Figure 31 Gene expression profiles of PDT treated MCF-7 cells with 0.5 μM ZnPcS_{mix} and 10 J/cm^2 was analysed using the Human Cell Death PathwayFinder Profiler™ PCR Array System. ZnPcS_{mix} mediated PDT induced changes in gene expression and DFFA, BCL-2 and CASP-2 genes were significantly up-regulated as represented with the 3D Profile (a) and

the volcano plot (b).

90



LIST OF TABLES

Table 1	Parameters of the lasers used in this study.	46
Table 2	Genomic DNA elimination reaction and various components.	59
Table 3	Reverse transcription reaction and various components.	60
Table 4	Functional gene grouping of the human cell death pathway finder profiler (updated from SABiosciences, PHAS-212A).	61
Table 5	Experimental cocktail preparation for RT-PCR application.	63
Table 6	Trypan blue percentage viability of different treatments. The percentage viability range from 99 to 32% and the lowest percentages were noted with 1 μM ZnPcS _{mix} treated samples. Significant differences ($p < 0.05^*$) ($p < 0.01^{**}$) ($p < 0.001^{***}$) were noted when compared to the untreated control cells (0 μM Hypericin and 0 J/cm^2). The Trypan blue exclusion assay was repeated six times ($n=6$). Cells treated with 4 μM of Hypericin and 10 J/cm^2 was found to have resulted in 53% cell viability.	75
Table 7	Trypan blue percentage viability of different	

treatments. The percentage viability range from 99 to 42% and the lowest percentages were noted with 1 μM $\text{ZnPcS}_{\text{mix}}$ treated samples. Significant differences ($p < 0.05^*$) ($p < 0.01^{**}$) ($p < 0.001^{***}$) were noted when compared to the untreated control cells only. The Trypan blue exclusion assay was repeated six times ($n=6$). Cells treated with 0.5 μM $\text{ZnPcS}_{\text{mix}}$ and 10 J/cm^2 was found to have resulted in 54% cell viability.

78

Table 8 Percentage of various cell populations after flow cytometric analysis. Normal cells were both negative for Annexin V-FITC and PI, early apoptotic cells were positive for Annexin V-FITC but negative for PI, late apoptotic cells were positive for both Annexin V-FITC and PI, and necrotic cells stained positive for PI. The lowest percentage of cell death (apoptotic and necrotic) were obtained with untreated and $\text{ZnPcS}_{\text{mix}}$ controls. These apoptotic populations significantly increased (around 65%) in Actinomycin D and PDT treated cells. The experiments were repeated four times ($n=4$) and significant differences ($p < 0.01^{**}$) and ($p < 0.001^{***}$) were noted when compared to the untreated control cells.

86

Table A1 List of consumables used throughout the study. 129

Table B1 List chemicals, solutions and media used during the study. 132

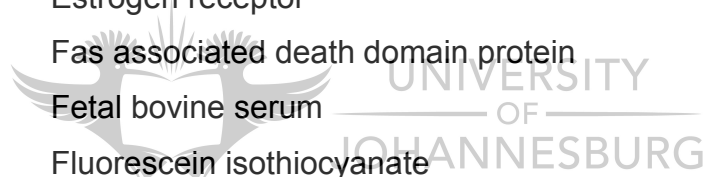
Table C1	Calculation of Hyperin (stock) volumes that were added for different concentrations.	138
Table C2	Calculation of ZnPcS _{mix} (stock) volumes that were added for different concentrations.	139
Table C3	Absorbance ratios of samples used for gene expression analysis.	140
Table D1	The p-values of genes analysed during the RT-PCR array.	142



LIST OF SYMBOLS AND ACRONYMS

x g	Gravitational force
λ	Wavelength(s)
~	Approximately
μg	Microgram(s)
μl	Microliter(s)
μM	Micromolar(s)
$^{\circ}\text{C}$	Degree celsius
$^1\text{O}_2$	Ground state oxygen
%	Percentage
2 D	Two dimensional
5-ALA	5-aminolevulinic acid
ADP	Adenosine diphosphate
AIF	Apoptosis initiator factor
αTNF	Alpha tumour necrosis factor
Al^{3-}	Aluminium ion
ASIR	Age standardised incidence rate
ATCC	American tissue culture collection
ATP	Adenosine triphosphate
Bak	BCL-2 associated antagonist/killer-1
Bax	BCL-2 associated X protein
BC	Before Christ
BCL-2	B-cell lymphoma-2
BH-3	BCL-2 Homology-3
BID	BH-3 interactin domain
Bok	BCL-2 related ovarian killer
BRCA	Breast cancer gene
CAD	Capase activated DNase
Ca^{+2}	Calcium ion

casp	Caspase
cDNA	Complementary DNA
Cl ⁻¹	Chlorine ion
cm	Centimetre(s)
CO ₂	Carbon dioxide
C _t	Threshold cycle value
Dapi	4'-6 diamidino-2- phenylindole
DCIS	Ductal carcinoma in situ
DFFA-1	DNA fragmentation factor-alpha
Disc	Death initialising signalling complex
DMEM	Dulbecco's Modified Eagle's Medium
DNA	Deoxyribonucleic acid
ELISA	Enzyme linked immunosorbent assay
ER	Estrogen receptor
FADD	Fas associated death domain protein
FBS	Fetal bovine serum
FITC	Fluorescein isothiocyanate
Ga ⁺²	Gallium ion
gDNA	Genomic DNA
h	Hour(s)
HBSS	Hank's balanced salt solution
HSP	Heat shock proteins
hv	Heat absorbed
IAP	Inhibitory apoptotic protein
IBC	Inflammatory breast cancer
ICAD	Inhibitor of caspase activated DNase
IDS	Invasive ductal carcinoma
ILC	Invasive lobular carcinoma
IMS	Internal membrane space
J/cm ²	Joule per centimeter square



K _f	Rate constant for fluorescence
K _{isc}	Rate constant for intersystem crossing
K _{nr}	Rate constant for nonradiative decay
K _p	Rate constant for phosphorescence
LCIS	Lobular carcinoma in situ
LDH	Lactate dehydrogenase
LILI	Low intensity laser irradiation
m	Meter(s)
MCF-7	Human breast cancer cell line
min	Minute(s)
ml	Mililiter(s)
mm	Milimeter(s)
MMP	Mitochondrial membrane potential
MOMP	Mitochondrial outer membrane permeabilisation
mPC	Metallated phthalocyanine
mw/cm ²	Miliwatt per centimetre square
MYB	Myeloblastosis
NADH	Nicotinamide adenine dinucleotide
NK	Natural killer
nm	Nanometer(s)
OH ⁻	Hydroxide ion
PARP	Poly ADP ribose polymerase
PBS	Phosphate buffered saline
PC	Phthalocyanine
PCD	Programmed cell death
PCR	Polymerase chain reaction
PDT	Photodynamic therapy
PI	Propidium iodide
PI3K	Phosphatidylinositol-3 kinase
PS	Photosensitiser

PT	Permeability transition
RLU	Relative light unit(s)
RNA	Ribonucleic acid
ROS	Reactive oxygen species
rpm	Rotation per minute
RT-PCR	Reverse transcriptase polymerase chain reaction
S	Second(s)
S ₀	Singlet electronic state zero order
S ₁	Singlet electronic state first order
S _n	Singlet electronic state n order
SO ³	Sulphuric anhydride
T ₁	Triplet state first order
T ₂	Triplet state second order
TM	Transmembrane
v/v	Volume per volume
W	watts
WHO	World health organisation
Zn ⁺²	Zinc ion
ZnPcS _{mix}	Zinc sulfophthalocyanine mixture



CHAPTER ONE

INTRODUCTION

1.1 Foreword

PDT is a therapeutic modality for cancer and non cancerous disorders characterised by proliferation of unwanted cells. PDT uses a photochemotherapeutic agent known as a PS, which has to be activated by light at a specific wavelength (600-900 nm) to undergo photochemical and photobiological processes that cause irreversible photodamage to cancer cells (Mitra and Stables, 2006). PDT offers an effective and specific means of killing cancer and is highly dependent upon the nature of the PS. The PS is able to recognise and rapidly enter neoplastic cells whereby after absorbing light at a specific wavelength, the PS produces ROS that kill the cells (Tsai *et al.*, 2004). In modern oncology, PDT research is of great importance forming the basis of clinical trials (Sieron and Kwiatek, 2006). The early clinical trials of PDT on breast cancer patients were performed using a Hematoporphyrin and skin photosensitivity was a major concern (Dougherty *et al.*, 1998; Usuda *et al.*, 2006). Hematoporphyrin, a first generation PS, has a poorly defined chemical composition and low absorption index in the therapeutic region of the electron magnetic spectrum (600-900 nm). This factor encourages research and since its approval in certain countries, efforts have been made to improve the outcomes of PDT, which have resulted in the synthesis and evaluation of new PSs. Phthalocyanine is a member of the second generation family of PSs that are currently studied as potential and efficient elements for photodynamic applications.

1.2 Problem Statement

The breast is an apocrine gland located in the upper ventral region of the torso of humans and produces milk during pregnancy. At puberty sex hormones, mainly estrogen, promote the development of the breasts in women (Ramsay *et al.*, 2004). The breast is susceptible to various benign and malignant conditions. In the last ten years, breast cancer has become the most diagnosed cancer in females worldwide. The incidence and death rate due to female breast cancer has decreased as a result of early detection, advanced treatment and increased awareness. Despite this decrease, the condition continues to be the most frequently diagnosed and the leading cancer faced by women worldwide, including in South Africa (Bray *et al.*, 2013; American Cancer Society, 2013; Siegel *et al.*, 2012; Molete, 2009). According to the World Health Organisation (WHO, 2006), breast cancer has become the most diagnosed cancer and common cause of death in women worldwide (American Cancer Society, 2013; Siegel *et al.*, 2012). New therapeutic means are required as conventional therapies such as radiotherapy and chemotherapy offer limited results, which are often associated with numerous side effects. PDT is already seen as a better treatment modality for malignant conditions with fewer side effects as this treatment is neoplastic specific. The PSs, which specifically localise in neoplastic cells, are the inducers of cell death upon light activation. Many clinical studies had reported PDT as a safer and efficient means of dealing with cancer, and for that reason better tumour localising PSs are required in order to enhance the therapeutic potential of PDT. This treatment can be used in conjunction with other treatments and thus it is referred to as an alternative cancer therapy rather than as a replacement therapy.

1.3 Aims and Objectives

The aims of this study were as follows:

- To identify subcellular localisation of ZnPcS_{mix} in malignant breast cancer cells.
- To determine and compare the effectiveness of Hypericin and ZnPcS_{mix} mediated PDT on cell viability.
- To determine cellular effects of ZnPcS_{mix} mediated PDT.
- To evaluate the expression of genes involved in cell death pathway following ZnPcS_{mix} mediated PDT.
- To identify the induced cell death pathway subsequent to PDT using ZnPcS_{mix}.



CHAPTER TWO

LITERATURE REVIEW

2.1 Cancer

Cancer has become one of the major challenges faced by the medical profession in modern societies. It is a genetic disorder, in which cells escape the control mechanisms and grow uncontrollably, thus invading surrounding normal cells. Cancer cells metastasise to other tissues and are transported through the bloodstream and lymphatic system. Cancerous cells differ from benign tumours, which do not metastasise and are self dependent entities. However, cancer is not a new phenomenon; it has affected humanity across time and space (Fayed, 2009; Karpozilos and Pavlidis, 2004; Tannock and Hill, 1998). Indeed, traces of cancer have been detected in fossils and Egyptian mummies. This is further corroborated by both pictures and writings describing malignant tumours. The analysis of skeletal residues from mummies, for instance, has revealed traces of osteosarcoma and cancer of the skull and neck. What is more, cancer also affects all higher animal species (American Cancer Society, 2010).

A study conducted by Newby and Howard in 2005 revealed a yearly diagnosis of more than 10 million cases of cancer worldwide. WHO predicts that this figure might increase to more than 15 million new cases annually by 2020 if no action is taken (Frankish, 2003). Cancer has been identified as the primary cause of death in industrialised countries and the second cause of mortality in developing countries (Jemal *et al.*, 2011). Clearly, there is an unequal distribution of cancer between developing regions/countries (Africa, Latin America, Asia and the Caribbean), where it is less prevalent, and developed regions/countries including Europe, North America, Australia, New

Zealand and Japan where it is more prevalent (International Agency for Research on Cancer, 2007). This led to the conception of cancer as a disease of industrialised countries. However, in a reversal of the situation, the WHO world cancer report for 2010 reveals that cancer is now predominant in the low and medium resource countries. In light of this rapid increase, cancer will soon supersede heart disease as the leading cause of mortality in the world. By 2010, the impact of increased incidences of cancer and the resulting deaths will be felt more severely in developing countries than in industrialised nations.

Cancer cells are dangerous for a number of reasons. Unlike normal cells, they can grow and age indeterminately. This leads to the formation of a tumour, as a result of an accumulation of cells in one area. Furthermore, cancer cells can conquer and disrupt the functioning of surrounding tissues. In other words, through a phenomenon called metastasis, cancer cells circulate in and affect other parts of the body. Many factors account for the immortality of cancer cells. But it suffices to note that most cancer cells activate an enzyme, telomerase, which is normally active only in stem cells (Hernandez, 2010). Cancerous cells are also characterised by their ability to multiply exponentially, until their telomeres shrink progressively and eventually die. The only way cells can avoid this fatal shrinkage is through up-regulation of telomerase, which prevents the shortening and enables the elongation of the telomeres (Willeit *et al.*, 2010). In addition, telomerase can prevent cell senescence and apoptosis (Philippi *et al.*, 2010).

2.2 Types of Cancer

There are various types of cancer. Most cancers form tumours except for a few such as Leukemia and Lymphoma (Varricchio, 2004). The classification

of cancers is based on the resemblance between the type of tissues and the formed tumour. The National Institute of Health's (2007) International Classification of Diseases for Oncology identifies the following categories of cancer:

- Carcinoma: represents more than 80% of all cancer cases, and includes the most common cancers such as breast, prostate, lung, and colon cancers which are derived from the epithelial tissues. Carcinomas are subdivided into adenocarcinoma and squamous carcinoma.
- Sarcoma: refers to tumours originating from connective or mesenchymal tissues. They are generally detected in young adults. The most common sarcomas are characterised by a painful mass on the bone.
- Lymphomas: are solid cancers which develop in the lymphatic system that is the network that purifies bodily fluids and produces lymphocytes. Because they could also occur in specific organs, they are designated as extra-nodal lymphomas. Diagnostically, the presence of Reed-Sternberg cells differentiates Hodgkin Lymphoma from Non Hodgkin Lymphoma.
- Leukaemia: refers to liquid or blood cancer which affects hematopoietic tissues. This form occurs in the bone marrow and is characterised by the patient's the inability to combat infections, as well as poor blood clotting, fatigue due to anaemia, and abnormal white and red blood cells.
- Germ cell tumour: relates to totipotent cells. It mostly affects the testicles and ovaries in adults; the body midline in fetuses, especially the tip of the tailbone, in babies, and young children; and the poll (base of the skull).
- Blastoma: a tumour (usually malignant) which resembles an immature or embryonic tissue. It is most common in children.

2.3 Carcinogenesis

The increase in cancer cases results from the aging and augmentation of the global population as well as the adoption of a cancer conducive lifestyle (Jemal *et al.*, 2011). Any form of cancer begins in the body's basic unit of life, the cell. Carcinogenesis or development of cancer is a process whereby normal cells turn cancerous. Put differently, the body is normally constituted of millions of cells, which grow, divide and die in an orderly manner. However, this orderly process may be upset, causing damage to the genetic material of cell. This results in mutations that negatively affect the normal growth and division of cells (National Cancer Institute, 2010).

In light of the above, carcinogens are cancer-causing agents. They can be classified into two categories. The first category comprises of genotoxins, which stick to DNA and engender permanent genetic damage. The second category encompasses non genotoxins (hormones and organic compounds), which stimulate growth without directly affecting DNA (Guyton *et al.*, 2009). Carcinogenesis is caused by various mutations to specific types of genes (Figure 1). These abnormal mutations in genes regulating cell division, apoptosis, and DNA repair lead to a cell's loss of control over its proliferation process. Numerous factors account for the transformation of normal cells into cancerous cells. These factors can be categorised as internal and external. Internal factors include heredity, immunology, and hormones; whereas external factors consist of chemicals, viruses, diet and radiation. Regardless of their classification, all these factors impair the genetic material of cells which results in the destruction of cell growth and division regulating genes. Thus, cancer is viewed as a tissue growth regulation disease (Vogelstein and Kinzler, 2004; Fearon and Vogelstein, 1990)

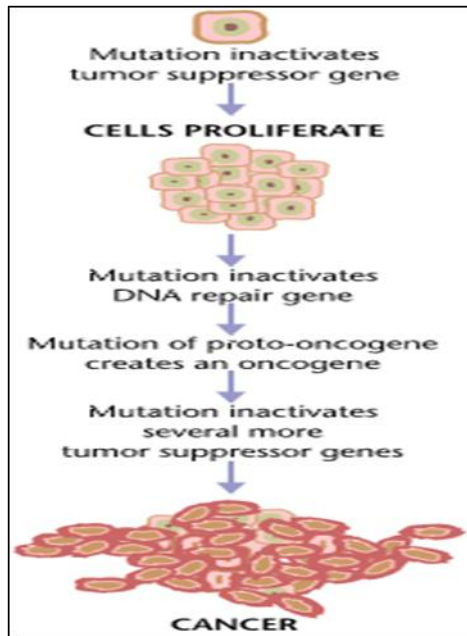


Figure 1 Cancers are caused by a sequence of changes; each change alters the behaviour of the cell in a certain manner (National Cancer Institute, 2004).



UNIVERSITY
OF
JOHANNESBURG

2.4 Breast Cancer

The breast is an apocrine gland that develops as an ingrowth from the ectoderm. A woman's breast comprises of milk-producing lobules, ducts which carry milk from the lobules to the nipple, fatty connective tissue, and blood and lymph vessels. The major secretory units consist of groups of terminal ductules equipped with alveoli (sac like-ends). These are imbedded in a fine specialised connective tissue to form the breast lobules (Figure 2).

Breast cancer refers to a malignant tumour that develops from cells in the breast. This malignancy is hormone dependent and may spread from the breast into other parts of the body. Breast cancer is believed to commence in the epithelium which lines the lobules terminal ductules (Ray and Mittra, 2003). Men are 100 safer from developing breast cancer than women. Breast

cancer has also become the most common form of cancer among women in developing and developed countries. Consequently, it accounts for most cancer-related deaths in the world, with the highest fatality rate in low and middle income nations. This prevalence resulted in cancer being declared an epidemic disease (Newby and Howard, 2005; Parkin and Fernandez, 2006).

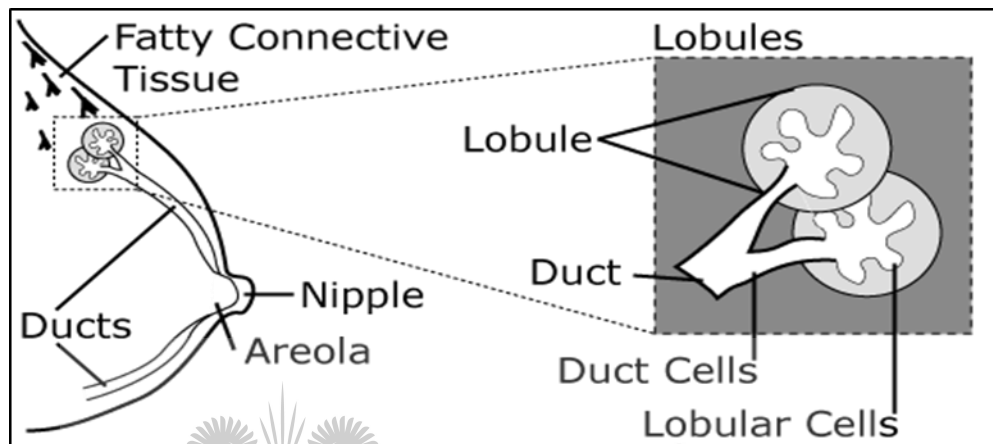


Figure 2 Anatomy of the breast, updated from Atossa Genetics (2010).

2.4.1 Types of breast cancer

There are many types of breast cancer; however, a breast tumour may be a combination of various types. The most common types of breast cancer are (CancerNet, 2012):

- Ductal carcinoma in situ (DCIS): it is located in the ducts. An early treatment of this condition maximises the patient's chance of healing. Most non-invasive breast tumours are of this type.
- Lobular carcinoma in situ (LCIS): it is located in the lobules. At this stage, it is not yet a cancer. However, individuals with LCIS are at risk of developing cancer.

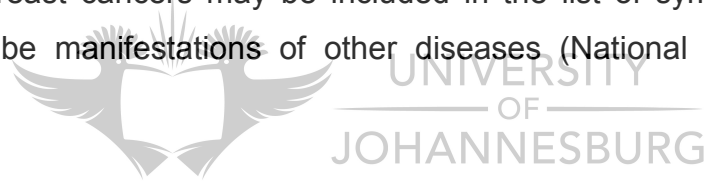
- Invasive ductal carcinoma (IDC): this is the most common type of cancer which accounts for 80% of all the invasive breast cancers. It originates from the ducts, and has the ability to invade other breast tissues by spreading through the duct walls. Most importantly, it can metastasise to other tissues.
- Invasive lobular carcinoma (ILC): this type begins in the lobules and can pass through the lobule walls into peripheral tissues. It accounts for 10% of invasive breast cancers.
- Inflammatory breast cancer (IBC): it causes breasts' skin to feel warmer than normal. This is accompanied by a reddish appearance. IBC is very uncommon and accounts for 4% of invasive breast cancers. It is usually misdiagnosed as an infection due to no lump in the breast.

2.4.2 Symptoms of breast cancer

Symptoms are the visible manifestations of a particular condition. However, the insignificant size of cancer cell clumps at the earliest stages renders prompt detection difficult, if not impossible. This is because an unusual tissue lump in the breast is the first noticeable symptom of breast cancer. Most cases of breast cancer are detected through feeling the woman's breast. Generally, the detection of a lump implies that the tumour has been developing for years. In this context, Mammography screening, that is, an X-ray type of breast examination, remains the only means of early detection of cancerous abnormalities in the breast (Merk, 2003; Gotzsche and Nielsen, 2009).

However, many other symptoms of breast cancer exist. These include modifications in the shape and size of the breast, dimpling of the skin,

inversion of the nipple, or unprompted single-nipple release (Merk, 2003; eMedicine, 2006). IBC, which is a swelling of the skin, also happens when cancer cells metastasise to lymph vessels located in the skin of the breast. Pain, inflammation, redness and orange peel texture of the breast's skin are the common symptoms of IBC (Merk, 2003). Paget's disease, which is characterised by redness and mild flaking of the nipple skin, is yet another symptom of breast cancer. The development of the condition may bring more symptoms such as tingling, itching, increased sensitivity, burning and pain. Generally, diagnosis of Paget's disease will be accompanied by the presence of a lump in the woman's breast (National Cancer Institute, 2005). It suffices to note that breast cancers can affect other organs such as bones, the liver, lungs, and the brain. These are known as metastatic breast cancers (Lacroix, 2006). Consequently, bone or joint pains, jaundice or neural signs ascribed to invading breast cancers may be included in the list of symptoms, although they may be manifestations of other diseases (National Cancer Institute, 2004).

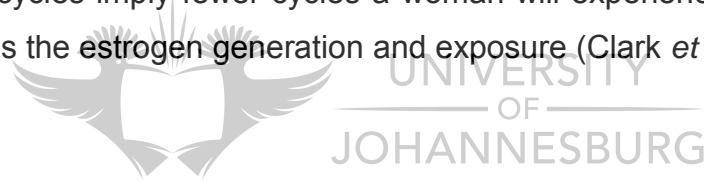


2.4.3 Etiology of breast cancer

Environmental influences account for the occurrence of most cancers (Vorobiof and Ruff, 2011). People of all ages, races, genders, and socio-economic status can be affected by cancer at any time. However, the socio-economic background largely influences the predominance of particular types of cancer. Although the development of breast cancer has been linked to a variety of factors, experimental research attributes its initiation and promotion to the elevated levels of endogenous estrogen metabolites (Yager, 2000). Estrogen is a hormone that is involved in the development of breast tissue and in the reproduction system of a woman. It is central to the normal functioning of a woman's reproductive system and influences the

development of her breasts. Prolonged exposure to this hormone stimulates breast cancer development in a woman.

A post menopausal woman's ovaries stop generating estrogen, which originates mainly from her body fat. This means that estrogen generation is dependent on the fat tissue in a woman. However, the quantity of estrogen in circulation in the body is strongly linked to alcohol intake. Alcohol has a stimulating effect on breast cancer development. Evidence suggests that the levels of estrogen in circulation in the body decreases with exercise. This is because fat tissue is used up and degraded to generate energy during exercise through beta-oxidation in the mitochondria. Furthermore, exercise is believed to lengthen the duration of the menstrual cycle of a woman. Longer menstrual cycles imply fewer cycles a woman will experience during her life; this reduces the estrogen generation and exposure (Clark *et al.*, 2002).



The female hormone estrogen stimulates the gene, MYB, which is a gene associated with breast cancer. MYB originates from myeloblastosis, which is a form of leukemia or blood cell cancer. This gene (6q23 chromosome) is present in most cases of breast cancer. It is responsible for the encoding of the transcription factor that is determinant in tumorigenesis. The prevalence of MYB in human breast cancer is strongly linked to the positivity of estrogen receptors (ER) (Drabsch *et al.*, 2007). The breast cancer gene (BRCA) situated on chromosome 17q21, stimulates mammary epithelial cell differentiation and the reduction of mammary stem cells that are conducive to the development of cancer. Mutations in the BRCA gene are linked to the occurrence of ovarian cancer and account for 20 to 40% of hereditary breast cancers affecting various populations around the world (Hu, 2009).

Breast cancer is the most occurring cancer in women the world over; this is true for South African women (American Cancer Society, 2013; Siegel *et al.*, 2012). Most cancer occurrences are related to the stimulation of tumour growth by estrogen. This is because of the central role played by estrogen metabolites and receptors in the development of the cancer (Rosen *et al.*, 2008). The risk of developing breast cancer is doubled for a woman whose immediate female family members, such as mother, sister or daughter, were diagnosed with this ailment. Research shows that 20 to 30% of women diagnosed with breast cancer are not the first in the family to have this condition. This means that most breast cancer cases originate from genetic transformations occasioned by aging and lifestyle, instead of heredity. Breast cancer cases attributed to aging in women over the age of 50 years represents 81%. Most of these cases are in the 50 to 69 years category.



2.4.4 Incidence and mortality

The global cancer report is released every 5 years and the latest one (2008) stated that breast cancer remained the most diagnosed cancer in women worldwide (American Cancer Society, 2013; Siegel *et al.*, 2012, Benn, 2009; Boyle and Levin, 2008; Molete, 2009; Van zyl *et al.*, 2008). Incidence refers to the likelihood of developing a given disorder in a set period of time. In this context, mortality is the outcome of incidence and the fatality for a specific type of cancer (Parkin *et al.*, 2005). Cancer incidence and mortality translate into absolute number of annual cases or an annual rate per 100,000 persons (American Cancer Society, 2013). Mortality is the figure of recorded deaths, its rate is construed as the yearly recorded dead people in a 100,000 populations. It suffices to note that regardless of the level of industrialisation, cancer is still a leading cause of death in the world. With around 100,000 people diagnosed with cancer, 60,000 of which result in death, South Africa has the highest yearly cancer incidence and fatality in Africa with roughly

100,000. South Africa has a 40% survival rate of cancer, which is higher than the global average of 37% (Vorobiof and Ruff, 2011). The latest 2002 statistics reported that one in four South Africans is affected by cancer (National Cancer Registry, 2008).

Men with a global age standardised incidence rate (ASIR) of 135.89 per 100,000 have a 1 in 7 lifetime risk of developing cancer. In contrast, women have an ASIR of 115.53 per 100,000; this translates in a 1 in 8 lifetime risk. With risk rates of 1 in 23 and 1 in 29 respectively, prostate cancer and breast cancer were the most prevalent in men and women respectively (Vorobiof and Ruff, 2011). Breast cancer is the most common cancer in women, and is responsible for more than one-fifth of new cancer cases and has been identified as the primary cause of cancer-related fatalities in women around the world (American Cancer Society 2013). Worldwide around 160,000 new cases of breast cancer are detected each year (Moleté, 2009). Although cancer has become an increasing health issue, breast cancer remains the most prevalent among South African women (Benn, 2009).

The incidence of breast cancer is significantly lower in teenagers and increases by more than a hundred fold at the age of 45. The world ASIR and mortality rate of breast cancer per 100,000 is presented in Figure 3 (American Cancer Society, 2004). The Southern African region has a mortality rate that is almost half its incidence, this means half of the women diagnosed with the condition in this region of Africa would die due to this cancer. Research conducted by Vorobiof *et al.*, (2001) observed that the population of black South African women have the lowest incidence of breast cancer in the country. The population of white women, with an ASIR of 70.2 per 100,000 is 6 times higher than that of black women. This ASIR was related to those of

industrialised countries including the United Kingdom and United States with an ASIR of 56.1 and 89.2 per 100,000 respectively.

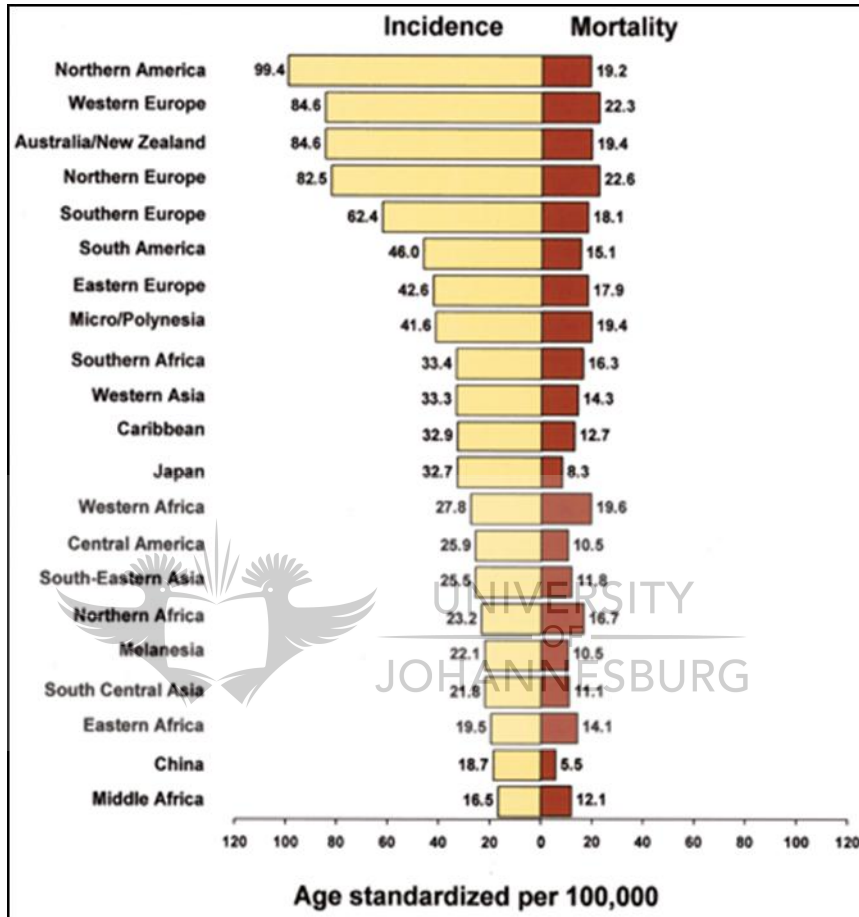


Figure 3 Age standardised incidence and mortality rates for breast cancer (Boyle and Levin, 2008).

This low ASIR in South African black women was due to the factors that used to be associated with rural inhabitants such as late menarche and limited or lack of access to contraceptives, which are believed to intensify the risk of hormone related cancer. In rural areas a high fibre and low animal fat intake, which is less predominant in urban areas and early pregnancy are believed to have played an important role in decreasing the risk. A demographic survey

revealed that 17.8% of black teenage females were pregnant as opposed to 2.2% of white females of the same age group (UNAIDS organisation, 2010). Breast cancer used to be related to a high income population, but the situation has progressively changed with a global incidence rate increase of 5% annually in low income populations. Despite the recent increase in the number of cancer associations in Africa, the challenge of implementing WHO recommendations remains a major issue. Cancer registries are providing data that will be indispensable for government agencies to make policies that suit these recommendations.

2.5 Cancer Therapy

2.5.1 Conventional therapies

Cancer therapy refers to a post diagnostic attempt to remedy the situation. An appropriate cancer treatment can be selected from a variety of options. However, the option is dependent on a number of factors such as the size of the tumour, the grade of cancer cells, and the type and stage of the cancer. Surgery, radiotherapy, hormone therapy, and chemotherapy are the main treatments for breast cancer.

- **Surgery** is the oldest cancer treatment. Its application to breast cancer implies the removal of the entire breast (mastectomy) or the cancerous portion together with peripheral tissues (lumpectomy). Generally, the side effects are inevitable and can considerably affect the patient's quality of life. Indeed, subsequent to having breast cancer surgery, some women have symptoms ranging from numbness, swelling, weakness, or tingling in the arm and shoulder area. These manifestations occur mainly after mastectomy surgery. Surgical removal of lymph nodes often leads to tingling sensation in the arm or shoulder (Breast Cancer Organisation, 2009).

- **Radiotherapy or radiation therapy** is a highly targeted and efficient method of directly killing cancer cells by means of high energy beams. Radiotherapy reduces breast cancer's recurrence risk by about 70%. This procedure is generally less complicated. However, the treatment damages both cancer cells and surrounding normal cells. Interestingly, the benefits and side effects of this treatment occur progressively. The most gradual and irritating side effect is the sunburn-like discoloration of the skin, that is, a mild to moderate redness accompanied by itching and soreness (Breast Cancer Organisation, 2009).
- **Hormone (anti estrogen) therapy** targets hormone receptor positive breast cancer cells and aims to decrease the quantity of estrogen in the body which, in turn, diminishes its effect on breast cancer cells. As observed elsewhere, estrogen is responsible for the stimulation of the growth of hormone receptor positive breast cancer cells. The entirety of estrogen in a woman's body is secreted by her ovaries. In certain instances of therapy, the treatment of hormone receptor positive cancer or the prevention of breast cancer requires the surgical removal of the ovaries and fallopian tubes. The ovaries may also be physiologically inhibited through medication uptake (Breast Cancer Organisation, 2009).
- **Chemotherapy** is the treatment of disease through the use of drugs designed to destroy microorganisms or unusual cells. The term chemotherapy was originally used to refer to the treatment of infectious diseases. However, it has come to refer primarily to the treatment of mental illness and cancer. The application of chemotherapy to breast cancer consists in the use of cytotoxic drugs to weaken and destroy cancer cells at the original site and any metastatic tumours. The cure particularly targets highly proliferating cells such as cancer cells. However, because they grow faster, some normal body cells located in the blood, the mouth, the intestinal tract, the nose, nails, the vagina,

and hair are accidentally targeted by these drugs (Breast Cancer Organisation, 2009).

2.5.2 Photodynamic therapy (PDT)

PDT is a third level treatment which uses light, in the presence of molecular oxygen, to activate a chemotherapeutic agent which stimulates the production of ROS (Figure 4). PDT was introduced in the early 1980s at various institutes (Konopka and Goslinski, 2007). The effects of ROS on cell metabolism are localised photodamage, nuclear damage, oxidation of amino acids in proteins, inhibition of particular enzymes due to oxidation of cofactors and cell death (Rada and Leto, 2008). The main benefits of PDT are its discerning accumulation into tumour tissues, the quasi absence of systemic drug caused toxicity, its capacity to treat many lesions concurrently and to retreat tumours (Luksiene, 2003). Because it specifically targets neoplastic tissues, the side effects of PDT are significantly minimal in comparison to other types of therapy.

The ability of PSs to accumulate in the tumour is attributed to biological and structural transformations that distinguish cancer cells from ordinary cells. Tumours display 7 key distinguishing features: they have larger interstitial volume and fraction of macrophages; leaky microvasculature; poor lymphatic drainage; low extracellular pH in the tumour; a relatively high level of synthesised collagen and numerous receptors for lipoproteins.

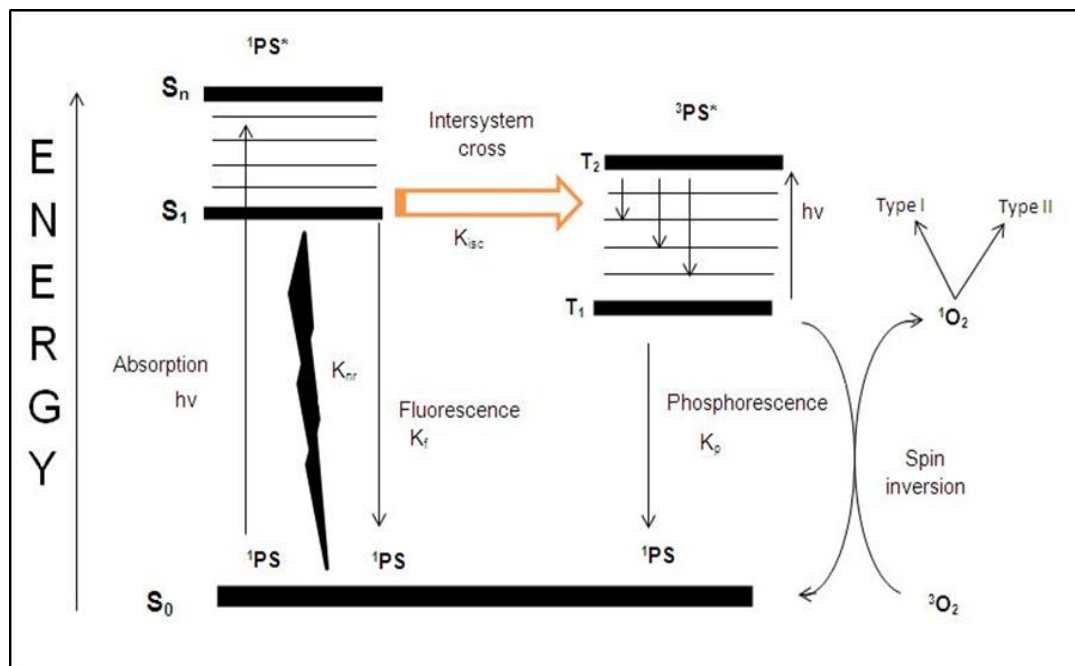


Figure 4 Modified Jablonski energy diagram. Energy level diagram of photon excited PS. S_0 , S_1 and S_n indicate ground or zero, first and n order of the singlet electronic state of PS respectively while T_1 and T_2 represent the first and second triplet state of the excited PS respectively. The molecule relaxes back to the ground state S_0 from S_1 or T_1 radiatively or nonradiatively. K_{nr} , K_{isc} , K_f and K_p are rate constants for nonradiative decay, intersystem crossing, fluorescence and phosphorescence respectively (Josefsen and Boyle, 2007).

2.5.2.1 PDT seen as a photochemical and photophysical process

PDT is a multi-stage process (Figure 5). The systemic or topic administration of PS is the initial step. A suitable PS for PDT has minimal toxic effects in the dark. The attainment of the optimal ratio of PS in diseased tissues as opposed to healthy ones resulted in the activation of the PS through exposure to a regulated light dose. The latter is directly shone onto the PS accumulated in the diseased tissue for a particular period of time. The toxic response in the tissue is associated with the light triggered form of the PS. The PS absorbs light energy (photons) and is promoted from its ground inactive state to the excited short life singlet state (S_1). This short transitional state of the PS lasts 10^{-9} to 10^{-6} seconds (Figure 4) (Josefsen and Boyle, 2007).

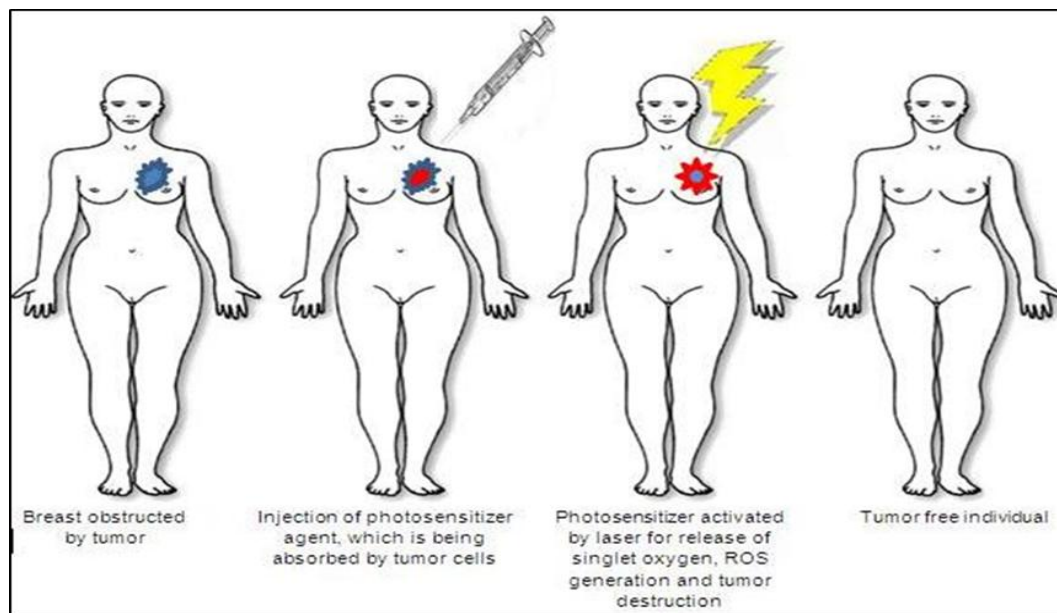


Figure 5 Mechanism of PDT, adapted from Ho *et al.*, (2008).

Interestingly, the stimulated PS molecule can experience further transitions (Figure 4), which are embodied by the singlet (S_0 to S_n) and the triplet states (T_1 and T_2) states. The singlet-excited PS can return to a radiation free decay state through heat generation (K_{nr}) or fluorescence (K_f). The singlet excited PS undergoes intersystem crossing when the constant K_{isc} is greater than both the constant of the heat generated (K_{nr}) and fluorescence (K_f). After intersystem crossing over, the excited PS in its triplet state has a longer life (10^{-3} seconds). For neoplasm obliteration, the triplet state is preferable and more chemically reactive than the singlet state. This new state of PS stimulates most physiological photochemical reactions (Figure 4) and interacts with peripheral molecular oxygen via spin reversal, and generates two photo oxidative responses (McNaught and Wilkinson, 1997; Turro *et al.*, 2008).

2.5.2.2 Mechanisms of PDT

PDT fuses the preferential accretion of a nontoxic PS into cancer tissues and irradiation using a perceptible light at a wavelength to be absorbed that matches the absorption specificity of the PS. After light activation, the tumour localised PS provides the selectivity of this treatment in the presence of molecular oxygen (Figure 5). The PS excited triplet state can undertake two different pathways labelled type I and type II reactions (Mroz *et al.*, 2010; Josefsen and Boyle, 2007). In type I reactions, the triplet PS can interchange an electron and an adjacent molecule (Castano *et al.*, 2005). This amalgamation of nontoxic components (PS, light, and oxygen) stimulates the selective damage of cancer tissues while minimising the obliteration of contiguous healthy tissues. This means that the properties of each constituent used in PDT are essential and determine the outcomes of the treatment (Josefsen and Boyle, 2007; Luksiene, 2003).



2.5.2.3 Properties of photosensitiser (PS)

Radiation therapy targets and destroys a cell's DNA directly, whereas the direct incorporation of the PS into cells during PDT and its subsequent activation by irradiation facilitates the targeting of cellular structures such as nuclear envelopes (Foster *et al.*, 2005), mitochondria (Wilson *et al.*, 2005), and lysosomes (Kirste *et al.*, 2002). The importance of PSs as a therapeutic agent dates back to the ancient civilisations (Egypt, India, and Greece). These societies identified PSs as light stimulated plant extracts to treat psoriasis and vitiligo. The main distinctive characteristic of any PS suitable for PDT is its capacity to specially accrue in diseased tissues so as to engender the intended biological effects, by means of cytotoxic species generation (Luksiene, 2003).

PSs can be divided into six clusters: Porphyrins (5-aminolevulinic acid, 5-ALA), metallated Phthalocyanines (mPC), Porphycenes (17-tri-methoxyethyl porphycene), Chlorines (monoaspartyl chlorine), Pheophorbides (bacteriophephorbide), and PSs other than the cited ones. Porphyrins are a group of primarily synthesised compounds that have a porphin structure to which are attached numerous side chains (Figure 6).

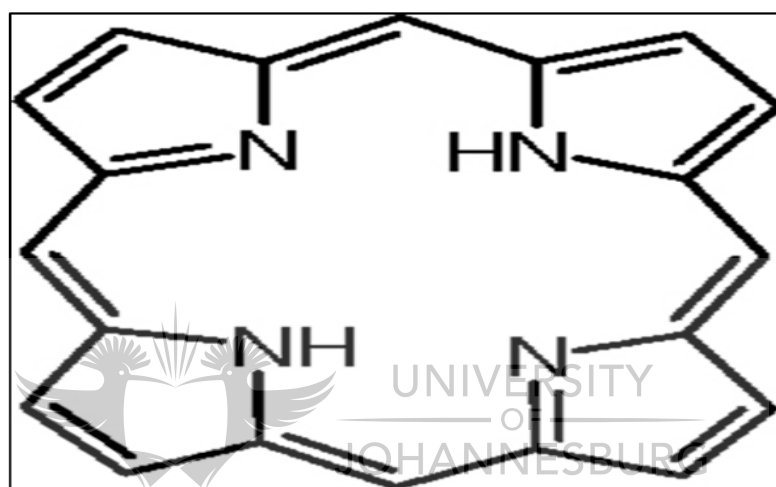


Figure 6 Porphyrin structure (Chemistry About, 2009).

Porphyrin family member PSs were effective in prompting phototoxicity and therefore recommended for the PDT treatment of some early stage superficial cancers. Their reduced tumour specificity, their poor tissue penetration due to their weak absorption spectrum in the near infrared region, their poor chemically defined structure and their durable skin photosensitisation after the treatment led to the development of new PSs (Rousset *et al.*, 2003).

mPC is an enhanced family of PSs derived from the preceding porphyrin PSs. PSs that belong to the family of mPC have an extra benzo ring on each of the

four pyrrolic subunits, which are interlinked by nitrogen atoms (Figure 7) (Lukšienė, 2003). These modifications result in a red shift in the absorption spectrum between 675 to 700 nm. They have a higher molar absorption coefficient ($105 \text{ m}^{-1} \cdot \text{cm}^{-1}$) that gives them an enhanced tissue infiltration compared to the previous generation of PSs. PC is a stable complex constituted by dissimilar fundamental metal ions; hence, it is referred to as metallated PC (mPC). mPCs comprise benzene rings fused to the β -positions of each of the four pyrrolic subunits (Figure 7) and a high triplet quantum yield ($\Phi_T \geq 0.5$). These benzo rings reinforce the absorption of the chromophore at longer wavelengths. However, it has a short lifespan of nearly 490 femto seconds (Lukšienė, 2003). The photophysical traits of mPCs depend on their structures and are influenced by the type of central metal ion.

Given that the majority of unaltered PCs are not water indissoluble, their chemical alterations are essential to their improvement, that is, the augmentation of their solubility. Regardless of their low quantities, water solvable PSs can only melt in physiological diluents in the absence of detergents and lipophilic environments. Solid composites alone are photoactive and therefore essential for the light based cures. PCs have been split into two categories on the basis of their photo mediated biological attributes: hydrophilic PCs which are easily dissolvable in biological solvents and their hydrophobic counterparts whose dissolution in similar conditions requires special mixtures like oil combination, liposome, and other colloidal methods. Hydrophilic sulfonated PC, which is derived from the sulfonation of its corresponding unsubstituted PC whether through the fuming of sulfuric acid with phthalic acid, phthalonitrile, phthalamide or phthalic acid, is soluble in water (Brasseur, 2003).

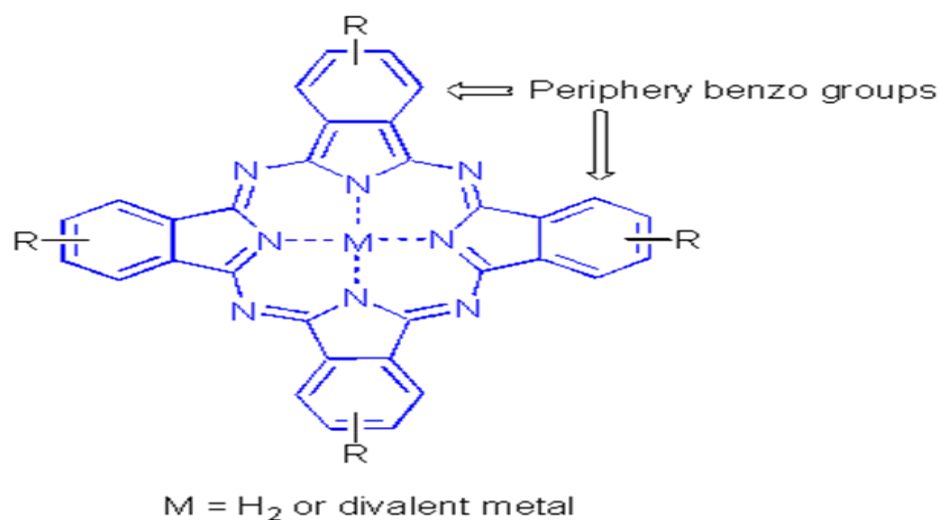


Figure 7 Structure of metallated phthalocyanine (O'Malley *et al.*, 2007).

An amphiphilic (with various components) PC comprises two contiguous benzo ring and achieves better photo activity and cell infiltration attributes. Localisation studies reveal that the mono and disulfonated Al⁺² and Cl⁻¹-PC diffuse and localise in the cytoplasm, whereas the same happens in the lysosomes for the tri and tetra forms. Zinc phthalocyanine (ZnPcS) is an encouraging second group PS which possesses photosensitising properties deriving from its intense absorbance in the red region of visible light.

Profounder infiltration of light into tissues improves cell annihilation in contrast to Porphyrin treated cells (Sazgarnia *et al.*, 2010; Abrahamse *et al.*, 2006; Ogunsipe *et al.*, 2004; Decreau *et al.*, 1999). In most instances, once ZnPC is absorbed by cells, it is localised predominantly in the Golgi apparatus. Its localisation mainly in the mitochondria is subsequent to prolonged exposure. Mitochondria constitute a significant location and element for the promotion of apoptosis which is regarded as the primary death pathway of PDT (Fabrics *et al.*, 2001). The success of PDT depends on the protracted accretion of ZnPcS and its ability to successfully produce singlet oxygen or other highly

responsive species in damaged tissues (Josefsen and Boyle, 2007). ZnPcS complexes have attracted increased interest due to their significantly long triplet lifespans which are advantageous since the number of diffusional encounters between triplet excited state and ground state of molecular oxygen augments with triplet state lifespan (Ogunsipe *et al.*, 2004).

2.5.2.4 Properties of light

PDT requires a special light source to initiate the PS at its peak absorption spectrum. Laser, which is an acronym for Light Amplification by Stimulated Emission of Radiation, is a mechanism of producing electromagnetic radiation through the process of stimulated emission in a form of monochromatic and directed light (Figure 8) (Osborne, 2007). The five primary attributes of light are intensity, frequency or wavelength, polarisation, phase, and orbital angular momentum. Light particles or photons display the characteristics of both waves and particles (Fonseca *et al.*, 1999).

Laser light differs from normal white light, which comprises of numerous dissimilar wavelengths (or colour of light) combined together. A laser light consists of a single wavelength, hence the term monochromatic. An additional difference between laser and normal light is that all wavelengths in laser light are in phase and aligned. Unlike ordinary light sources (flashlight, light bulb, sunlight) whose beam spreads in all directions, laser light waves are collimated. This means that they travel parallel to one other, in one direction. Because laser light beams are fine, all the energy can be focused on one central point with intense power (Netting and Fisher, 2011). Photons are absorbed by PSs when the wavelength of the light and the absorption spectrum of PSs correlate. The range of light used in PDT is between 600-

900 nm. This is because some endogenous proteins such as hemoglobin absorb light below 600 nm (Tayyaba et al., 2000).

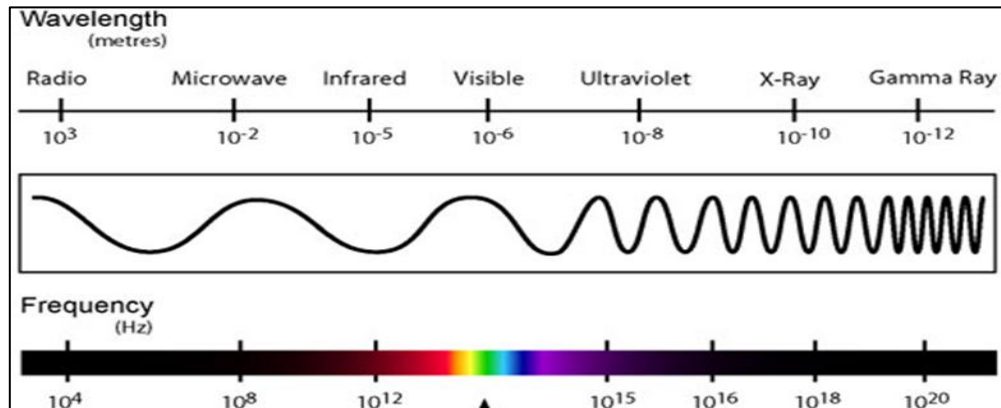


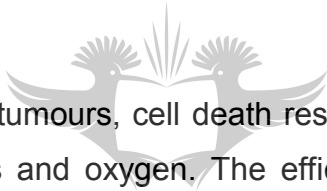
Figure 8 The electromagnetic spectrum with different wavelengths and the frequencies. As the wavelength of light decreases, the frequency increases. The visible spectrum of light is around a wavelength of 10^{-6} (adapted from Zebu.uoregon.edu., 2010).

The 900 nm maximum is motivated by the fact that the energy content of photons, at higher wavelengths, is inappropriate for the stimulation of singlet oxygen production. Light at such wavelengths was shown to infiltrate deeper into tissue and the actual penetration depth depends on optical characteristics such as absorption and scattering of irradiated tissue. Light dose in a tissue is influenced by depth. For instance, during a similar period of irradiation, a penetration depth of 2 to 3 mm will be achieved at 630 nm and this depth will be doubled using a wavelength of 700-800 nm (Tromberg *et al.*, 2000). The X-ray innovation in the 1890s propagated the use of light for medical applications, sterilisation and therapeutic radiation. The visible region of the spectrum is the most utilised and each coloured light can offer a specific preferred therapeutic effect. For instance, whereas red light only stimulates, blue light destroys biological organelles (Ryer, 1997). The laser is the main source of light for PDT and the preferred wavelengths are red and

near the infrared region, which offers better penetration into tissue (Wilson, 2006).

2.5.2.5 Properties of molecular oxygen

Oxygen is one of the most important molecules for life as it is involved in many metabolic processes. It has two unpaired electrons in its lowest energy state and these electrons confer oxygen its high biochemical reactivity. It has been shown that PDT efficiency depends on oxygen, which accepts energy carried by the electrons from excited PSs during photosensitised reactions in PDT. The ensuing energy rich singlet/triplet oxygen triggers oxidation and the generation of reactive molecules such radical species, which are the effectors of photodynamic damages (Grossweiner, 1992).



UNIVERSITY
JOHANNESBURG

In hypoxic tumours, cell death results from necrosis caused by the depletion of nutrients and oxygen. The efficacy of PDT, which is also dependent on oxygen, may be reduced by depletion of oxygen. On the one hand, the oxygen dependence of PDT is linked to the type of PS used. For instance, in Photofrin mediated PDT, the damage is directly proportional to oxygen pressure; whereas the photodamage observed during Chloroaluminium mediated PDT is inversely proportional to the same pressure. On the other hand, exhaustion of oxygen leads to ineffective tumour destruction after PDT. It is accepted that a prolonged illumination *in vivo*, leads to high rates of oxygen depletion and inadequate tumour reperfusion to produce insufficient PDT effects. Oxygen is a limiting factor in PDT and an *in vitro* study showed that oxygen depletion led to several changes in intermediate pathways and cell death (Tayyaba *et al.*, 2000; Gomer *et al.*, 1989).

2.6 Mechanisms of Cell Death

In photodynamic reactions, a lethal dose of PDT causes cell damage and death. Subcellular localisation of PSs in cells is a primary factor in PDT. Oxygen rich structures that are likely to accumulate PSs would be damaged upon illumination. Death is a fundamental process of life, in particular at the cellular level, where it plays critical roles in eradicating damaged cells (Alberts *et al.*, 2002; Engelberg *et al.*, 2006). Active cells degrade and remove damaged or dying cells through three standard cell death pathways, namely, apoptosis, autophagy, and necrosis. These pathways may occur depending on the types of cellular damage and participate in cell regeneration, growth, degradation and homeostatic responses (Green, 2011). Both apoptosis and autophagy are genetically regulated processes and known as programmed cell death, while necrosis is an accident event. Sometimes, autophagy responses are associated with starvation in cultured cells. Biochemical events of apoptosis are the best studied and understood of cell death pathways (Reape *et al.*, 2008; Zong and Thompson, 2006).

2.6.1 Apoptosis

Apoptosis means leaves falling from a tree and is also known as cell suicide. It is an active regulated process of destroying cells by combined actions of macrophages, fibroblasts, epithelial and immature dendritic cells (Youle and Strasser, 2008; Botto, 2004). The absence of inflammatory reactions is one of the distinguishing features of the apoptotic pathway (Figure 9) among many others including ATP level alternation, casapase activation, cell budding, cell shrinkage, chromatin margination, nuclear condensation, DNA fragmentation and formation of apoptotic bodies. Phagocytic cells take up cellular debris and the transport system of the debris across the plasma membrane, mitochondria and lysosome is maintained even towards the end of the pathway (Gewies, 2003; Luksiene, 2003).

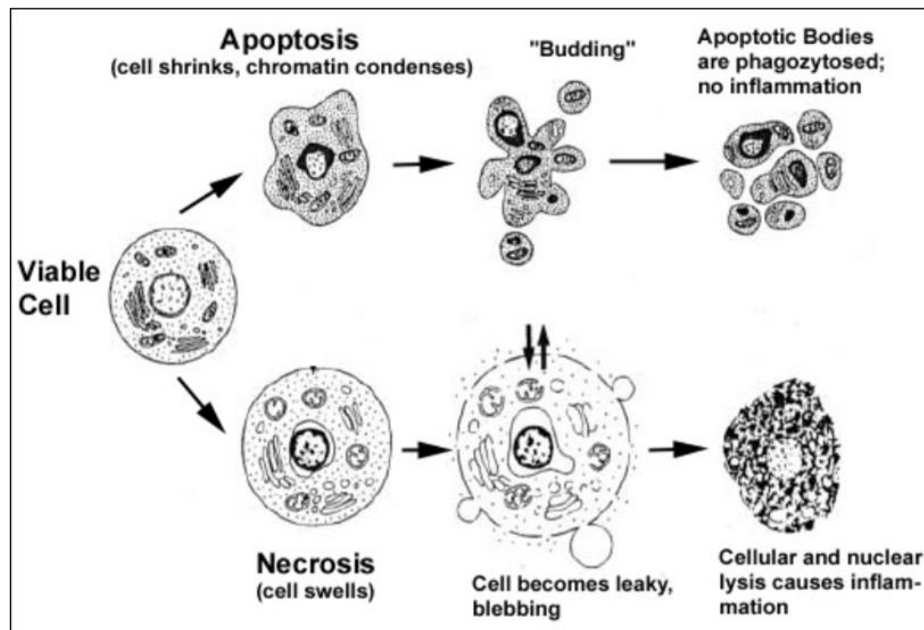


Figure 9 Apoptosis includes cellular shrinking, chromatin condensation and margination at the nuclear periphery with the eventual formation of membrane-bound apoptotic bodies that contain organelles, cytosol and nuclear fragments and are phagocytised without triggering inflammatory processes. The necrotic cell swells, becomes leaky and is finally disrupted and releases its contents into the surrounding tissue resulting in inflammation (Gewies, 2003).

In the inner cellular membrane, a phospholipid component, which is also known as phosphatidylserine, translocates to the exposed membrane surface. This translocation to the cell surface is an important signalling apoptotic event that will provoke further cell death events such as the activation, propagation and completion phases of apoptosis (Botto, 2004). These processes involve mediators on the outer surface membrane, which are cell receptors, and inner mediators generated due to nuclei damage, oncogene action and oxygen depletion (Luksiene, 2003). Apoptosis is the most studied of cell death mechanisms and PDT mediated apoptosis has been reported. When compared to PSs that primarily localise in the plasma membrane and lysosome, mitochondrial localising PSs are efficient inducers of apoptosis.

The cytochrome C discharge from mitochondria during cell death is one of the main signals of the intrinsic pathway, which together with its extrinsic counterpart form the two standard apoptotic pathways in mammalian cells. Stimulation of either of these pathways leads to the cascade activation of caspase, a family of prominent proteases involved in cell death (Fulda, 2009). Most neoplasms have defective apoptotic machinery with increased expression of prosurvival BCL-2 and tumour suppressor gene TP53 and is one of the well-known abnormalities of such cells. High expression of the guardian of the genome or tumour suppressor gene TP53, which encodes for the p53 tumour protein, is an initiator of cell death in response to nuclear damage caused by radiation, chemical agents and oxidative stress. Apoptosis is advantageous for the health of any multicellular organisms and without this essential process; organs would have grown such that an octogenarian would have accumulated more than two tons of bony mass and a 16 kilometer long intestine (Melino, 2001).



UNIVERSITY
OF
JOHANNESBURG

2.6.2 Autophagy

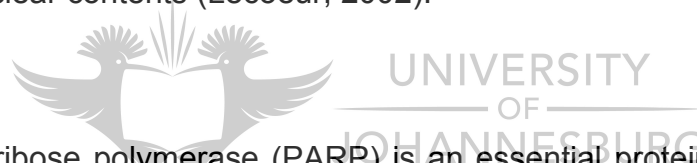
Autophagy is an adaptive response to starvation such as the lack of nutrients. This type of cell death plays an important role in homeostasis and in a catabolic means through lysosomal degradation. It also originated and translated from the ancient Greek words, which means self-destruction, and initially used to designate single or double lysosomal derived vesicle filled with cytoplasmic residues that were identified by electron microscopy (Watanabe *et al.*, 2009). Cytoplasmic contents are being degraded via the formation of an autophagosome, which is a large vacuole. The autophagosomic assemblage and its proteolytic lysosome mediated degradation lead to the production of micro substances, which in turn are used up for cell metabolism in energy generation and membrane formation (Smith and Yellon, 2011). In case of exhaustion of resources, autophagy

offers an alternative means of self-generation of energy and maintenance of healthy state of cells and tissues through the substitution of useless and impaired cellular contents with new ones. It is more a survival mechanism than a cell death pathway (Rabinowitz and White, 2010; Levine *et al.*, 2011).

According to the lysosomal destruction mechanism; different autophagic forms have been identified. Macro autophagy is a double membrane structure and also called an autophagosome which engulfs targeted particles before fusion with lysosomes. An autophagosome is regulated by a protein complex made up of class III phosphatidylinositol-3-kinase (PI3K) and beclin-1, which are part of the B-cell lymphoma 2 (BCL-2), family members. This family of proteins has a BCL-2 Homology 3 (BH 3) only domain. Furthermore, autophagosomic assemblage can be inhibited by Sirolimus, which is a mammalian target of rapamycin and a specific serine-threonine kinase through the addition of various cellular nutrients, growth factors and cellular redox state (Levine and Deretic, 2007). Micro autophagy is the degradation of target particles by lysosomes and the process is facilitated by heat shock proteins (HSPs), which make target particles available for lysosomal degradation, known as chaperone mediated autophagy (Klionsky, 2007). There is not enough evidence to establish a firm link between the increased population of autophagosomes and cell death mechanisms. The process is therefore referred to as autophagy associated cell death (Galluzzi *et al.*, 2009). Autophagy has two major advantages that is the induction of the survival pathway by providing alternative sources of nutrients under extreme conditions such as nutrient depletion, and a protection mechanism by eradication of damaged mitochondria, which constitute in this case a major source of ROS and toxic misfolded proteins that may damage the nervous system (Kroemer *et al.*, 2009).

2.6.3 Necrosis

Necrosis is referred to as a nonprogrammed cell death caused due to cell swelling or breaks that led to intracellular component leakage into the cytoplasm. In neoplasms, it occurs when the proliferation rate is greater than angiogenesis. The presence of an inflammatory reaction, plasma membrane disturbance and release from the cytoplasm are the defining features of necrosis (Figure 9). Major necrotic effects include unregulated or impaired functions, osmotic stress, flocculent mitochondria and cell bursting (Lemasters, 2005; Majno and Joris, 1995). In situ, a local inflammatory response followed by the discharge of cellular debris into peripheral tissues. Exposure of Propidium Iodide (PI) to the DNA molecules may reveal that PI is often used to distinguish between necrotic, apoptotic and normal cells (Josefsen and Boyle, 2007). PI is an important intercalating dye and used to assess nuclear contents (Lecoeur, 2002).



Poly-ADP-ribose polymerase (PARP) is an essential protein in necrosis that has a DNA restoring function. A certain extent of cellular ATP is required for storing and repairing activities in damaged cells. Under apoptotic conditions, this enzyme is in its cleaved and inactive form to allow the organism to cope with the high energy demand during the execution phase (Jagtap and Szabo, 2005). An increase in calcium ion (Ca^{+2}) levels in cells is a determinant stimulating factor for necrosis. The influx of Ca^{+2} across the plasma membrane has been reported to occur during necrosis and a discharge from the endoplasmic reticulum may be enough to promote apoptosis (Vanlangenakker *et al.*, 2008).

Contrary to the general view, necrosis is a sequential process rather than an accidental process. Under necrotic conditions, the first cells to be damaged

are chemotaxins and cytokines. These cells activate phagocytes and immune cells, which destroy foreign substances and induce an inflammatory response. Although little proof exists to establish a genetically regulated mechanism; it has been shown with the discovery of intracellular protease inhibitors including Serpin that necrotic reactions are the result of harmful invasion and can be regulated through protein stress response pathways (Luke *et al.*, 2007).

2.6.4 Mitochondria as a critical regulator of cell death

Cellular respiration and energy production take place in the mitochondria. These cellular organelles play a central role in all three types of cell death modes and in the integration of stress and/or cell death signals in both plants and animals. Release of apoptogenic proteins from the mitochondrial internal membrane space (IMS) through the aperture of the permeability transition (PT) pores triggers the activation of proteolytic enzymes and promotion of apoptosis in mammalian cells. Mitochondrial release of cell death initiating molecules may also be as a consequence of a temperature increase to 55°C (Reape *et al.*, 2008).

In mammalian cells, most proapoptotic signals converge to the mitochondria. The effect of these signals in conjunction with the membrane potential disturbance, leads to the release of mitochondrial IMS proteins (Luksiene, 2003). The disruption of the mitochondrial membrane leads to a sequential and progressive cell death response (Lemasters, 2005). On occasion, autophagy follows the destruction of the mitochondrial membrane of a limited number of cells. The destructed mitochondria are degraded and removed by the lysosomes. Conversely, apoptosis occurs when higher quantities of mitochondria are permeable, possibly as a result of an increased discharge of

apoptogenic factors (Reape *et al.*, 2008). Such discharges are regulated by both proapoptotic (Bax, Bak, Bid, and Bin) and antiapoptotic (BCL-2, BCL-X, and BCL-W) proteins. Caspase- 8 and -9 are the effectors of apoptosis and are initiated by death receptors such as Fas and cytochrome C, respectively.

These caspases in turn stimulate downstream caspases, which execute the programmed cell death via the obliteration of cellular organelles and nuclear materials (Luksiene, 2003). A severe disturbance in the mitochondrial membrane potential (MMP) leads to ATP depletion and disastrous cell impairment as a result of permeable mitochondrial membranes. Necrotic cell death would be the logical consequence (Reape *et al.*, 2008). Mitochondria are indeed important in both internal and external cell death pathways of apoptosis. The release of proapoptotic proteins leads to mitochondrial outer membrane permeabilisation (MOMP) in the internal pathway. Conversely, the external pathway is triggered by the action of cell death receptors and stimulated by the activation of BH3-interactin domain death agonist (Bid), which is a caspase mediated mechanism (Chipuk and Green, 2005).

2.6.5 Caspase family

Caspases are cysteine proteases which are proteins mostly related to degradation processes in an organism. They are involved in wound healing, immunomodulation, digestion, and neoplastic illnesses (Salas *et al.*, 2008). In other words, caspases are essential proteases and are directly connected to cell death. They are key initiators, diffusers and executioners of apoptosis. Thus, it is not surprisingly that the utmost morphological transformations that occur during apoptosis are associated with caspases, but that they also possess other essential non cell death functions (Lamkanfi *et al.*, 2007). Under normal conditions, caspases exist as proenzymes in their inactive form

and need to be activated through proteolytic cleavage either by other proteins or receptors in active complexes (Gewies, 2003). These proenzymes do not localise in mitochondria, but are commonly found in the cytosol (Van Loo *et al.*, 2002).

Caspase-8 is a key initiator caspase by virtue of the centrality of its initial role in the initiation of the caspase cascade. It is crucial for the regulation of programmed cell death (PCD) as well as the appropriate signalling of the external apoptotic path (Fulda, 2009). The external (death receptor) or internal (mitochondrial) initiation of pathway apoptosis is influenced by stimuli. The tying of specific ligands (Fas and CD95/TNFR/TRAIL) to their corresponding death receptors constitutes the first step in the extrinsic pathway. This is followed by the recruitment of adaptor molecules through the cytoplasmic death domain. The ultimate result is the formation of a trimeric death receptor structure. The autoproteolytic initiation of caspase-8, subsequent to the constitution and disassembling of the death initialising signalling complex (DISC) (Figure 10), is the outcome of the combination of this trimeric structure and procaspase-8. The cleaving and activation of caspase-3/-9, for the execution of apoptosis are achieved by caspase-8 (Kantari and Walczak, 2011).

In certain instances, mitochondrial apoptotic pathway activation results from DNA destruction. However, the initialising of this pathway is usually activated by death signals resulting from the simultaneous action of caspase-8 onto Bid protein and procaspase-9. The resulting shortened, essential Bid protein promotes the disturbance and permeability of the external mitochondrial membrane. It also enables the mitochondrial discharge of smac, AIF and cytochrome C into the cytosol. An apoptosome is a complex constituted by

the assemblage of cytochrome C with the caspase-9 and Apaf-1 protein, and initiates other effectors of apoptosis (Figure 10) (Kantari and Walczak, 2011).

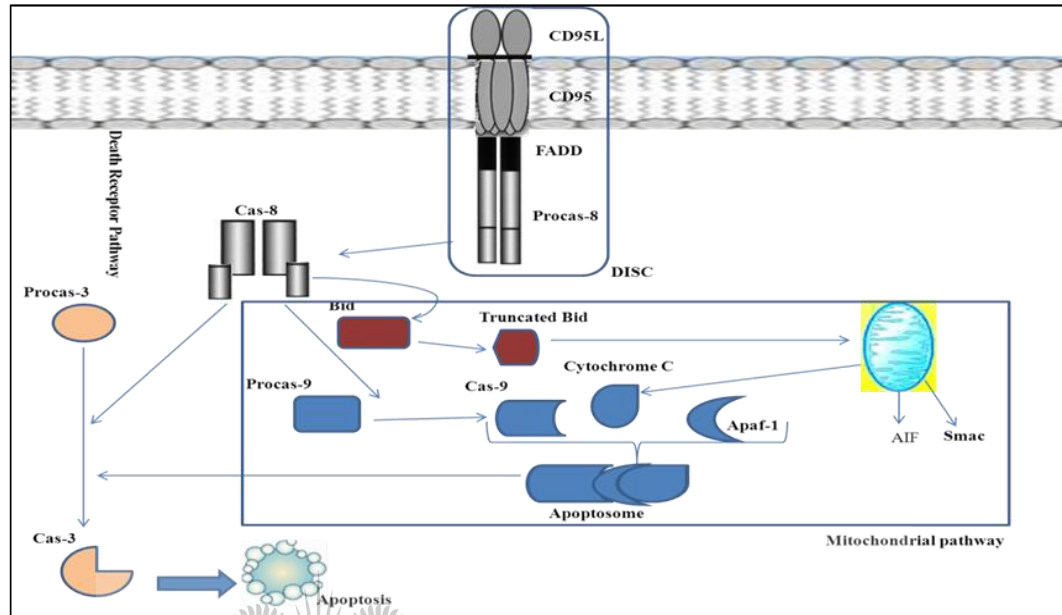


Figure 10 Apoptosis signalling pathways. The death receptor pathway is stimulated by the binding of death receptor ligand (CD95/TNFR/ TRAIL ligands) to death receptors (CD95/TNFR/ TRAILRs). The ligation triggers receptor trimerisation, recruitment of the adaptor Fas associated death domain protein (FADD) and procaspase-8 to form the death inducing signalling complex (DISC) and activation of caspase-8 through induced proximity at this complex. The cross talk between the extrinsic and intrinsic pathway is initiated by a proapoptotic truncated Bid (tBid), processed by caspase-8. tBid translocates to the mitochondria and favours Smac, AIF and cytochrome C release from the mitochondria into the cytosol. Cytochrome C together with caspase-9 and Apaf-1 forms the apoptosome, and triggers caspase-3 activation, while AIF and Smac promote apoptosis, the latter by neutralising “Inhibitor of Apoptosis Proteins” (IAPs) (Tynga and Abrahamse, 2012).

2.6.6 BCL-2 family

BCL-2 is a family of proteins that controls the discharge of toxic proteins such as cytochrome C from the mitochondrial intermembrane area (Taylor *et al.*, 2008). Every BCL-2 protein has a minimum of one preserved BH domain. This enables the protein to prompt or prevent apoptosis by attaching itself to

other proteins through intermolecular forces (Hockenbery *et al.*, 1991). The family is divided into proapoptotic and antiapoptotic subfamilies, and the ratio between these subfamilies controls the mitochondrial apoptotic pathway. The antiapoptotic subfamily contains a maximum of four BH domains (Figure 11) and encompasses BCL-XL, MCL1, BCL2A1, BCL-W, and BCL-B. The proapoptotic subfamily is further subdivided into multidomain and BH-3-only groups. The multidomain proteins comprise Bax (BCL-2-associated X protein), Bak (BCL-2-antagonist/killer-1), and Bok (BCL-2-related ovarian killer). Because of their lack of the BH-4 domain, these proteins enable the formation of pores in the external mitochondrial membrane (Kaufmann *et al.*, 2007).

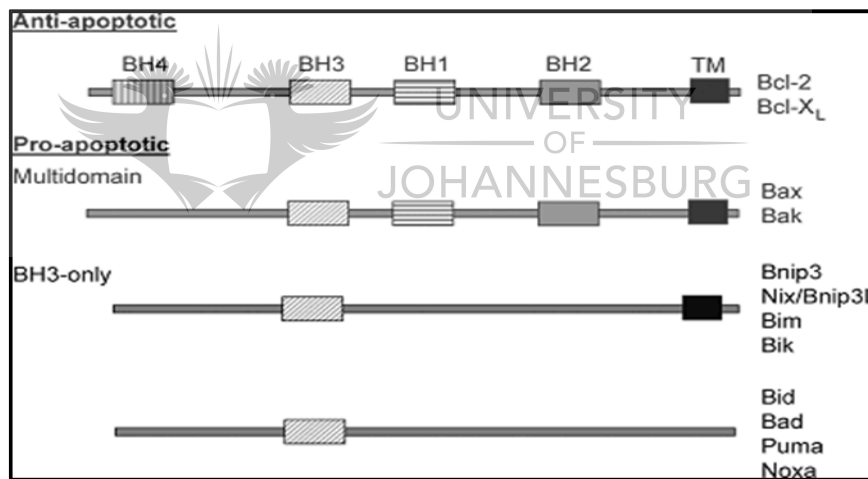


Figure 11 Domain structure of BCL-2 family proteins, depending on subfamily proteins, BCL-2 can inhibit (antiapoptotic members) or induce (proapoptotic members) apoptosis. BCL-2 subfamily (antiapoptotic): BCL-2, BCL-XL, BCL-W, MCL-1 and A1; the multidomain (proapoptotic): Bax, Bak and Bok; and BH3 only proteins (proapoptotic): Bad, Bid, Bik, Bim, Hrk, BNIP3 and BimL (Gustafsson and Gottlieb, 2007).

The gene products of Bid, Bad, Bim, Bik, Bmf, Noxa, Puma and HRK form the mammalian BH-3 only group. The BH-3 only proteins connect to and deter

antiapoptotic BCL-2 proteins. This results in the release of proapoptotic Bax and Bak proteins and engenders more mitochondrial membrane integrity loss (Taylor *et al.*, 2008). Puma stimulates apoptosis due to DNA damage, Bim does the same in a context marked by limitedness of growth factors. Conversely, other BH-3 only proteins resist the inhibitory action of antiapoptotic proteins and/or trigger the multidomain proapoptotic proteins (Taylor *et al.*, 2008). Antiapoptotic BCL-2 proteins inhibit the BH-3 only protein mediated oligomerisation of the proapoptotic multidomain proteins in the outward mitochondrial membrane. This is the source of cytochrome C and other mitochondrial proteins release. The BCL-2 protein family regulates apoptosis through the activation of Bax and Bak proteins in response to apoptotic signals. This results in the permeabilisation of the outer mitochondrial membrane. Thus, the fate of a cell is sealed by the balance between activators of Bax/Bak and antiapoptotic BCL-2 proteins (Taylor *et al.*, 2008).



2.7 Effects of PDT *in Vivo*

Some of the most documented effects of PDT, which enable the destruction of tumorous masses, include modification in the membrane permeability, fluidity reduction, and inaction of the enzymatic systems and receptors. The observation of the effects of PDT *in vivo*, reveals its ability to activate neoplastic destruction in numerous, synchronous or asynchronous manners. Clinically, vascular damage is predominantly caused by Photofrin mediated PDT and is the most dominant tumour death mechanism. Its macroscopic manifestations include acute erythema, edema, blanching and occasionally necrosis triggered by the stimulation of inflammatory mechanisms. Conversely, its microscopic manifestations include endothelial cell damage, platelet aggregation, vasoconstriction and hemorrhagic reactions in the treated tissues. At irradiation time; a high concentration of PS in tumour cells

facilitates cellular destruction by means of apoptotic or necrotic pathways. PDT is an effective means of inducing mitochondrial damages and apoptosis both in *vivo* and *in vitro* (Calin and Parasca, 2006; Moor *et al.*, 2003).

PDT trials conducted in cats revealed a good degree of tolerance and presented promising pharmacokinetic prospects. In contrast, the PDT treatment of rats with ALA exhibited extreme antitumour effects; an 85% viability reduction and a direct cytotoxicity, in addition to vascular damage (Buchholz *et al.*, 2005). However, the use of PDT in mice revealed significant tumour necrosis, the prolonging of mice's survival and substantial effects in experimental melanoma (Keller *et al.*, 2003). Subsequent studies indicated the stimulating effect of PDT on the immune system through the mediation of natural killer (NK) cells and macrophages. Although various cell types had been used in the stimulation of antitumour responses, the effect of NK cells following PDT was significant and encouraging for the treatment. This is due to the ability of NK cells to diminish the metastatic potential of surviving tumour cells. Indeed, an increase in tumour immunity was observed in PDT treated mice. This highlights the foremost role of neutrophils in initial tumour responses (Korbelik and Cecic, 1998), although macrophages have now been identified as one of the most effective initiators of the antitumour immunity. This is because the associated macrophages accumulate up to 9-fold in tumour cells. In other words, macrophages contribute to PDT induced cytotoxicity. Notwithstanding the current limitation in the understanding of the complexity of the *in situ* effects of PDT, this treatment has proven to be an advanced method of fighting cancer; hence its clinical use as a cancer therapy in a few countries (Moor *et al.*, 2003).

CHAPTER THREE

MATERIALS AND METHODS

3.1 Experimental Design

A flow diagram showing an overview of this project is presented in Figure 12.

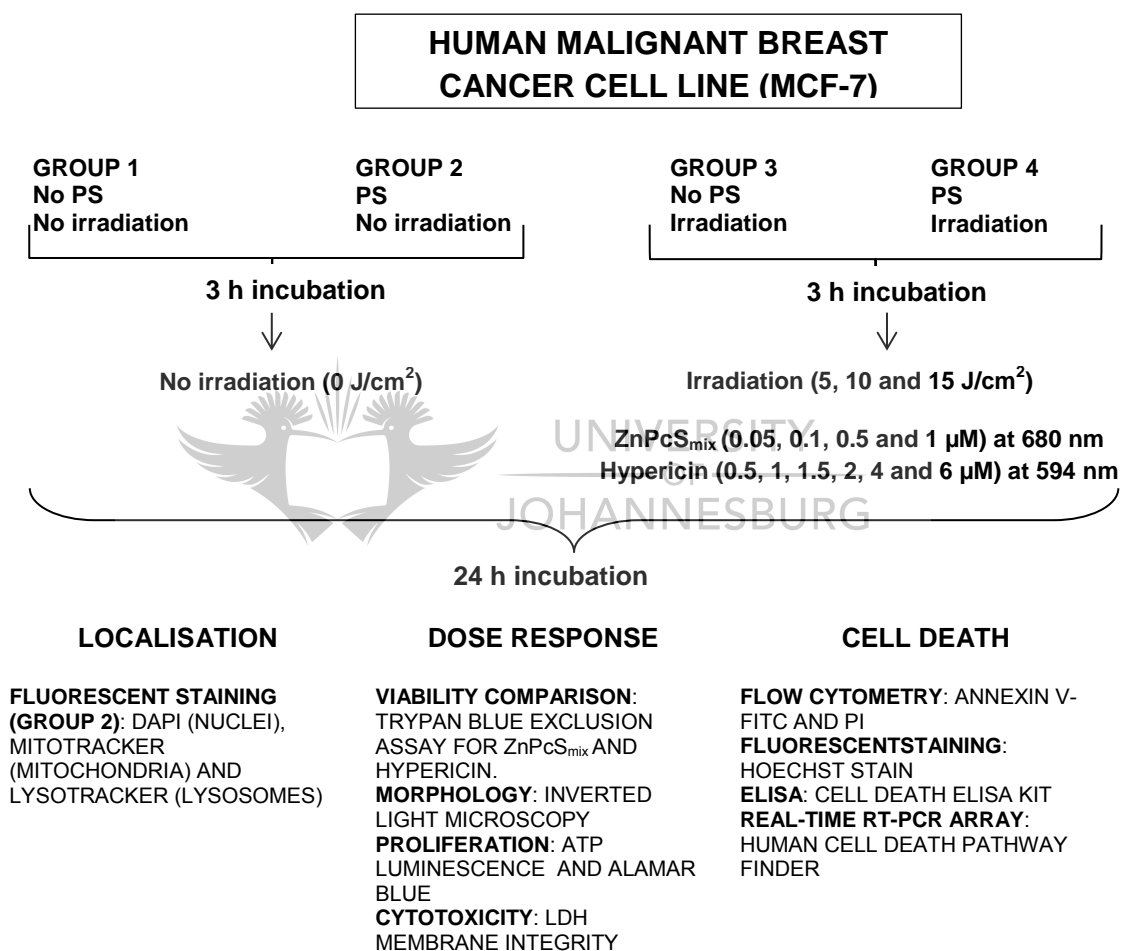


Figure 12

Flow diagram of ZnPcS_{mix} and Hypericin mediated PDT. The project comprised of localisation, dose response and cell death studies. MCF-7 cell cultures were divided into 4 study groups. Group 1 was an untreated control, group 2 received PS but was not irradiated and group 3 was irradiated with a 594 or 680 nm diode laser for Hypericin and ZnPcS_{mix} respectively but received no PS. Group 4 was irradiated and received PS. All samples were incubated for 24 h (except for PCR array, 3 h) and thereafter localisation, dose response and cell death studies were performed.

A list of consumables (Appendix A), chemical solutions and medium constituents (Appendix B) and calculations (Appendix C) performed within this methodology are provided. Ethics approval was obtained from the Faculty of Health Sciences Academic Ethics committee of the University of Johannesburg to perform this research project (AEC58/01-2010) (Appendix D).

3.2 Human Breast Cancer Cells (MCF-7)

Cell lines are isolated cells that are grown outside their natural environments and under precise conditions (pH, temperature, nutrients, and growth factors) in culture flasks, which are appropriate for cell attachment and growth. The cell growth can be monitored on a regular basis. While some cells have a limited passage capability before becoming senescent and dying, cancer cell lines can grow and proliferate indefinitely. Thus, cell culture refers to the controlled multiplication of primary cells, isolated from tissues of multicellular organisms. Cell lines are identified according to properties including cell strain, chromosome number, membrane receptors and growth factors. Culture conditions are cell line dependent and can result in different phenotypes. Many cells are cultured as a monolayer on flat plastic dishes (flasks) and are also known as a two dimensional (2 D) cell line (Freshney, 2005).

MCF-7 cells are a human breast cancer cell line and were first isolated from a Sexagenarian lady at the Barbara Ann Karmanos Cancer Institute in Detroit. The cancer institute was formerly known as the **Michigan Cancer Foundation-7**, from which the acronym MCF-7 was derived (Soule *et al.*, 1973). MCF-7 cells have ER and the ability to process estrogen in the form of estradiol. The cell line is therefore an ER positive control cell line (Pratt and Pollack, 1993).

Cells form clumps and grow as monolayers and this growth can be inhibited by both alpha tumour necrosis factor (α -TNF) and anti estrogen actions. Genetic studies have revealed that the karyotype of this cell line is 69 chromosomes. A MCF-7 cell line from the American Type Culture Collection (ATCC) was used for this research project.

3.2.1 Cell culture

The MCF-7 breast cancer cell line (ATCC: HTB 22) is an adherent cell line and was used throughout this project. MCF-7 cells were grown as a monolayer and attached to the bottom of cell culture flasks. Cells were grown to 85% confluence in 25 ml complete DMEM (Gibco Invitrogen Corporation, 41966). DMEM was supplemented with 10% (v/v) FBS (Gibco Invitrogen Corporation, 10106), 1% (v/v) penicillin-streptomycin (PAA Laboratories GmbH, P11-010) and 1 μ g/ml Amphotericin B (PAA Laboratories GmbH, P11-001) in an 85% humidified atmosphere at 37°C and 5% CO₂. The cells were incubated at 37°C, in 5% CO₂ and 85% humidity throughout the project and observed on a daily basis to monitor cell growth.

Tissue culture media has a pH indicator (phenol red) added to monitor cell growth. When cells have used up nutrients in the media and produced by products/waste, the pH changes and induces a subsequent change in the colour of the media. The colour of the media changed from red to yellow as an indication of the decrease in pH value when this occurred the media was discarded and replaced with fresh complete DMEM after cells were washed twice with 4 ml Hanks balanced salt solution (HBSS, Gibco Invitrogen Corporation, 14170088). Upon reaching confluence, the media was discarded and cells were washed twice with HBSS, trypsinised with 1 ml/25 cm² TrypLEExpress (Gibco Invitrogen Corporation, 12604) and incubated at 37°C,

5% CO₂ and 85% humidity for 5 min, to allow the cells to detach from the culturing surface of the flasks. Four millilitres of HBSS was added, the cell suspension was transferred into a 50 ml tube and centrifuged at 2,200 rpm (Laboratory Scientific Equipment, Hermle Labortechnik Centrifuge, 60090391) for 4 min. The supernatant was discarded and the cells were resuspended in 1 ml HBSS for cell counting (Trypan blue exclusion assay). After performing a cell count and spinning down, cells were resuspended in complete DMEM and used for cell stocks, experimentation or further culturing.

3.2.2 Cell stock preparation

After performing a cell count and centrifugation, cells were resuspended either with complete DMEM for cell culture or in freezing media for storage at low temperatures. Cells were cultured from passage 8 to 15 and were frozen to ensure continuous availability at every passage of the cell line. Cells were resuspended at a concentration of 4×10^6 cells/ml in freezing media (Biochrom AG, F2270). One millilitre of the cell freezing media was transferred to 2 ml cryovial tubes and placed in a polystyrene box at -20°C to stabilise the temperature. Frozen cell stocks were then transferred to the -80°C freezer and at a later stage stored at the appropriate temperature (-150°C cryofreezer or in liquid nitrogen). When the 15th passage was reached a frozen stock at a low passage number was thawed in the water bath at 37°C for 2-3 min until a small amount of ice remained in the vial. The contents of the cryovial tubes was pipetted into prewarmed complete DMEM containing 20% FBS (v/v), to dilute out the freezing media, and the culture flasks were incubated at 37°C, 5% CO₂ and 85% humidity overnight before they were examined under the microscope.

3.2.3 Preparation of cells for experimentation

After cell counting and centrifugation, cells were resuspended and seeded at a concentration of 6×10^5 cells in 3 ml culture media in 3.4 cm² diameter culture dishes. Culture dishes were incubated for 4 h to allow the cells to attach. Cells were then ready for experimental applications. For better examination of cells during the subcellular localisation study and Hoechst staining, cells were seeded at a concentration of 2×10^5 cells in 3 ml.

3.3 Photosensitisers

A mixed isomer of ZnPcS_{mix} was used in this study and its effects in PDT in MCF-7 cells were investigated. It is a mixture of several sulfophthalocyanines and was synthesised by Prof Tebello Nyokong (Department of Chemistry, Rhodes University, South Africa) from (OH₂) ZnPc and fuming sulphuric acid (30% SO₃) (Seotsanyana-Makhosi *et al.*, 2006). Such compounds with central atoms have triplet state quantum yields and an extended lifespan of their excited state (Ogunsipe *et al.*, 2004; Kessel and Oleinick, 2010). The ZnPcS_{mix} has a peak absorbance at 680 nm and four concentrations of this PS was used (0.05, 0.1, 0.5 and 1 µM) to determine which would be the most suitable to monitor and induce cell toxicity and death using PDT *in vitro*.

Hypericin belongs to the 6th class of PSs (section 2.5.2.3) and is a naturally occurring photosensitising agent and is isolated from the plant *Hypericum Perforatum*. Due to its photophysical and photochemical properties, this PS generates superoxides and generates a high quantum yield of singlet oxygen. It is a potent antitumor agent with optimal tumoricidal responses around 593 nm and induces apoptosis and /or necrosis of cancer cells following PDT. A commercially available Hypericin (Sigma Aldrich, 56690) was used to determine the concentration of Hypericin coupled with laser irradiation that

led to a 50% decrease in viability. This second PS was activated using a 594 nm diode laser.

3.4 Laser Irradiation

All laser irradiations were conducted in a dark room using 594 or 680 nm diode lasers (Figure 13), which were provided by the National Laser Centre (South Africa). Cells in the culture dishes, without lids on, were continuously irradiated from above at different fluences (irradiation times). A FieldMate laser power meter was used to measure the output power of lasers and laser parameters used in this study are presented in Table 1.

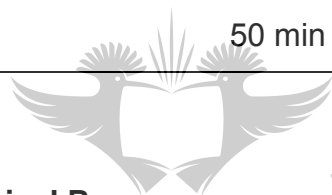
Unirradiated cells (group 1 and 2) were kept in the dark at room temperature during irradiations. Dosage was calculated as follows: Irradiance (J/cm^2) = time (sec) x [power (W)/surface (cm^2)] (Chen *et al.*, 2008).



Figure 13 The 680 nm diode laser used to irradiate the human breast cancer cells.

Table 1 Parameters of the lasers used in this study.

Parameters	Diode laser	Diode laser
Manufacturer	Oriel Corporation	Optoelectronics Technology
Wavelength	680 nm	594 nm
Wave emission	continuous	continuous
Spot size	9.1 cm ²	9.1 cm ²
Output power	52 mW	99 mW
Power density	5.73 mW/cm ²	11.58 mW/cm ²
Fluences	5 J/cm ²	5 J/cm ²
	10 J/cm ²	10 J/cm ²
	15 J/cm ²	15 J/cm ²
Irradiation times	16 min 50 s	7 min 11 s
	33 min 40 s	14 min 23 s
	50 min 30 s	21 min 35 s



UNIVERSITY
OF
JOHANNESBURG

3.5. Biological Responses

3.5.1 ZnPcS_{mix} localisation

Staining is the application of stains/dyes to samples to colour either the cells or cellular organelles. Fluorescent dyes absorb photons at a specific wavelength and emit back energy at a longer wavelength. They are covalently bound to macromolecules and are used for fluorescent imaging or spectroscopy (Tsien and Waggoner, 1995). Most stains can be used on either live or dead cells. Prior to staining, cells were fixed and permeabilised to allow the stain access to the cellular organelles. A mounting step followed to attach the coverslip cell preparations to glass microscope slides. For the localisation study (organelle staining), cells from group 2 (ZnPcS_{mix} and no irradiation) were used.

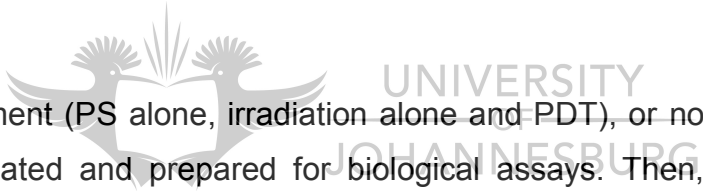
The subcellular localisation of ZnPcS_{mix} in MCF-7 cells was investigated due to the autofluorescence ability of the PS. Cells were grown at a concentration of 2×10^5 cells in 3 ml on sterile coverslips in 3.4 cm² diameter culture dishes and treated with 1 μ M of ZnPcS_{mix}. After 24 h incubation, the media was discarded and culture dishes were washed twice with Phosphate buffered saline (PBS, Sigma Aldrich, P3744). Cells were fixed with 200 μ l of 3.5% (v/v) formaldehyde (Sigma Aldrich, F8775) in DMEM and incubated at 37°C for 15 min. Cells were washed twice with PBS and then treated with 200 μ l of 0.5% (v/v) TritonX-100 (Sigma Aldrich, T9284) in PBS and incubated at 37°C for 10 min for cell permeabilisation. Cells from group 2 were washed with PBS and treated with 50 μ l of 35 nM of either Mitotracker (Invitrogen, M7514) for mitochondrial staining or LysoTracker (Invitrogen, L7526) for lysosomal staining. Following incubation at 37°C for 20 min, cells were then washed with PBS and 50 μ l of 0.1 mg/ml 4', 6-diamidino-2-phenylindole (DAPI, Invitrogen, D1306) was used to stain the nuclei. After 5 min of incubation, the preparations were rinsed with PBS and transferred to glass microscope slides which were previously treated with 30 μ l of 20% (v/v) mounting media (Propyl gallate, Sigma Aldrich, 02370) in distilled water for attachment. The coverslip borders were sealed with nail polish. Slides were examined and micrographs taken using the Carl Zeiss microscope (Axio Z1 Observer).

3.5.2 Dose response study

MCF-7 cells were treated with 0.5, 1, 1.5, 2, 4 or 6 μ M Hypericin and irradiated to deliver 3 energy densities (5, 10 and 15 J/cm²) using a 594 nm diode laser. Cells were divided into 4 groups; untreated control cells (group 1: no Hypericin and no irradiation), Hypericin treated cells (group 2: no irradiation), irradiated cells (group 3: no Hypericin) and PDT treated cells with Hypericin (group 4). After treatment and 24 h incubation, cells were washed, trypsinised, incubated and transferred to eppendorf tubes for centrifugation.

The Trypan blue exclusion assay was then performed to determine the effects of Hypericin mediated PDT on cell viability. After PDT, the effect of Hypericin, a naturally occurring phototherapeutic agent, was compared to the laboratory synthetic agent (ZnPcS_{mix}) for cancer photodynamic applications after the Trypan blue exclusion assay.

Another dose response study was performed on MCF-7 cells using concentrations of 0.05, 0.1, 0.5 and 1 μM of ZnPcS_{mix} and laser fluences of 5, 10 and 15 J/cm^2 . Cells were divided into 4 groups: untreated cells (group 1: no ZnPcS_{mix} and no irradiation), ZnPcS_{mix} treated cells (group 2: no irradiation), irradiated cells (group 3: no ZnPcS_{mix}) and PDT treated cells with ZnPcS_{mix} (group 4). Here the dual effect of ZnPcS_{mix} and laser irradiation was tested.



After treatment (PS alone, irradiation alone and PDT), or not (group 1), cells were incubated and prepared for biological assays. Then, the media was removed, cells were rinsed with prewarmed HBSS and replaced with 1 ml of prewarmed fresh complete media. The appropriate amount of PS was added to the relevant culture plates (group 2 and 4) and incubated at 37°C, 5% CO₂ and 85% humidity for 24 h. The media was then removed; cells were rinsed with prewarmed HBSS and replaced with 1 ml of prewarmed fresh complete media before the relevant culture plates (group 3 and 4) were irradiated at 5, 10 or 15 J/cm^2 . The unirradiated culture plates were placed in a dark container on the bench during irradiation. It is critical to rinse the culture plates before irradiation to remove all traces of PS that does not enter the cells. The excess PS will be activated during irradiation and result in false results as a consequence of excess ROS production. After 24 h incubation at 37°C, 5% CO₂ and 85% humidity, media was collected and stored at room temperature for cytotoxicity analysis (ZnPcS_{mix} treated cells). Cells were

washed twice with 1 ml HBSS, trypsinised with 0.5 ml TrypLEExpress for 5 min at 37°C, 5% CO₂ and 85% humidity. One millilitre of HBSS was added to remove all traces of the trypsinised cells and the cell suspensions were transferred into eppendorf tubes for centrifugation at 22,000 rpm (Laboratory Scientific Equipment, Hermle Labortechnik Centrifuge, 60090391) for 5 min. The supernatants were discarded and the cell pellets were resuspended in 600 µl HBSS. The newly obtained cell suspensions were used to conduct the viability (Hypericin and ZnPcS_{mix} treated cells) and proliferation assays (ZnPcS_{mix} treated cells).

3.5.2.1 Cellular morphology

After 24 h incubation and before media was collected for cytotoxicity analysis, morphology pictures of ZnPcS_{mix} treated cells were taken. Changes in cell structure were examined using an inverted microscope (Olympus, CKX41) and morphological pictures were taken using the SC30 Olympus camera. Each image was compared to that of the untreated control (group 1). Indicators such as debris, cellular fragments and the number of free floating cells were taken into consideration to determine the degree of change in cell viability and increased mortality.

3.5.2.2 Cellular viability: Trypan blue exclusion assay

The Trypan blue exclusion assay was used to determine the percentage viability of each cell suspension. Cells with an intact cellular membrane did not take up the dye and maintained a clear appearance under a microscope while damaged cells were stained blue as they took up the dye. A Trypan blue exclusion assay was performed to determine the cell count and percentage viability after PDT and the concentration of PS coupled with laser irradiation that induced a 50% decrease in viability.

Ten microliters of cell suspension was added to 90 μ l of 0.4% Trypan blue (Sigma Aldrich, T8154) in HBSS (1:10 dilution) and carefully mixed. The Trypan blue cell suspension mixtures were allowed to stand for 3 min before a small volume (10 μ l) was transferred to both counting chambers on either side of a Bright-Line™ hemocytometer by placing a pipette tip at the edge of the coverslip and allowing each chamber to fill by capillary action. The hemocytometer was viewed under a microscope (Olympus, CKX41) and the total number of cells (intact and damaged) in both chambers was counted. Total number of cells was determined by multiplying the average number of cells per square by 10^5 (dilution factor $\times 10^4$). Percentage viability was obtained by multiplying the fraction of the number of viable cells over the total number of cells by 100.

3.5.2.3 Cellular proliferation ATP luminescence

ATP is the specialised carrier of energy within a cell. The quantification of ATP indicates the presence of metabolically active cells. The ATP luminescence assay was performed to assess cell proliferation using the CellTiter-Glo® luminescent cell proliferation assay (Promega, G7570). The ATP assay exploits the properties of luciferase to generate a sensitive stable luminescent signal and prevents endogenous ATP release during cell lysis.

Fifty microliters of ATP CellTiter-Glo® reagent was added to an equivalent volume of cell suspension (from the 600 μ l, section 3.5.2) for each different treatment in an opaque-walled 96 well plate (BD Biosciences, 353296). The plate was mixed on an orbital shaker at 250 rpm (Heidolph Polymax Orbital, Labotec, 1040) for 2 min to induce lysis and incubated for 10 min at room temperature in the dark. The application led to the production of a

luminescent signal that was measured using a Multilabel Counter (Perkin Elmer, VICTOR3™, 1420) in relative light units (RLU). A background control well containing 50 µl of media was included and the RLU value obtained from the background control well was deducted from all the RLU values of the other wells.

alamarBlue®

Intact cells maintain a reducing state within their cytosolic environment. This reducing cellular potential converts redox indicators (alamarBlue®, Invitrogen, DAL 1025) into a detectable fluorescent product. A mitochondrial flavoprotein, also known as diaphorase, catalyzes the oxidation of alamarblue® reagent into its reduced red form. The amount of fluorescence or absorbance is proportional to the number of living cells and corresponds to cellular metabolic activity. Damaged cells have a lower metabolic activity and thus generate a lower signal than intact cells. This assay incorporates an oxidation-reduction indicator that can both fluoresce and undergo colorimetric changes. Cellular metabolic activities induce a shift from the oxidised and non fluorescent blue indicator form to the reduced fluorescent red form.

In the assay 10 µl alamarBlue® was added to 90 µl of cell suspension (section 3.5.2) to a final concentration of 10% (v/v) in a 96 well plate. The plate was thoroughly shaken on an orbital shaker at 250 rpm (Heidolph Polymax Orbital, Labotec, 1040) for 2 min and incubated for 2 h at 37°C, 5% CO₂ and 85% humidity in the dark. Following incubation, the generated signal was first referenced at 620 nm and then the absorbance value was measured at 550 nm, using a Multilabel Counter (Perkin Elmer, VICTOR3™, 1420). A background well containing 90 µl of media was included and the absorbance

value obtained with the background control was deducted from the absorbance value of the other wells.

3.5.2.4 Cytotoxicity

Cytotoxicity was assessed by measuring the amount of LDH released from the cytosol due to membrane damage. This oxidoreductase interconverts lactate into pyruvate. Its discharge from the cytosol leads to an unusual increase of the enzyme in the bloodstream *in vivo* or culture media *in vitro*. In the nonradioactive colometric assay, LDH reacted to convert a tetrazolium salt (in the reconstituted reagent, oxidised form) into a quantifiable red-formazan product (reduced form) in a NADH dependent reaction. The product of this enzymatic reaction is proportional to the number of cells that have been lysed or damaged.



Cytotoxicity was evaluated using the CytoTox96® nonradioactive cytotoxicity assay (Promega, G400). Fifty microliters of reconstituted reagent was added to an equal volume of culture media (section 3.5.2) in a 96 well plate and incubated in the dark at room temperature for 30 min. The colorimetric compound was measured spectrophotometrically at 490 nm using a Multilabel Counter (Perkin Elmer, VICTOR3™, 1420).

3.5.3 Cell death study

Subsequent to cell dose response studies, 0.5 μM ZnPcS_{mix} and 10 J/cm² was identified as the PDT combination that caused a 50% decrease in cell viability. Using these parameters, enough cells were available to carry on with the cell death study. In this study, two groups were considered; the untreated control cells, which received no ZnPcS_{mix} or laser irradiation, and the

experimental group, which received 0.5 μM ZnPcS_{mix} and irradiation at 680 nm with 10 J/cm² 4 h post incubation. Twenty four hours post irradiation, cell suspensions were obtained in the same way as stated in section 3.5.2.

3.5.3.1 Flow cytometry

Flow cytometry is a technique used for the classification of particles/cells in a flow system to deliver them individually past a point of measurement. Light is scattered at 2 directions and large number of cells are examined in a short time period (Davey and Kell, 1996).

Annexin V- fluorescein isothiocyanate (FITC) apoptosis detection (Sigma Aldrich, APO-AF) was used to determine the cell death events after PDT. The kit uses a combined Annexin V-FITC to detect phosphatidyl serine sites on the membrane of apoptotic cells and has PI to label necrotic cells at sites of membrane damage. Therefore this assay measured two parameters and gave an overview of the cell population; apoptotic cells (Annexin V-FITC positive, PI negative; or positive for both), necrotic cells (Annexin V-FITC negative, PI positive) and viable cells (Annexin V-FITC negative, PI negative).

Actinomycin D is a chemotherapy drug used for neoplastic conditions and a cytotoxic inducer of apoptosis. An apoptotic control sample, which was treated with Actinomycin D, was included for the Annexin V-FITC and PI staining. MCF-7 cells were grown according to the standard protocol and the sample was treated with 1 $\mu\text{g/ml}$ Actinomycin D (Sigma Aldrich, A9415) 24 h prior to Annexin V-FITC and PI staining.

Cells were treated with 0.5 μM ZnPcS_{mix} and irradiated at 10 J/cm². After incubation, cells were trypsinised and washed with HBSS. Cells were resuspended in 1X binding buffer at a concentration of 1 x 10⁶ cells/ml and 100 μl of the cell suspension was transferred into flow cytometry tubes. Five microliters of each Annexin V-FITC and PI reagents were added and the tubes were thoroughly mixed and incubated for 10 min at room temperature in the dark. Within 1 h, flow cytometric analysis was performed on the BD FACSAria (BD Biosciences, 642226) and Annexin V-FITC and PI were detected as a green and red fluorescence, respectively.

3.5.3.2 Hoechst staining

Hoechst is a blue fluorescent dye used to stain nucleic acids and has a high affinity for AT rich regions. It is excited at 343 nm and emits light at 483 nm. This staining was performed to determine nuclear changes after PDT. Hoechst 3328 (Sigma Aldrich, H6024) is a sensitive bis benzimide derivative compound that binds to double stranded DNA in the minor groove forming a new fluorescent complex. Thus cells with intact double stranded DNA and nuclei show high nuclear fluorescence, while damaged cells show a low dense cytoplasmic fluorescent signal (Allen *et al.*, 2001).

After cell permeabilisation and fixation as previously described (section 3.5.1), cells from the untreated control (group 1) and PDT treated cells (group 4) were washed with PBS and stained with 50 μl of 0.5% (v/v) Hoechst stain in HBSS. Cells were incubated for 5 min before coverslips were inverted onto glass microscope slides, which had 30 μl of 20% (v/v) mounting media on and the coverslip borders were sealed with nail polish. Slides were examined using the Carl Zeiss microscope (Axio Z1 Observer).

3.5.3.3 Cell death Enzyme Linked Immunosorbent Assay (ELISA)

ELISA is a biochemical assay used to detect and measure the presence of a substance in a sample. During ELISA, target analytes/substances have a high affinity for a specialised type of protein, which is produced by the immune system and known as antibodies. The assay is based on the principle of sandwich enzyme immunoassay; monoclonal antibodies are directed against DNA and histone associated DNA fragments, allowing the determination of mono- and oligonucleosomes following cell damage (Ning *et al.*, 2000). A cell death ELISA kit (Roche, 11 774 425 001) was used to detect and quantify the DNA histone complexes formed during nuclear fragmentation.

Twenty microliters from each sample; untreated control, ZnPcS_{mix} control, irradiated control, positive control (DNA-histones complex), negative control (lysis buffer), background control (ABTS substrate buffer) and PDT treated cells was transferred into a microplate well. The positive, negative and background control samples were all supplied with the kit. After adding 80 µl of immune reagent to each well, the microplate was covered with foil and incubated for 2 h at room temperature in a Labcon shaking incubator (Amersham) set at 300 rpm. The solution was discarded and the wells rinsed 3 times with 150 µl of incubation buffer and then 100 µl of ABTS solution was added to the wells. The microplate was incubated for 20 min at room temperature on a plate shaker (Heidolph Polymax Orbital, Labotec, 1040), set at 250 rpm. In the final step, 100 µl of ABTS stop solution was added to the wells and the microplate was read at 405 nm and referenced at 490 nm using a Multilabel Counter (Perkin Elmer, VICTOR3™, 1420).

3.5.3.4 Real-time Reverse Transcriptase Polymerase Chain Reaction

Gene expression analysis was performed using real-time Reverse Transcriptase Polymerase Chain Reaction (RT-PCR). The technology monitors the amplification of gene products during cycles in real-time. Gene expression analysis is performed due to the real-time RT-PCR selectivity and the multigene profiling capacity of microarray. SYBR Green is a dye used to detect any double stranded DNA molecule and binds to their nitrogenous bases leading to a high fluorescent signal in the presence of double stranded DNA (Bustin *et al.*, 2005; Wang *et al.*, 2006).

Complementary DNA (cDNA) is the template used for RT-PCR and is synthesised from RNA. The RNeasy kit (Qiagen, 74104) with QIAshredder homogenisers (Qiagen, 79654) was utilised to extract RNA from the MCF-7 cells due to the specific binding properties of a silica-membrane and the speed of microspin technology. The use of a high salt buffer allows the extraction of up to 100 µg of RNA longer than 200 bases bound to the RNeasy Silica-membrane.

Such extraction of nucleic acid depends on the properties of the Silica-materials. Silica-membranes are cation rich components and these ions, such as sodium ions, form cation bridges. In solution, and under high salt concentration (pH<7), these ions disrupt hydrogen bonds between water molecules ($\text{O} \cdots \text{H}^+$). The cation bridges in the Silica-membranes attract negatively charged oxygen in the backbone phosphate groups of nucleic acids. Nucleic acids thus become tightly bound to the Silica-membranes and during extraction washing processes remove all unbound substances and contaminants. Under low ionic strength (pH>7), during the elution phase, purified nucleic acids are eluted (Lai *et al.*, 2007).

Extraction of ribonucleic acid (RNA)

RNA extraction was performed using the RNeasy kit (Qiagen, 74104) with QIAshredder homogenisers (Qiagen, 79654) on treated MCF-7 cells, which were incubated for 30 min prior to RNA extraction. Cells were trypsinised, the supernatants discarded, and cells washed with PBS to remove all traces of culture medium. A volume of 600 μ l of RLT buffer was added to the cells, which were mixed by vortexing. RLT buffer inactivates RNase to guarantee purification of intact RNA. Reagents and cell suspensions were loaded on the QIAcube (Qiagen) and RNA isolation was performed. Thirty microliters of eluted RNA was collected and kept on ice.

RNA quantification

The eluted RNA was quantified using the Quant-iT™ RNA Assay kit (Invitrogen, Q32852) on the Qubit™ fluorometer. Thin-walled, clear 0.5 ml optical-grade PCR tubes were used to quantify the RNA. The working solution of the assay was prepared by diluting Quant-iT™ RNA reagent in Quant-iT™ RNA buffer in a 1:200 ratio and stored at room temperature. A volume of 190 μ l working solution was loaded into two tubes for standards (1 and 2) and 10 μ l of each Quant-iT™ standard was added to the appropriate tube and mixed. For isolated RNA, 199 μ l working solution and 1 μ l of the eluted RNA sample was mixed. Both standard and sample tubes had a final volume of 200 μ l. The mixtures were incubated at room temperature for 2 min and then measured in the Qubit™ fluorometer. The Qubit™ fluorometer was calibrated using the two standard tubes and then RNA sample concentration (μ g/ml) was calculated by the instrument once the volume of sample (1 μ l) was selected. The total concentration of RNA isolated was calculated by multiplying the concentration of the RNA (μ g/ml) by the total eluted volume (30 μ l).

RNA purity

RNA purity was evaluated by obtaining the ratio of the absorbance value at 260 nm over the value at 280 nm using the Biomate 3 spectrophotometer (Thermospectronic, 335904P). One microliter RNA was added to 99 μ l buffer AE (Qiagen, 19077) in a quartz cuvette to quantify nucleic acids. The buffer consists of 10 mM Tris-Cl and 0.5 mM EDTA; pH 9.0.

The ratio $A_{260/280}$ nm is an important indicator of the quality of the RNA and it is used to evaluate the degree of purity. Due to the aromatic rings, proteins absorb light at 280 nm. An ideal RNA sample should have a ratio between 1.8 to 2 and a ratio less than 1.8 indicates protein contamination.

Complementary DNA (cDNA) synthesis

In molecular biology, the central dogma states that the flow of genetic information is from DNA to RNA through transcription and then RNA to protein through translation of the transcript. In some cases (RNA virus), the flow is from the transcript to DNA through reverse transcription, a reaction catalysed by a RNA dependent DNA polymerase, known as reverse transcriptase. Since then, reverse transcriptases have been utilised to convert RNA into its cDNA counterpart.

In this study, QuantiTect Reverse Transcriptase has a high affinity for RNA and the ability to synthesise cDNA from as little as 10 pg RNA. After RNA quantification and purity were performed, a volume containing 30 ng of RNA was used for RNA reverse transcription into cDNA using the QuantiTect Reverse Transcription kit (Qiagen, 205311). The PCR Array system used yields results with as little as 25 ng or as much as 5 μ g total RNA per array. A

genomic DNA (gDNA) elimination reaction mixture (final volume of 14 μ l) was prepared on ice and consisted of gDNA wipeout buffer, template RNA and RNase free water (Table 2).

Table 2 Genomic DNA elimination reaction and various components.

Component	Volume/reaction	Final concentration
gDNA wipeout buffer	2 μ l	1X
Template RNA	Variable (30 ng)	
RNase free water	Variable	
Final volume	14μl	-

gDNA elimination tubes were incubated for 8 min at 42°C and placed on ice. A final volume of 20 μ l of reverse transcription reaction was prepared on ice by adding Quantiscript Reverse Transcriptase, QuantiscriptRT Buffer, RT Primer Mix and 14 μ l of the gDNA elimination reaction according to Table 3. The reverse transcription reaction tubes were kept on ice, mixed and incubated for 15 min at 42°C. Then the reverse transcription reaction tubes were incubated for 3 min at 95°C to inactivate Quantiscript Reverse Transcriptase. The cDNA was stored at -20°C and/or used as a template in the real-time PCR array.

cDNA purity

Purity of the cDNA was determined before being used for real-time PCR. The purity was determined by the ratio between the absorbance values at 260 and 280 nm ($A_{260/280}$ nm). One microliter cDNA was added to 99 μ l buffer AE (Qiagen, 19077) in a quartz cuvette and read using the Biomate 3 spectrophotometer. Ratios between 1.82 and 1.94 were obtained and used for gene expression analysis (Appendix C).

Table 3 Reverse transcription reaction and various components.

Component	Volume/reaction
Reverse-Transcription master mix	
Quantiscript Reverse Transcriptase	1µl
Quantiscript RT Buffer	4µl
RT Primer Mix	1µl
Template RNA	
gDNA elimination reaction	14µl
Final volume	20 µl

Gene expression

The synthesised cDNA was used for real-time PCR to study the expression of a panel of genes involved in death and senescence using the Human Cell Death PathwayFinder™ PCR Array (SABiosciences, PAHS-212A) and Stratagene Mx3000p®. The RT² Profiler PCR Array profiles the expression of 84 genes; all involved in the mechanisms of cellular death (Table 4). The RT² Profiler PCR Array System takes advantage of real-time PCR performance and combines it with the ability of microarrays to detect the expression of many genes simultaneously.

The PCR plate contains 96 wells arranged in 12 columns (1 to 12) and 8 rows (A to H). The first 84 genes (wells A1 to G12) are important for the different cell death pathways and the remaining 12 consist of 5 housekeeping genes (wells H1 to H5) inserted for normalisation of the PCR Array data, 1 gDNA control gene (well H6) for gDNA contamination, 3 Reverse Transcription Controls (RTC, wells H7 to H9) and 3 Positive PCR Control genes (PPC, wells H10 to H12) for assessment of the efficiency of the primer set provided

in the kit and of a predisposed artificial DNA sequence, respectively (Figure 14).

Table 4 Functional gene grouping of the human cell death pathway finder profiler (updated from SABiosciences, PHAS-212A).

Cell death	Gene subunits
Pro-Apoptotic	ABL1, APAF1, BCL2L11, BIRC2 (c-IAP2), CASP1 (ICE), CASP2, CASP6, CASP7, CASP9, CD40 (TNFRSF5), CD40LG (TNFSF5), CFLAR (CASPER), DFFA, FASLG (TNFSF6), GADD45A, NOL3, TNFRSF10A (TRAIL-R).
Anti-Apoptotic	BCL2A1 (Bfl-1/A1), BIRC3 (c-IAP1), IGF1R, MCL1, TNFRSF11B, TRAF2, XIAP.
Apoptosis and Autophagy	AKT1, BAX, BCL2, BCL2L1 (BCL-X), CASP3, FAS (TNFRSF6), TNF, TP53.
Apoptosis and Necrosis	ATP6V1G2, CYLD, SPATA2, SYCP2, TNFRSF1A
Autophagy	APP, ATG12, ATG16L1, ATG3, ATG5, ATG7, BECN1, CTSB, CTSS, ESR1 (ERa), GAA, HTT, IFNG, IGF1, INS, IRGM, MAP1LC3A, MAPK8 (JNK1), NFKB1, PIK3C3 (VPS34), RPS6KB1, SNCA, SQSTM1, ULK1.
Necrosis	BMF, C1orf159, CCDC103, COMMD4, DEFB1, DENND4A, DPYSL4, EIF5B, FOXI1, GALNT5, GRB2, HSPBAP1, JPH3, KCNIP1, MAG, OR10J3, PARP1 (ADPRT1), PARP2, PVR, RAB25, S100A7A, TMEM57, TXNL4B.

The cDNA was thawed on ice and 92 µl of RNase-DNase free water was added to make a final volume of 111 µl. An experimental cocktail was

prepared and the SABiosciences RT² qPCR master mix, the diluted cDNA mixture and RNase-DNase free water were mixed in a 50 ml RNase-DNase free tube according to the manufacturer protocol (Table 5). The SABiosciences RT² qPCR Master mix is specifically designed for the Stratagene Mx3000p® and consists of a RT² SYBR Green (detected dye) and ROX (reference dye) qPCR components.

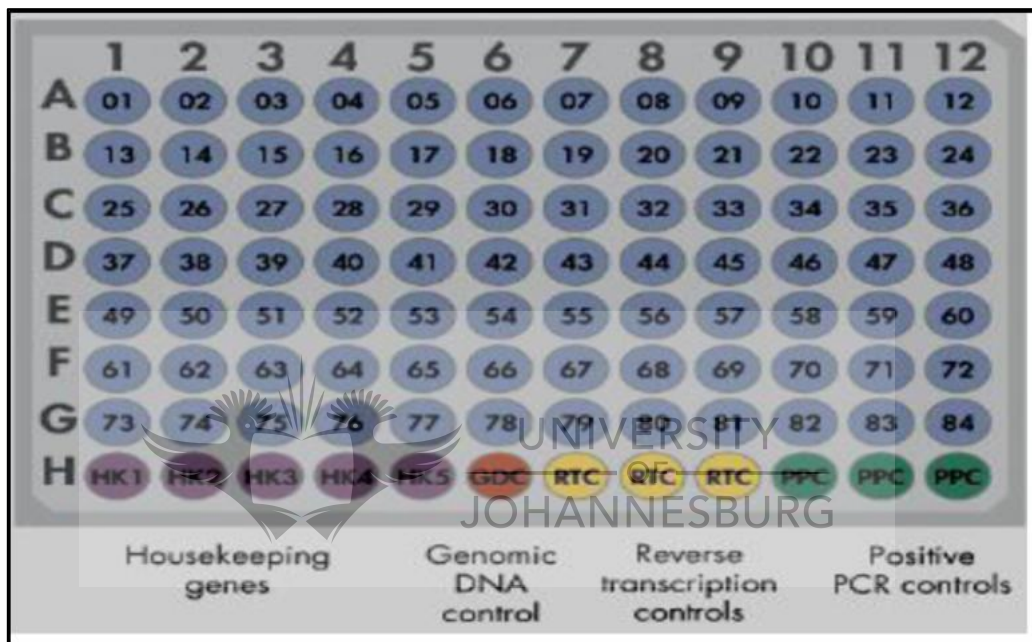


Figure 14 Layout of the catalogued 96 well PCR Array. Wells A1 through G12 contain individual qPCR assays for the 84 genes relevant to the human cell death pathway. Wells H1 through H5 contain a panel of housekeeping genes (HK1-HK5) used for normalising the PCR array data. Well H6 to H12 contain controls namely genomic DNA contamination (GDC), Reverse Transcription Controls (RTC), and Positive PCR Control (PPC).

The 96 well PCR array plate was loaded by adding 25 µl of the experimental cocktail to each well. The PCR array plate was sealed with the optical thin walled 8-cap strips and kept on ice. The plate was centrifuged for 1 min at room temperature at 1,000 xg using a Heraeus Labofuge 400 centrifuge (Thermo Scientific) to remove all air bubbles. The Stratagene Mx3000p® was

programmed as follows: 1 cycle, 10 min at 95°C to activate the HotStart DNA polymerase, 40 cycles of 15 sec and 1 min at 95°C and 60°C respectively (the annealing step). During the annealing step of each cycle, SYBR Green intercalates and detects double stranded DNA from every well.

Table 5 Experimental cocktail preparation for RT-PCR application.

Plate format:	96 well
2x SABiosciences RT ² qPCR Master mix	1,350 µl
Diluted First Strand cDNA Synthesis Reaction	102 µl
Water	1,248 µl
Final Volume	2,700 µl

The annealing step is followed by an amplification step. It is at this stage that the target DNA sequence will be amplified through a thermal process of repeated heating (for DNA melting) and cooling (for enzyme dependent replication) steps. The DNA melting step unwinds the double stranded helical molecule into two single stranded DNA molecules. Both single stranded DNA molecules are used as a template by DNA polymerase for the amplification of the target DNA sequence in the cooling step. SYBR Green is not specific and detects any other double stranded DNA such as the target DNA in each well, primer dimers, contaminant DNA or products from misannealed primers.

After PCR cycling, it is important to do a melt curve analysis, which is an evaluation of the dissociation of the helical molecule. During the heating step, hydrogen bonds between the nitrogenous bases are destabilised and the double stranded DNA starts to dissociate. As the dissociation occurs, the molecule becomes hyperchromic due to the increase in the absorbance

intensity. The melting point is the temperature at which 50% of hydrogen bonds are disrupted. This physical property is dependent on the G-C content of nucleic acid molecules and it is used for identification purposes. Therefore, the identification of a single peak in each well indicates the amplification of one specific gene. The software of the Stratagene Mx3000p® has a melting curve program that was run immediately after the above cycling program and the instrument was preprogrammed as follows: 95°C, 1 min; 65°C, 2 min (optics off) and 65 to 95°C at 2°C per min (optics on). A melt curve with one peak for each well in the plate at temperatures greater than 80°C had to be obtained.

Real-time PCR array data analysis

After programming the instrument, a loaded PCR array plate was placed on the real-time thermal cycler and the program was run. The threshold cycle (C_t) value for each well was calculated using the instrument software. All C_t values equal to or greater than 35 were considered as absence of amplicon (negative). A gDNA control well (well H6) with a C_t value greater than 35 indicates that there was no gDNA contamination. A positive C_t value ($C_t < 35$) indicates gDNA contamination. PCR control wells (PPC, wells H10 to H12) with a positive C_t value indicated successful amplification and the C_t value should be 20 ± 2 (should not vary by more than 2 cycles between PCR Arrays being compared). Larger differences in average C_t PPC values between plates and wells on the same plate indicates different amounts of starting template or the presence of PCR amplification inhibitors in each sample, which then requires purification steps. An average C_t PPC value above 22 indicates a problem with the cycling condition or sensitivity of the instrument. The software used the average C_t values of all 5 housekeeping genes to normalise the 84 genes studied; the average C_t value of all 5 of the housekeeping genes was deducted from the gene C_t value.

The C_t values were exported to a blank Excel spread sheet for use with the SABioscience PCR array Data Analysis Template available from the SABioscience website with the suitable pathway focused genes (PAHS-212A). The PCR Array Data Analysis software automatically performed the calculations and interpretation of the control wells upon including C_t data from the real-time instrument. The results are presented in a tabular format, a scatter plot, a three-dimensional profile, and a volcano plot (when replicates are included). The Student t-test is used to calculate the p value and the significant difference of gene expression. Fold-change ($2^{\Delta\Delta C_t}$) was calculated by dividing the normalised gene expression ($2^{\Delta C_t}$) of the test sample by the normalised gene expression ($2^{\Delta C_t}$) of the control sample. Fold-change values greater than one indicate a positive or an up-regulation, and the fold-regulation is equal to the fold-change, while fold-change values less than one indicate a negative or down-regulation. The fold-regulation is the negative inverse of the fold-change. The p values were calculated based on the Student's t-test of the replicate $2^{\Delta C_t}$ values for each gene in the control group and treatment groups. A value of $p < 0.05$ was considered significant.

3.6 Statistical Analysis

Dose response study experiments were repeated six times ($n=6$), gene expression experiments were performed three times ($n=3$) and cell death experiments were repeated four times ($n=4$) on different MCF-7 cell populations. Each biochemical assay was done in duplicate, the average of which was used and the mean, standard deviation, standard error and significant changes were calculated using SigmaPlot Version 11.0 software, manufactured by Systat Software Incorporation. The results were recorded for statistical analysis and the one-tailed Student t-test (difference between control and experimental group) and one-way analysis of variance (ANOVA,

difference between treated groups) was used for each independent variable. Statistical significance is shown as $p < 0.05$ (*), $p < 0.01$ (**) or $p < 0.001$ (***) when compared to the untreated control cell and graphs and tables are represented as the mean \pm standard error.



CHAPTER FOUR

RESULTS

4.1 Cell Culture

Breast cancer cells (MCF-7) were cultured in supplemented DMEM. When confluent (Figure 15), cells were seeded at a final concentration of 6×10^5 cells in 3 ml culture media in 3.4 cm² diameter culture dishes. Four hours later, cells were treated with different doses of ZnPcS_{mix} (0; 0.05; 0.1; 0.5 and 1 μM) or Hypericin (0.5, 1, 1.5, 2, 4 and 6 μM). Cells were then incubated for 3 h to allow the respective PS to enter the cells and irradiated either with a 680 nm diode laser (0; 5; 10 and 15 J/cm²) for ZnPcS_{mix} treated cells or with a 594 nm diode laser (0, 5, 10 and 15 J/cm²) for Hypericin treated cells. Twenty four hours post irradiation, cellular morphology, viability, proliferation, cytotoxicity and cell death assays were performed to evaluate cellular responses subsequent to ZnPcS_{mix} treated cells. Trypan blue exclusion assay was performed on Hypericin treated cells and compared to ZnPcS_{mix} treated cells.

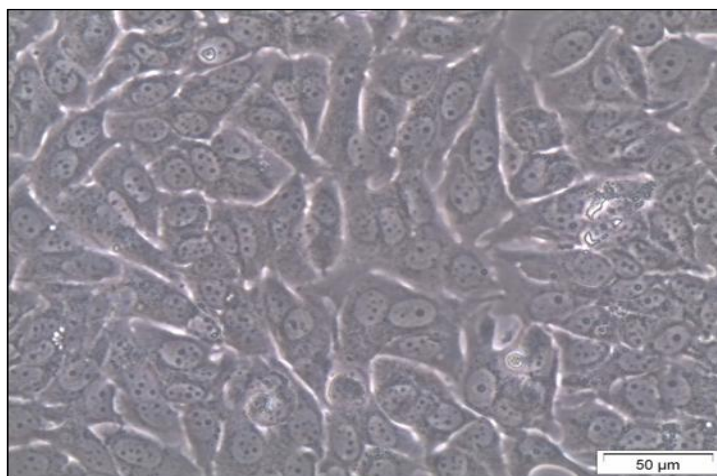


Figure 15 Microscopic representation of confluent breast cancer cells. Cells grew as an anchored, flat monolayer sheet.

4.2 Biological Responses

4.2.1 ZnPcS_{mix} localisation

Fluorescent staining was performed to determine the primary subcellular localisation sites of ZnPcS_{mix} in MCF-7 cells 3 h after the PS was added (Figure 16). Nuclei were stained with DAPI (blue, Figure 16a, e and i), mitochondria were stained with Mitotracker (green, Figure 16d) and lysosomes were stained with LysoTracker (green, Figure 16h).

ZnPcS_{mix} autofluoresced red (Figure 16b, f and j) and did not localise in the nuclei as there was no overlapping of fluorescence (Figure 16c). Red fluorescence was seen around the nuclei and therefore this PS has perinuclear localisation. When stained with mitotracker, there was an overlap with ZnPcS_{mix} fluorescence when the images were merged, as seen by the yellow fluorescence (Figure 16g). The same overlap in fluorescence was seen when MCF-7 cells were stained with LysoTracker (Figure 16k). Thus it can be said that ZnPcS_{mix} localises within both the mitochondria and lysosomes of MCF-7 cells.

4.2.2 Dose response study

A dose response study was performed to identify the combination of ZnPcS_{mix} concentration and laser fluence that induced approximately 50% cell death. Four concentrations of ZnPcS_{mix} and three laser fluences were used during this dose response study. Twelve distinct experimental samples were treated with both ZnPcS_{mix} and laser irradiation and incubated for 24 h before cellular responses were assessed. Cell viability (Trypan blue exclusion assay) was used for comparison between ZnPcS_{mix} and Hypericin, cell proliferation (ATP luminescence and alamarBlue®) and cytotoxicity (LDH membrane integrity) were examined to determine the effectiveness of ZnPcS_{mix} mediated PDT.

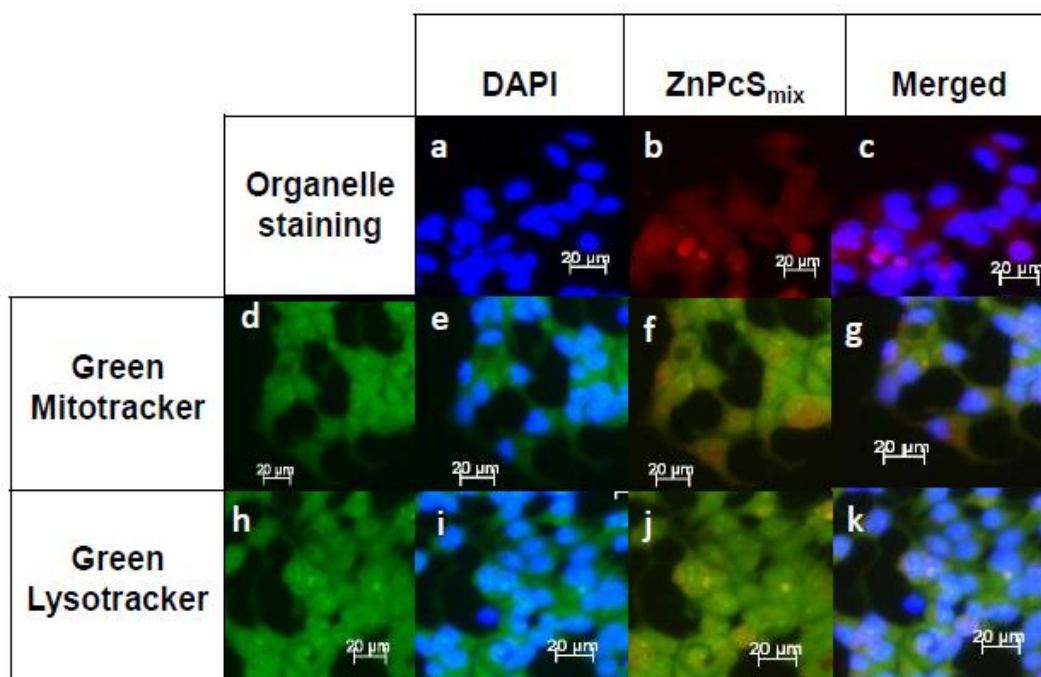


Figure 16 Subcellular localisation of ZnPcS_{mix} in MCF-7 cells. DAPI stained the nuclei (blue a, e and i), Mito- and LysoTracker stained mitochondria (green, d) and lysosomes (green, h), respectively. ZnPcS_{mix} (red, b, f and j) localised in both the mitochondria and lysosomes as the red and green fluorescence overlapped as indicated by the yellow fluorescence (g and k). Distinct red and blue fluorescence were seen (merged) as ZnPcS_{mix} does not localise in the nuclei and ZnPcS_{mix} localised in the perinuclear area (c).

4.2.2.1 Cellular morphology

Before cells were used for biological assays, the morphology of all treated cells were examined by inverted light microscopy and compared to the untreated control cells (no irradiation and no ZnPcS_{mix}). Digital images were taken and are shown in Figures 17 to 21.

Laser irradiated and ZnPcS_{mix} treated cells did not present any morphological disparity as they preserved the MCF-7 cell morphological features which include spindle shaped cells with strong proliferation and adhesion properties

(Figure 17). Neither laser irradiation alone (Figure 17 b-d) nor ZnPcS_{mix} alone (Figure 17 e-h) had damaging effects on the MCF-7 cells. These cells did not present any morphological disparity as compared to untreated control cells (Figure 17 a). All cells grew as spindle shaped cells with strong proliferation and adhesion properties.

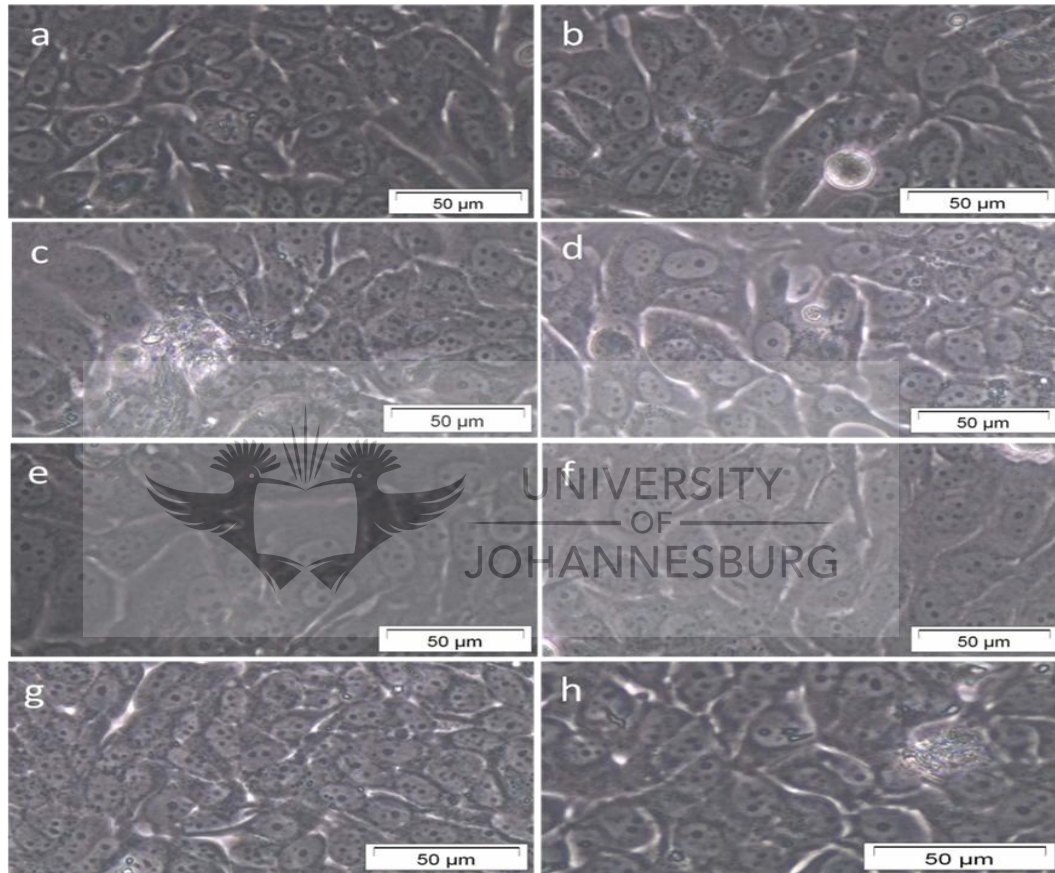


Figure 17 Morphology of MCF-7 cells treated with either laser irradiation or ZnPcS_{mix}. The untreated control (a) received no PS and was not irradiated. Cells were irradiated at 5 (b), 10 (c) and 15 J/cm² (d). ZnPcS_{mix} treated cells received 0.05 (e), 0.1 (f), 0.5 (g) and 1 μM (h) of the PS. No morphological change was noted (200 x magnification).

PDT treated cells showed morphological changes and these changes were more pronounced with the increase in ZnPcS_{mix} concentration (Figures 18,

19, 20 and 21). At a concentration of $0.05 \mu\text{M}$ $\text{ZnPcS}_{\text{mix}}$, cells remained identical to the untreated control cells (Figure 18). Cells treated with $0.1 \mu\text{M}$ $\text{ZnPcS}_{\text{mix}}$ showed signs of a decrease in cell density as the laser fluence increased (Figure 19 c and d).

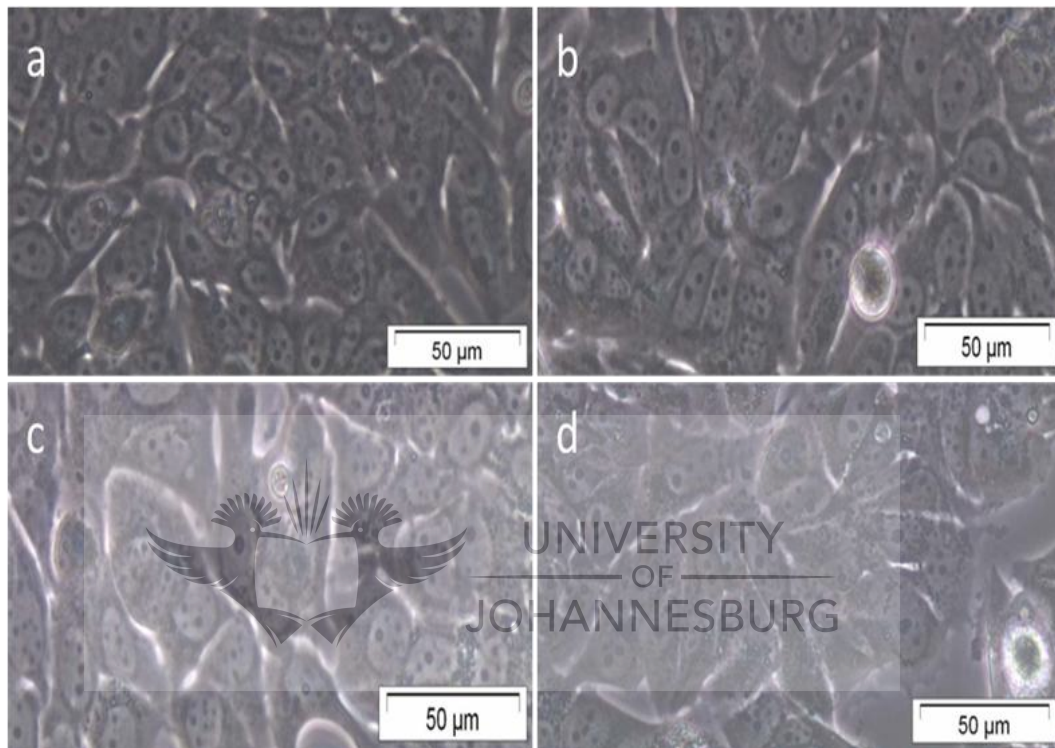


Figure 18 Morphology of PDT treated MCF-7 cells with $0.05 \mu\text{M}$ $\text{ZnPcS}_{\text{mix}}$. The untreated control (a) received no PS and was not irradiated. Three hours after receiving the PS, cells were irradiated at 5 (b), 10 (c) and 15 J/cm^2 (d) using a 680 nm diode laser. At this concentration of $\text{ZnPcS}_{\text{mix}}$, PDT treated cells showed no morphological changes when compared to the untreated control cells (200x magnification).

With higher concentrations of $\text{ZnPcS}_{\text{mix}}$ during PDT (Figures 20 and 21), cells lost their characteristic shape, became rounded as they detached from the culture surface and appeared as free floating round structures at higher fluences (Figure 20 d) and at the highest $\text{ZnPcS}_{\text{mix}}$ concentration (Figure 21). It was seen that the morphological changes were also a function of the

irradiation time; the longer the cells were irradiated, the more the changes were noticeable. Slight cellular elongation was the first sign of morphological change, followed by the decrease in the number of attached cells and the rounding up of cells (Figure 20 b, c and d, respectively). The majority of PDT treated cells with $1 \mu\text{M}$ $\text{ZnPcS}_{\text{mix}}$ were round irrespective of the laser fluence used (Figure 21 b, c and d). This showed that the observed morphological changes depend mainly on the concentration of PS used. The major observed changes included abnormal elongation (swelling), rounding up, detachment from culture plates and blebbing, which is the irregular bulge in the plasma membrane of the cell.

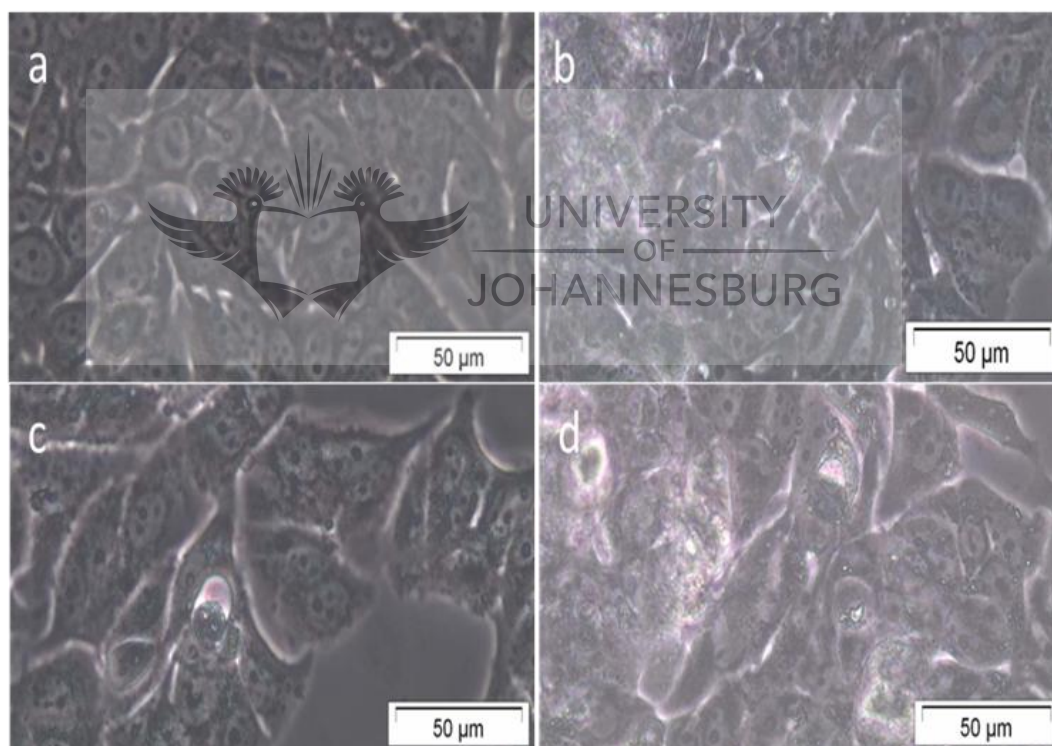


Figure 19 Morphology of PDT treated MCF-7 cells with $0.1 \mu\text{M}$ $\text{ZnPcS}_{\text{mix}}$. The untreated control (a) received no PS and was not irradiated. Three hours after receiving the PS, cells were irradiated at 5 (b), 10 (c) and 15 J/cm^2 (d) using a 680 nm diode laser. When compared to the untreated control, all PDT treated cells showed a slight decrease in cell density and cell morphology started to change as cells became elongated (200x magnification).

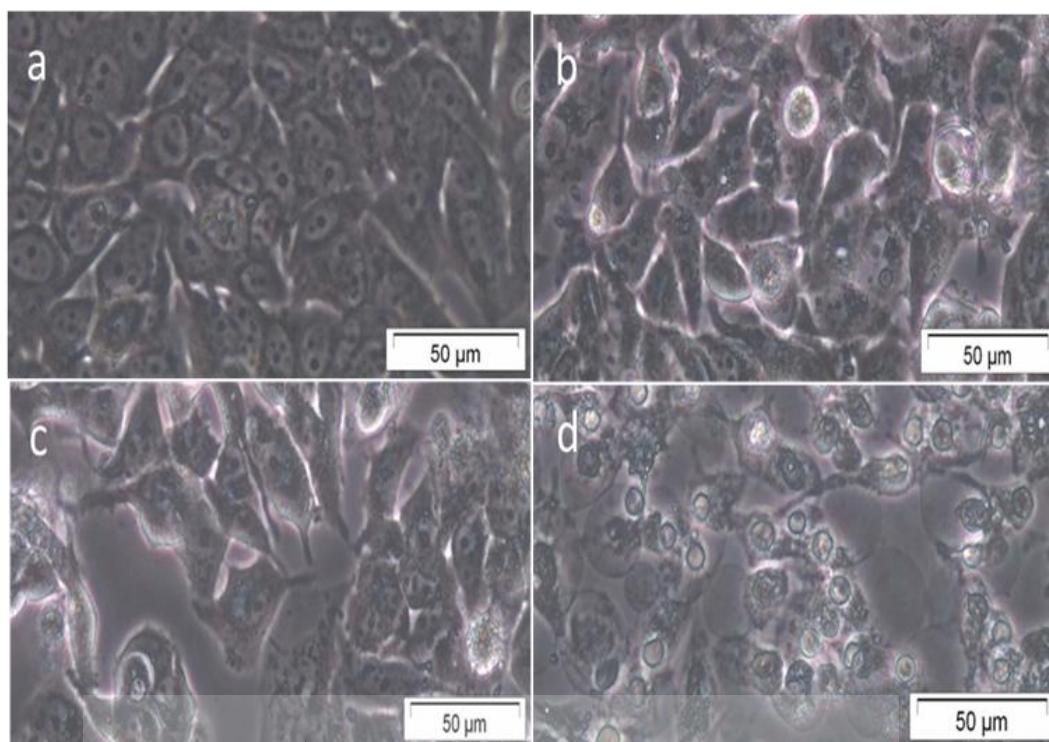


Figure 20

Morphology of PDT treated MCF-7 cells with 0.5 μM ZnPcS_{mix}. The untreated control (a) received no PS and was not irradiated. Three hours after receiving the PS, cells were irradiated at 5 (b), 10 (c) and 15 J/cm² (d) using a 680 nm diode laser. Morphological change was observed in a fluence dependent manner; the longer the cells were irradiated, the more cell changes were noted when compared to the untreated control. These changes included an elongation of cells (b), decrease in cell number and detachment (c) and rounding off (d) (200x magnification).

4.2.2.2 Cellular viability

Trypan blue exclusion assay for Hypericin

The proportion of viable and damaged cells was determined after the Trypan blue exclusion assay was performed and the percentage viability obtained (Table 6). The untreated control cells were not treated with laser irradiation or Hypericin. These cells were 99% viable and no major change in percentage viability was noted with cells treated with either laser irradiation alone or Hypericin alone (at any concentration).

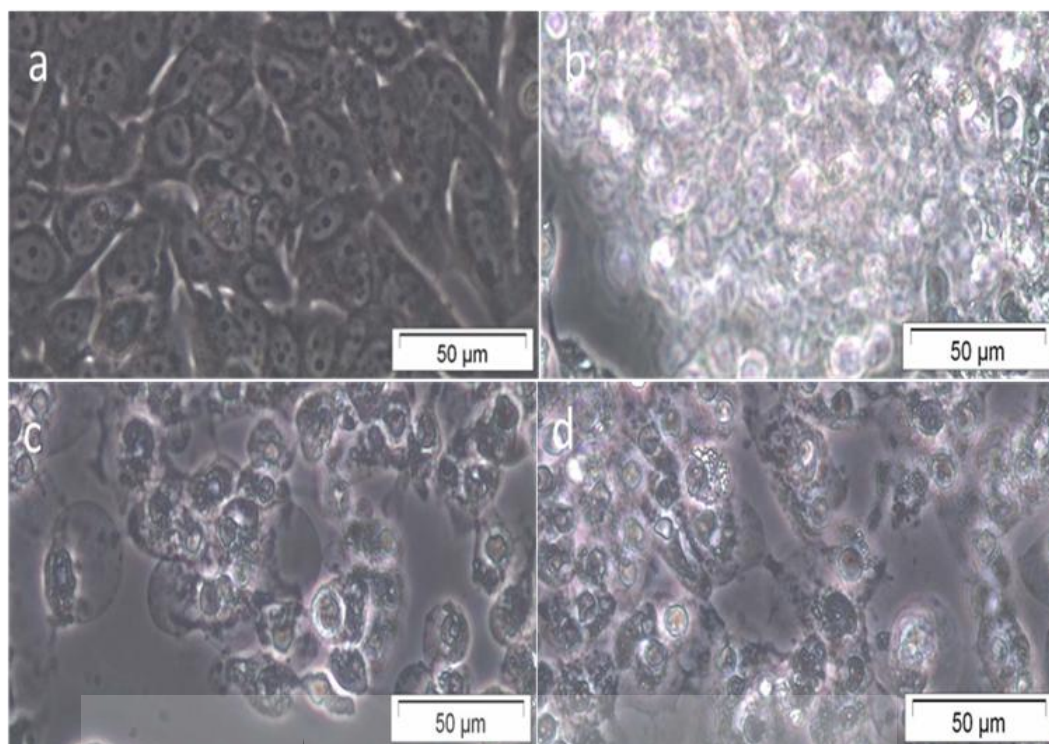


Figure 21 Morphology of PDT treated MCF-7 cells with 1 μM ZnPcS_{mix}. The untreated control (a) received no PS and was not irradiated. Three hours after receiving the PS, cells were irradiated at 5 (b), 10 (c) and 15 J/cm^2 (d) using a 680 nm diode laser. Morphological features of PDT treated cells had totally changed when compared to the untreated control. Most cells have already rounded off as they detached from the culture surface (200x magnification).

Significant decreases in cell viability were seen with cells treated with the following concentrations of Hypericin in PDT: 1 μM irradiated at 15 J/cm^2 ($p < 0.05$); 1.5 μM irradiated at 15 J/cm^2 ($p < 0.01$), 2 μM irradiated at 10 or 15 J/cm^2 ($p < 0.05$ and $p < 0.01$ respectively), and 4 and 6 μM irradiated at 5, 10 and 15 J/cm^2 ($p < 0.05$, $p < 0.01$ and $p < 0.001$, respectively). It was observed that the percentage viability did not decrease below 60% when 0.5, 1 and 1.5 μM Hypericin were used in PDT. A decrease below the same mark was observed with the other 3 concentrations (2, 4 and 6 μM). Two combinations of Hypericin and laser fluence were found to have resulted in 48 and 53% cell viability, which corresponded to 2 μM Hypericin coupled with 15 J/cm^2 and

4 μM Hypericin coupled with 10 J/cm^2 , respectively. The treatment of 4 μM Hypericin and 10 J/cm^2 was identified as the combination of Hypericin concentration and laser fluence that induced a decreased viability of around 50%.

Table 6 Trypan blue percentage viability of different treatments. The percentage viability ranged from 99 to 32%. Significant differences ($p < 0.05^*$) ($p < 0.01^{**}$) ($p < 0.001^{***}$) were noted when compared to the untreated control cells (0 μM Hypericin and 0 J/cm^2). The Trypan blue exclusion assay was repeated six times ($n=6$). Cells treated with 4 μM of Hypericin and 10 J/cm^2 was found to have resulted in 53% cell viability.

Laser fluence	0 μM Hypericin	0.5 μM Hypericin	1 μM Hypericin	1.5 μM Hypericin	2 μM Hypericin	4 μM Hypericin	6 μM Hypericin
0 J/cm^2	99 \pm 1.24	98 \pm 1.11	99 \pm 1.25	99 \pm 0.85	99 \pm 1.08	98 \pm 0.86	97 \pm 1.49
5 J/cm^2	98 \pm 0.59	99 \pm 0.91	94 \pm 0.86	92 \pm 1.08	88 \pm 0.69	76 \pm 1.34*	69 \pm 2.54*
10 J/cm^2	99 \pm 0.76	98 \pm 0.48	84 \pm 0.91	83 \pm 0.64	62 \pm 1.08**	53 \pm 1.47**	46 \pm 1.44**
15 J/cm^2	99 \pm 1.64	97 \pm 0.65	68 \pm 0.86*	63 \pm 1.47**	48 \pm 1.32**	38 \pm 2.16***	32 \pm 1.25***

Data shown are means plus standard errors \pm .

When treated cells were compared between each other, changes in PDT treated cells with 1 μM Hypericin at 15 J/cm^2 were found to be significant ($p < 0.05$) when compared to all the irradiated cells, Hypericin treated cells, all PDT treated cells with 0.5 μM Hypericin, and PDT treated cells with 1 μM Hypericin at 5 J/cm^2 and 1.5 μM Hypericin at 5 J/cm^2 . Changes in PDT treated cells with 1.5 μM Hypericin at 15 J/cm^2 were found to be significant ($p < 0.05$) when compared to PDT treated cells with 1 μM Hypericin at 5 J/cm^2 , 1.5 μM Hypericin at 5 J/cm^2 , 2 μM Hypericin at 5 J/cm^2 . Changes in PDT treated cells with 1.5 μM Hypericin at 15 J/cm^2 were found to be significant ($p < 0.01$) when compared to all the irradiated cells, all Hypericin treated cells,

all PDT treated cells with 0.5 μM Hypericin. Changes in PDT treated cells with 2 μM Hypericin at 10 J/cm^2 were found to be significant ($p < 0.05$) when compared to PDT treated cells with 1 μM Hypericin at 5 J/cm^2 , 1.5 μM Hypericin at 5 J/cm^2 , 2 μM Hypericin at 5 J/cm^2 . Changes in PDT treated cells with 2 μM Hypericin at 10 J/cm^2 were found to be significant ($p < 0.01$) when compared to all the irradiated cells, all Hypericin treated cells, all PDT treated cells with 0.5 μM Hypericin. Changes in PDT treated cells with 2 μM Hypericin at 15 J/cm^2 were found to be significant ($p < 0.05$) when compared to PDT treated cells with 1 μM Hypericin at 5 J/cm^2 , 1 μM Hypericin at 10 J/cm^2 , 1.5 μM Hypericin at 5 J/cm^2 , 1.5 μM Hypericin at 10 J/cm^2 , 2 μM Hypericin at 5 J/cm^2 , 4 μM Hypericin at 5 J/cm^2 . Changes in PDT treated cells with 2 μM Hypericin at 15 J/cm^2 were found to be significant ($p < 0.01$) when compared to all the irradiated cells, all Hypericin treated cells, all PDT treated cells with 0.5 μM Hypericin.



UNIVERSITY
OF
JOHANNESBURG

Changes in PDT treated cells with 4 μM Hypericin at 5 J/cm^2 were found to be significant ($p < 0.05$) when compared to all the irradiated cells, all Hypericin treated cells, all PDT treated cells with 0.5 μM Hypericin. Changes in PDT treated cells with 4 μM Hypericin at 10 J/cm^2 were found to be significant ($p < 0.05$) when compared to PDT treated cells with 1 μM Hypericin at 5 J/cm^2 , 1 μM Hypericin at 10 J/cm^2 , 1.5 μM Hypericin at 5 J/cm^2 , 1.5 μM Hypericin at 10 J/cm^2 , 2 μM Hypericin at 5 J/cm^2 and 4 μM Hypericin at 5 J/cm^2 . Changes in PDT treated cells with 4 μM Hypericin at 10 J/cm^2 were found to be significant ($p < 0.01$) when compared to all the irradiated cells, all Hypericin treated cells, all PDT treated cells with 0.5 μM Hypericin. Changes in PDT treated cells with 4 μM Hypericin at 15 J/cm^2 were found to be significant ($p < 0.05$) when compared to PDT treated cells with 1 μM Hypericin at 10 J/cm^2 , 1 μM Hypericin at 15 J/cm^2 , 1.5 μM Hypericin at 10 J/cm^2 , 1.5 μM Hypericin at 15 J/cm^2 , 2 μM Hypericin at 5 J/cm^2 , 4 μM Hypericin at 5 J/cm^2

and 6 μM Hypericin at 5 J/cm^2 . Changes in PDT treated cells with 4 μM Hypericin at 15 J/cm^2 were found to be significant ($p < 0.01$) when compared to PDT treated cells with 1 μM Hypericin at 5 J/cm^2 , 1.5 μM Hypericin at 5 J/cm^2 . Changes in PDT treated cells with 4 μM Hypericin at 15 J/cm^2 were found to be significant ($p < 0.001$) when compared to all the irradiated cells, all Hypericin treated cells and all PDT treated cells with 0.5 μM Hypericin.

Changes in PDT treated cells with 6 μM Hypericin at 5 J/cm^2 were found to be significant ($p < 0.05$) when compared to all the irradiated cells, all Hypericin treated cells, all PDT treated cells with 0.5 μM Hypericin, and PDT treated cells with 1 μM Hypericin at 5 J/cm^2 and 1.5 μM Hypericin at 5 J/cm^2 . Changes in PDT treated cells with 6 μM Hypericin at 10 J/cm^2 were found to be significant ($p < 0.05$) when compared to PDT treated cells with 1 μM Hypericin at 5 J/cm^2 , 1 μM Hypericin at 10 J/cm^2 , 1.5 μM Hypericin at 5 J/cm^2 , 1.5 μM Hypericin at 10 J/cm^2 , 2 μM Hypericin at 5 J/cm^2 and 4 μM Hypericin at 5 J/cm^2 . Changes in PDT treated cells with 6 μM Hypericin at 10 J/cm^2 were found to be significant ($p < 0.01$) when compared to all the irradiated cells, all Hypericin treated cells, all PDT treated cells with 0.5 μM Hypericin. Changes in PDT treated cells with 6 μM Hypericin at 15 J/cm^2 were found to be significant ($p < 0.05$) when compared to PDT treated cells with 1 μM Hypericin at 15 J/cm^2 , 1.5 μM Hypericin at 15 J/cm^2 , 2 μM Hypericin at 10 J/cm^2 , 4 μM Hypericin at 5 J/cm^2 and 6 μM Hypericin at 5 J/cm^2 . Changes in PDT treated cells with 6 μM Hypericin at 15 J/cm^2 were found to be significant ($p < 0.01$) when compared to PDT treated cells with 1 μM Hypericin at 5 J/cm^2 , 1 μM Hypericin at 10 J/cm^2 , 1.5 μM Hypericin at 5 J/cm^2 , 1.5 μM Hypericin at 10 J/cm^2 and 2 μM Hypericin at 15 J/cm^2 . Changes in PDT treated cells with 6 μM Hypericin at 15 J/cm^2 were found to be significant ($p < 0.001$) when compared to all the irradiated cells, all Hypericin treated cells and all PDT treated cells with 0.5 μM Hypericin.

Trypan blue exclusion assay for ZnPcS_{mix}

The proportion of viable and damaged cells was obtained after the Trypan blue exclusion assay was performed. The percentage viabilities after the ZnPcS_{mix} mediated PDT are presented in Table 7. The untreated control had a high percentage viability (98%) and no major viability changes were observed when cells were either treated with laser irradiation alone or with ZnPcS_{mix} alone (at any concentration). After PDT, the percentage viability decreased significantly to as low as 42% in ZnPcS_{mix} treated cells. The decrease occurred in a dose dependent manner.

Table 7 Trypan blue percentage viability of different treatments. The percentage viability range from 99 to 42% and the lowest percentages were noted with 1 μM ZnPcS_{mix} treated samples. Significant differences ($p < 0.05^*$) ($p < 0.01^{**}$) ($p < 0.001^{***}$) were noted when compared to the untreated control cells only. The Trypan blue exclusion assay was repeated six times ($n=6$). Cells treated with 0.5 μM ZnPcS_{mix} and 10 J/cm^2 was found to have resulted in 54% cell viability.

Laser fluence	0 μM ZnPcS _{mix}	0.05 μM ZnPcS _{mix}	0.1 μM ZnPcS _{mix}	0.5 μM ZnPcS _{mix}	1 μM ZnPcS _{mix}
0 J/cm^2	98 \pm 0.62	98 \pm 0.36	98 \pm 0.26	94 \pm 0.57	93 \pm 0.62
5 J/cm^2	99 \pm 0.89	95 \pm 0.61	90 \pm 0.84	81 \pm 1.51	71 \pm 2.76 *
10 J/cm^2	98 \pm 1.26	95 \pm 0.72	90 \pm 0.88	54 \pm 1.38 **	42 \pm 1.45 **
15 J/cm^2	98 \pm 0.77	94 \pm 0.68	88 \pm 1.29	44 \pm 1.77 **	42 \pm 1.15 **

Data shown are means plus standard errors \pm .

The higher the concentration of PS and laser fluence used, the more cells were damaged and Trypan blue dye entered cells through damaged membranes. Significant decreases were obtained when cells were treated with 0.5 and 1 μM ZnPcS_{mix} and these treatments were: 0.5 μM irradiated at 10 or 15 J/cm^2 ($p < 0.01$), 1 μM irradiated at 5, 10 and 15 J/cm^2 ($p < 0.05$,

$p < 0.01$ and $p < 0.01$, respectively). The nearest 50% decrease in cell viability was obtained when cells were treated with $0.5 \mu\text{M}$ ZnPcS_{mix} and a laser fluence of 10 J/cm^2 and led to 54% viability.

Changes in PDT treated cells with $0.5 \mu\text{M}$ ZnPcS_{mix} at 10 and 15 J/cm^2 were significant ($p < 0.01$) when compared to all the irradiated cells, ZnPcS_{mix} treated cells, PDT treated cells with 0.05 and $0.1 \mu\text{M}$ and PDT treated cells with $0.5 \mu\text{M}$ at 5 J/cm^2 . Significant changes ($p < 0.05$) were also observed when PDT treated cells with $1 \mu\text{M}$ at 5 J/cm^2 were compared to all the irradiated cells and ZnPcS_{mix} treated cells with 0.05 and $0.1 \mu\text{M}$. Changes in PDT treated cells with $1 \mu\text{M}$ at 10 and 15 J/cm^2 were found to be significant ($p < 0.05$) when compared to PDT treated cells with $0.1 \mu\text{M}$ at 5 , 10 and 15 J/cm^2 ; and with 0.5 and $1 \mu\text{M}$ at 5 J/cm^2 . With the same PDT treated cells, higher variation degrees were made ($p < 0.01$) when compared to all the irradiated cells, ZnPcS_{mix} treated cells and PDT treated with $0.05 \mu\text{M}$.

4.2.2.3 Cellular proliferation

ATP luminescence

The Cell Titer-Glo ATP luminescence assay was performed to determine the rate of cellular proliferation and cellular metabolic activity after ZnPcS_{mix} mediated PDT. The level of ATP present was determined in all samples and treatments were compared to the untreated control. Cells treated with laser irradiation alone or ZnPcS_{mix} alone showed no significant change in ATP level (Figure 22). ZnPcS_{mix} in the absence of irradiation did not affect the mechanisms of ATP consumption and synthesis. No significant difference was seen when treated cells (irradiated and ZnPcS_{mix} treated) were compared to each other.

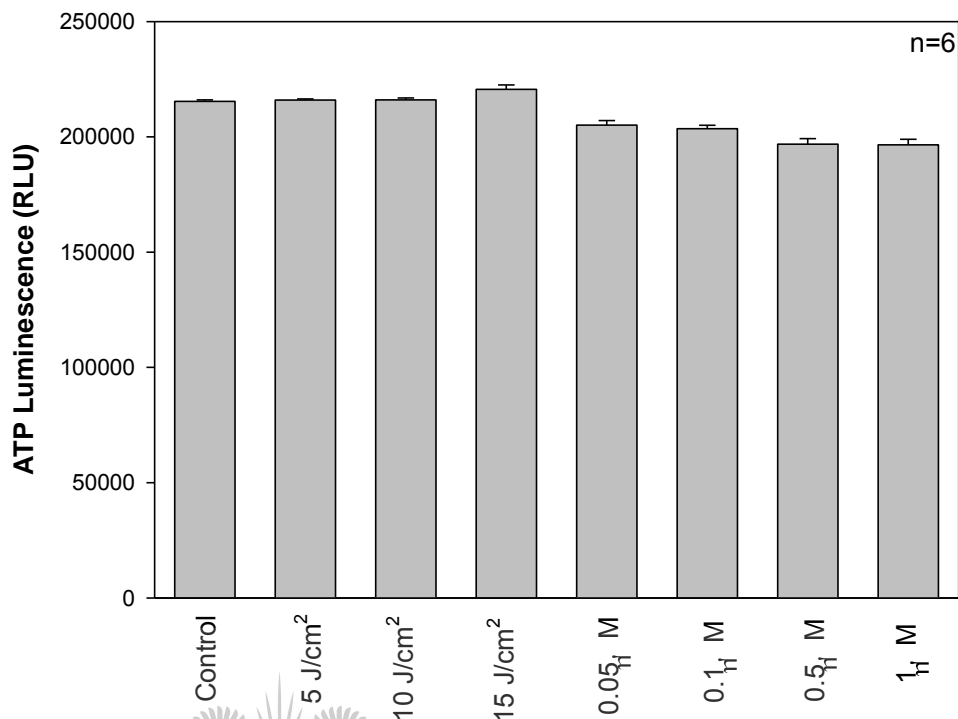


Figure 22 ATP luminescence cell proliferation assay in MCF-7 cells. When compared to untreated control cells, the relative light units (RLU) of both laser irradiated and ZnPcS_{mix} treated cells did not present any major change in cell proliferation and no significant change in ATP levels was noted.

A significant decrease in ATP levels was noted in all PDT treated cells with the exception of those treated with 0.05 μM ZnPcS_{mix} (Figure 23) that was inversely proportional to both the ZnPcS_{mix} concentration and the laser fluence used. An increase in ZnPcS_{mix} concentration during PDT resulted in lower detection of ATP luminescence. When irradiated at 5, 10 and 15 J/cm², PDT treated cells showed a significant decrease in ATP levels when treated with 0.1 μM (p<0.05, p<0.05 and p<0.01 respectively), 0.5 μM (p<0.01, p<0.01 and p<0.001 respectively) and 1 μM (p<0.01, p<0.001 and p<0.001 respectively). ZnPcS_{mix} showed significant ATP depletion in a dose dependent pattern.

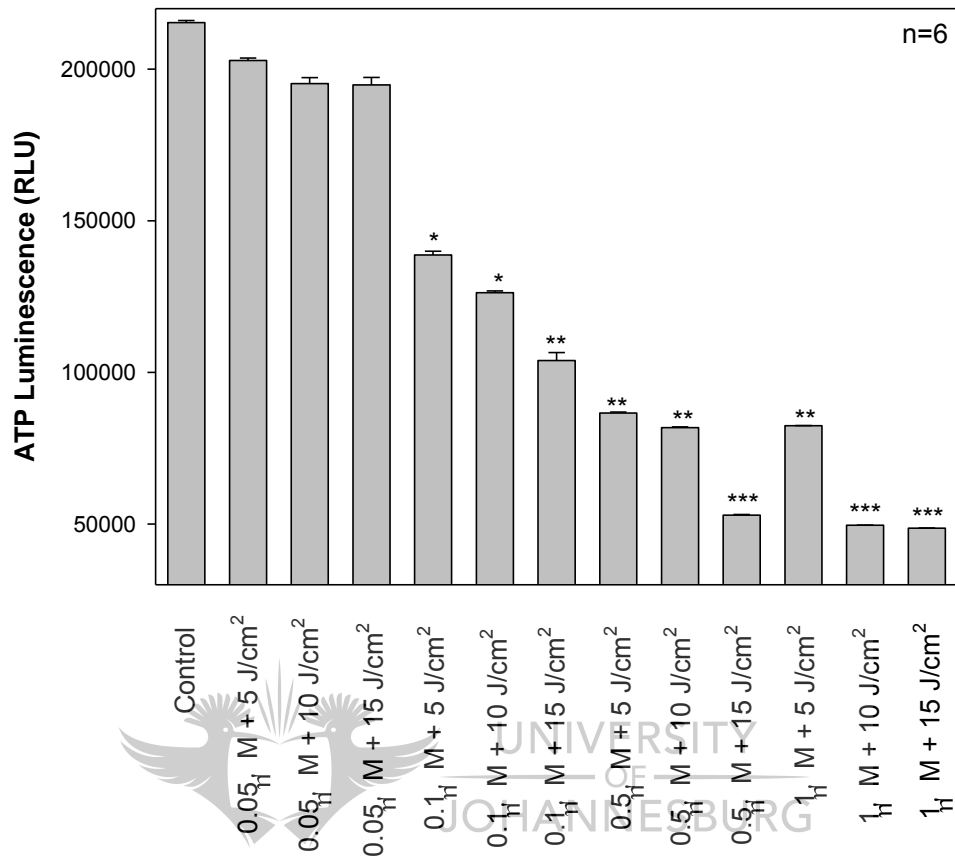


Figure 23 ATP luminescence cell proliferation assay in PDT treated MCF-7 cells. Activated ZnPcS_{mix} during PDT caused a decreased in cell proliferation. A decrease in ATP levels was observed with most of PDT treated cells when compared to the untreated control and significant differences (p<0.05*) (p<0.01**) (p<0.001***) were noted.

When PDT treated cells were compared between each other, PDT treated cells with 0.5 μM ZnPcS_{mix} at 5 J/cm² (p<0.05) and 0.5 μM ZnPcS_{mix} at 15 J/cm² (p<0.01), and 1 μM ZnPcS_{mix} at 5 J/cm² (p<0.05), 10 J/cm² (p<0.01) and 15 J/cm² (p<0.01) were found to be significant when compared to 0.05 μM ZnPcS_{mix} PDT treated cells. PDT treated cells with 0.5 μM ZnPcS_{mix} at 15 J/cm² and 1 μM ZnPcS_{mix} at 10 and 15 J/cm² were found to be significant (p<0.05) when compared to PDT treated cells with 0.1 μM ZnPcS_{mix} at 5 J/cm².

alamarBlue®

The alamarBlue® assay was performed to determine the rate of cellular proliferation. The absorbance values of untreated and treated cells were measured and the absorbance values were compared to that of the untreated control. No significant change in proliferation rate was noted when laser irradiated or ZnPcS_{mix} treated cells were compared to the untreated control (Figure 24). No significant difference was seen when treated cells (irradiated and ZnPcS_{mix} treated) were compared to each other.

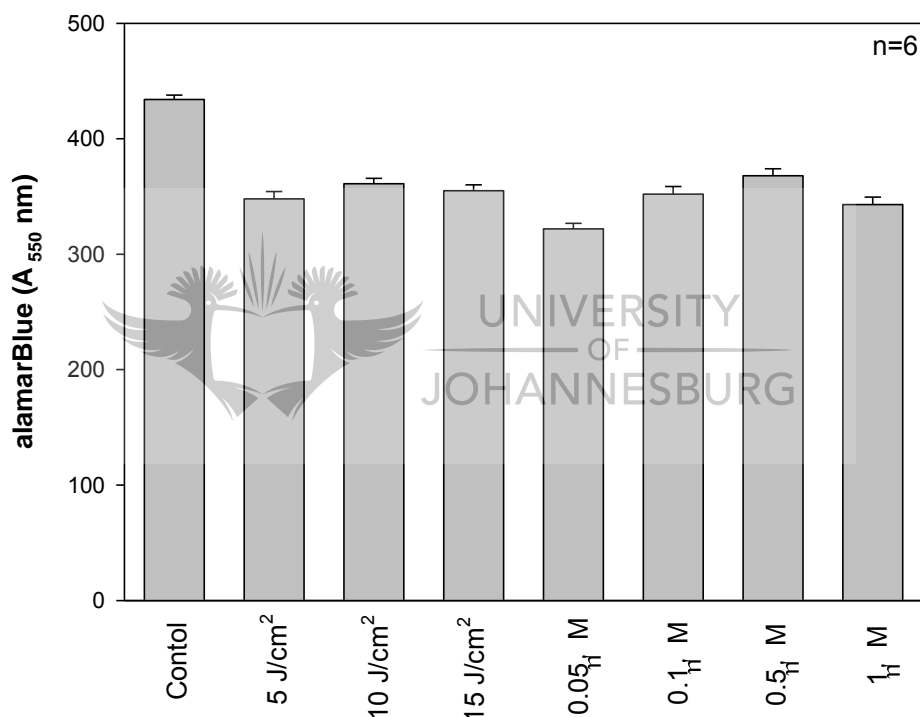


Figure 24 alamarBlue® cell proliferation in MCF-7 cells. Both irradiated alone and ZnPcS_{mix} treated cells did not show any significant proliferation change.

PDT treated cells showed a reduced proliferation rate (Figure 25). Significant changes in cell proliferation were observed when cells were treated with ZnPcS_{mix} at 0.1 μM and 15 J/cm² (p<0.05), 0.5 μM and 10 or 15 J/cm² (p<0.05), and 1 μM and 5, 10 or 15 J/cm² (p<0.05, p<0.01 and p<0.01

respectively). No significant difference was seen when PDT treated cells were compared to each other.

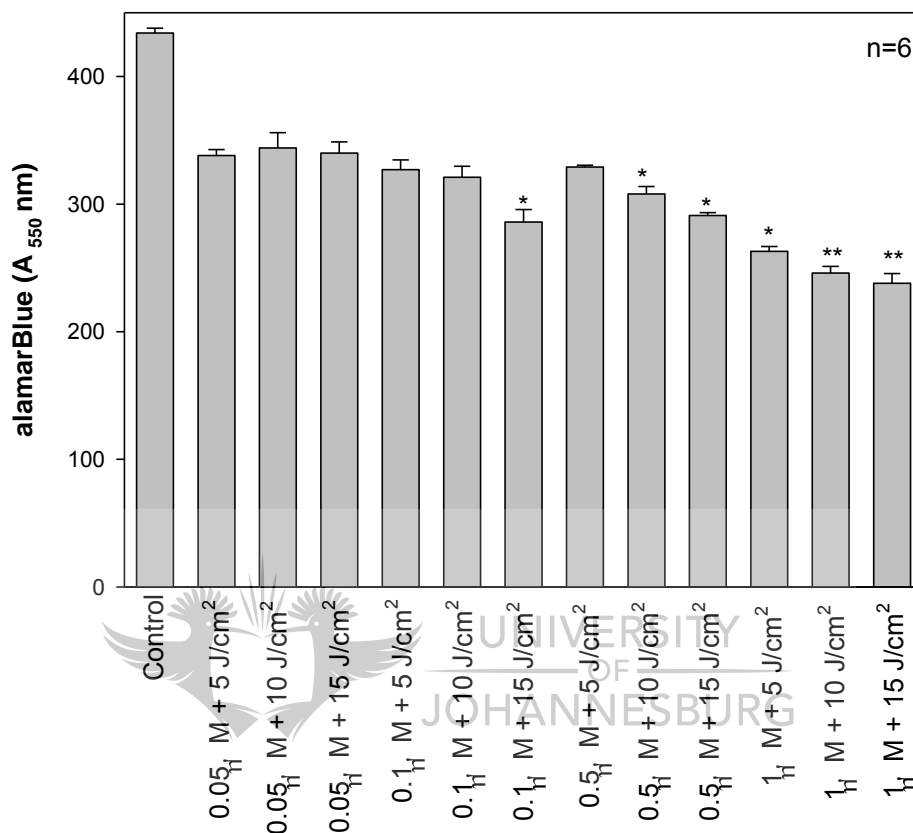


Figure 25 alamarBlue® cell proliferation in PDT treated MCF-7 cells. PDT treated cells had slow proliferation rates and significant differences ($p < 0.05^*$) and ($p < 0.01^{**}$) were noted when compared to the untreated control cells only.

4.2.2.4 Cytotoxicity

The CytoTox96® nonradioactive cytotoxicity assay was performed to assess the level of LDH released into the culture media and to determine the degree of cellular damage, in particular cellular membrane damage of the MCF-7 cells. The release of LDH from the cytosol into the culture media was quantified and the absorbance measured. Both laser irradiated cells alone and ZnPcS_{mix} treated cells alone released insignificant amounts of LDH

resulting in absorbance values similar to that of the untreated control cells (Figure 26). No significant difference was seen when treated cells (irradiated and ZnPcS_{mix} treated) were compared to each other.

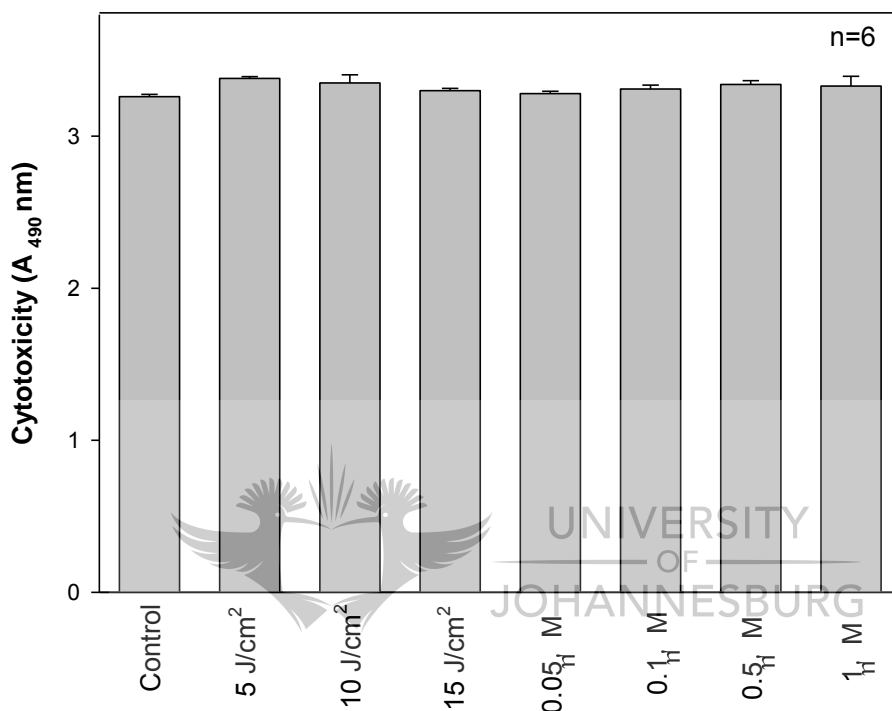


Figure 26 The CytoTox96® nonradioactive cytotoxicity assay in MCF-7 cells. Irradiated cells and ZnPcS_{mix} treated cells alone showed no significant change in LDH levels when compared to the untreated control cells only.

PDT treatment induced an increase in cell membrane damage, as noted by the significant increase in the level of LDH detected with 0.05 μ M ZnPcS_{mix} and the other concentrations ($p < 0.05$ and $p < 0.01$ respectively) when compared to the untreated control cells (Figure 27). Changes in PDT treated cells with 1 μ M ZnPcS_{mix} at 15 J/cm² were found to be significant ($p < 0.05$) when compared to those treated with 0.05 μ M ZnPcS_{mix} at 5 J/cm².

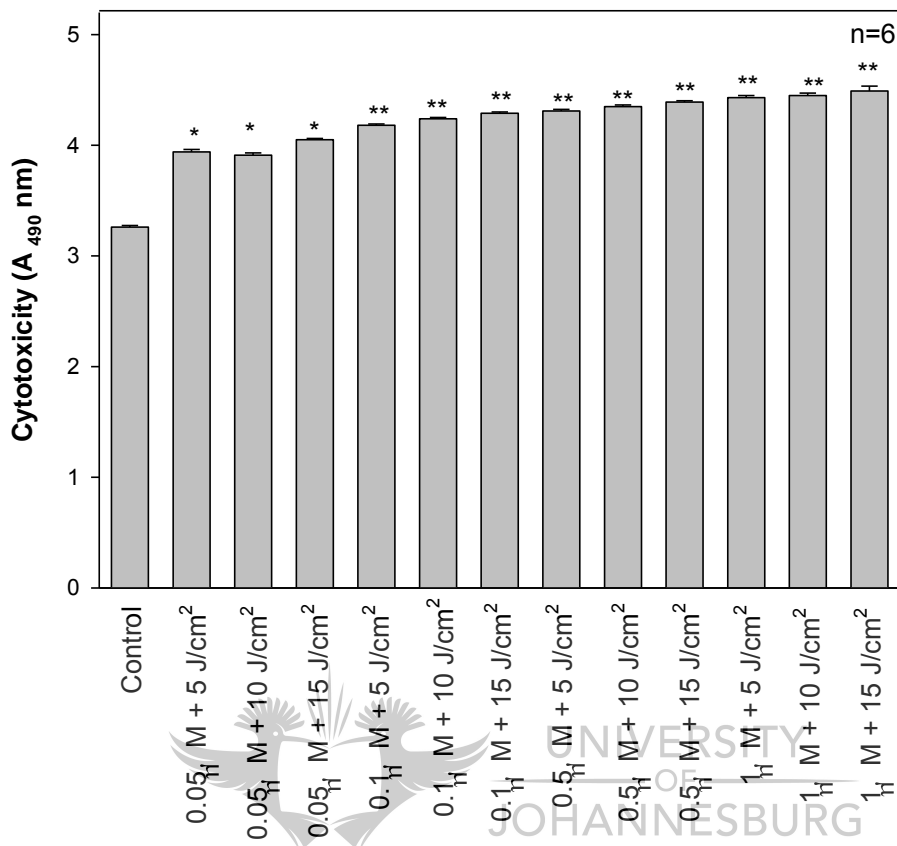


Figure 27 The CytoTox96® nonradioactive cytotoxicity assay in PDT treated MCF-7 cells. Cellular damage was significant in all PDT treated cells and significant levels of LDH were noted. Significant differences ($p < 0.05^*$) and ($p < 0.01^{**}$) were noted when compared to the untreated control cells only.

4.2.3 Cell death study

4.2.3.1 Flow cytometry

Annexin V-FITC was used in conjunction with PI to distinguish the types of cell population. One hour after staining, flow cytometric analysis was performed to identify the cell population of each sample. The majority of the cell population in untreated control cells and ZnPcS_{mix} treated MCF-7 cells were viable (89% and 91% respectively) and stained negative for both Annexin V-FITC and PI (Table 8). However, when compared to untreated

control cells, significant changes in cell population were noted with both Actinomycin D and PDT treated cells. More than 75% of cells were undergoing cell death; they were positive for both stains (late apoptotic, $p < 0.01$), positive for Annexin V-FITC (early apoptotic, $p < 0.01$), and the population of normal cells decreased significantly ($p < 0.001$).

Table 8 Percentage of various cell populations after flow cytometric analysis. Normal cells were both negative for Annexin V-FITC and PI, early apoptotic cells were positive for Annexin V-FITC but negative for PI, late apoptotic cells were positive for both Annexin V-FITC and PI, and necrotic cells stained positive for PI. The lowest percentage of cell death (apoptotic and necrotic) were obtained with untreated and ZnPcS_{mix} controls. These apoptotic populations significantly increased (around 65%) in Actinomycin D and PDT treated cells. Experiments were repeated four times (n=4) and significant differences ($p < 0.01^{**}$) and ($p < 0.001^{***}$) were noted when compared to the respective population type of the untreated control cells.

Cell population	Untreated control	ZnPcS _{mix} control	Actinomycin D	PDT
Normal	89±1.07	91±0.32	24±0.67 ^{***}	21±0.89 ^{***}
Early apoptotic	4±0.89	5±1.04	34±0.38 ^{**}	37±1.06 ^{**}
Necrotic	3±0.43	2±0.81	11±0.74	13±0.94
Late apoptotic	4±0.52	2±1.12	31±1.23 ^{**}	29±0.76 ^{**}

Data shown are means plus standard errors ±.

4.2.3.2 Hoechst staining

Hoechst staining was performed to assess nuclear changes and detect the degree of nucleic acid degradation. The Hoechst stain is a fluorescent permeable DNA dye that binds preferentially to AT base pairs. No difference in the size of the nucleus between the unirradiated ZnPcS_{mix} treated cells

(Figure 28 b) and the untreated control cells (Figure 28 a) was seen as the PS remained inactive in the absence of light. Smearing around the nuclear regions was seen 3 h after the activation (irradiation) of ZnPcSmix (Figure 28 c). With an increase in incubation time post irradiation (9 and 15 h), it appeared that the nuclear diameter kept on decreasing and the smear progressively disappeared (Figure 28 d and e respectively).

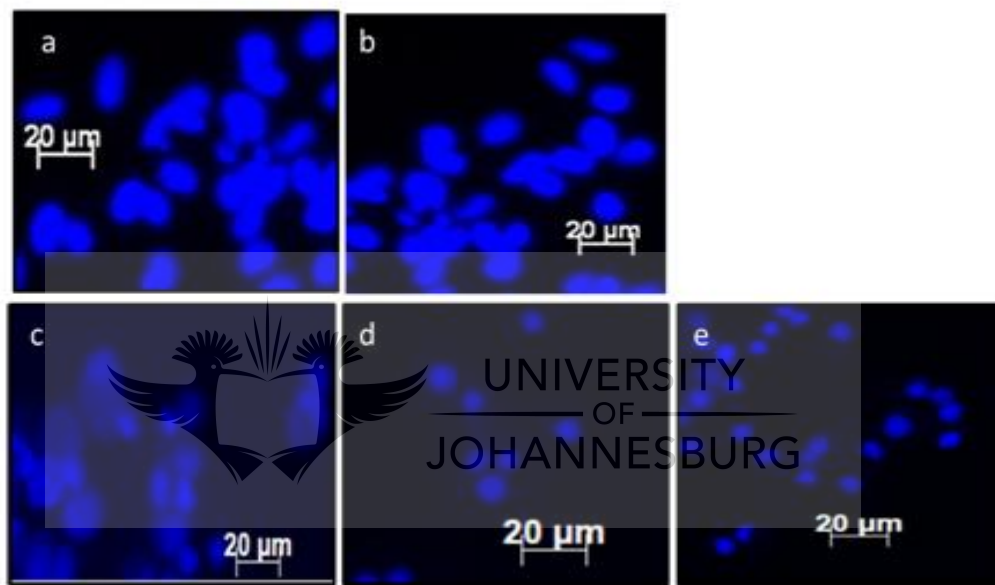


Figure 28 Hoechst immunofluorescence staining in MCF-7 cells. Intense fluorescence was seen when the nuclei of the untreated control (a) and unirradiated ZnPcS_{mix} treated (b) were analysed. After 3 h incubation post PDT (c), the nuclei appeared smaller in size with smears seen around them, an indication of nuclear condensation (damage). The smear cleared up and smaller distinct nuclear fluorescence was seen 9 and 15 h after irradiation (d and e respectively) (200x magnification).

4.2.3.3 Cell death ELISA

Apoptotic cell death is characterised by nuclear fragmentation and oligonucleosomal DNA degradation. A cell death photometric enzyme immunoassay was performed to determine cytoplasmic histone-associated

DNA fragments (mono- and oligonucleosomes) subsequent to PDT in MCF-7 cells. No significant quantity of DNA fragments was detected when cells were treated either with laser alone (10 J/cm^2) or $\text{ZnPcS}_{\text{mix}}$ alone (Figure 29). However, a significant increase in the quantity of DNA fragments as compared to the untreated control was noted after PDT ($p < 0.01$). The change in histones associated DNA fragment was found to be significant ($p < 0.01$) when PDT treated cells were compared to those treated with both irradiation and $\text{ZnPcS}_{\text{mix}}$ alone.

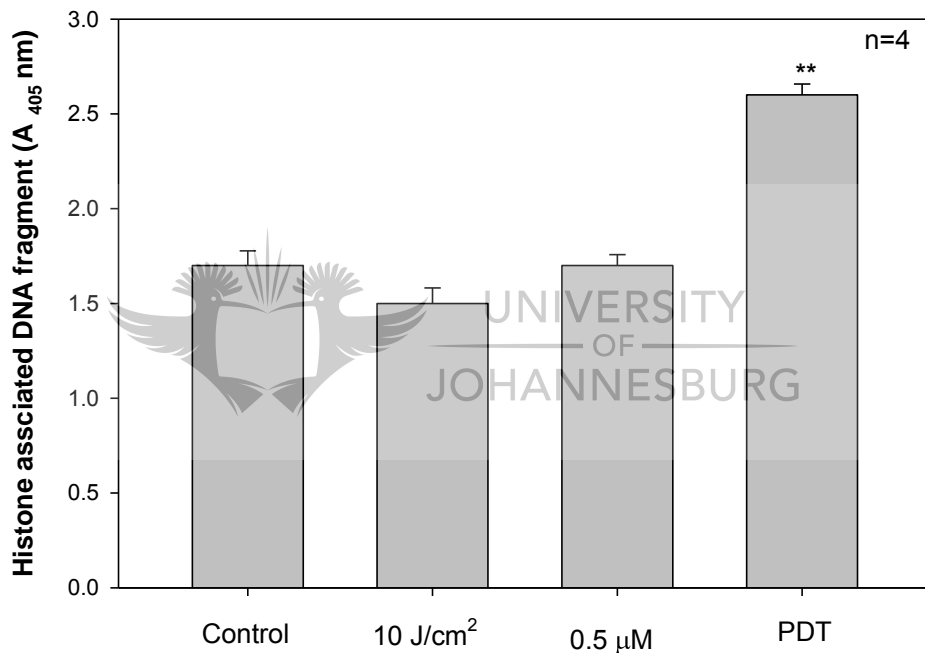


Figure 29 Evaluation of nuclear degradation using the Cell Death Detection ELISA assay. Untreated control cells (MCF-7) and both laser irradiated and $\text{ZnPcS}_{\text{mix}}$ treated MFC-7 cells showed low amounts of DNA fragmentation. After PDT, the amount of DNA fragmentation significantly increased ($p < 0.01^{**}$). Significant difference was noted when compared to the untreated control cells.

4.3.2.4 Real-time RT-PCR

Real-time RT-PCR was performed to identify the up- or down- regulation of 84 genes involved in different cellular death pathways 3 h after PDT. Along with the studied 84 genes, 12 other genes were incorporated, and these

included 5 housekeeping genes to normalise the genes of interest, 1 gDNA control gene, 3 reverse transcription control genes (RTC) and 3 positive PCR control genes (PPC). The SABioscience RT² First Strand kit was not used for cDNA synthesis and hence the RTC controls were not validated. All these controls do not appear in the results panel of expressed genes. Purity checks of all nucleic acid (RNA and cDNA) samples were performed and the all purities were between 1.82 and 1.94.

Real-time PCR array data analysis

Gene expression profiles of ZnPcS_{mix} treated MCF-7 cells

MCF-7 cells were treated with 0.5 µM ZnPcS_{mix} alone and incubated for 3 h, before RNA isolation was performed for real-time RT-PCR. Neither of the up-regulated or down-regulated genes was significantly expressed (Figure 30).

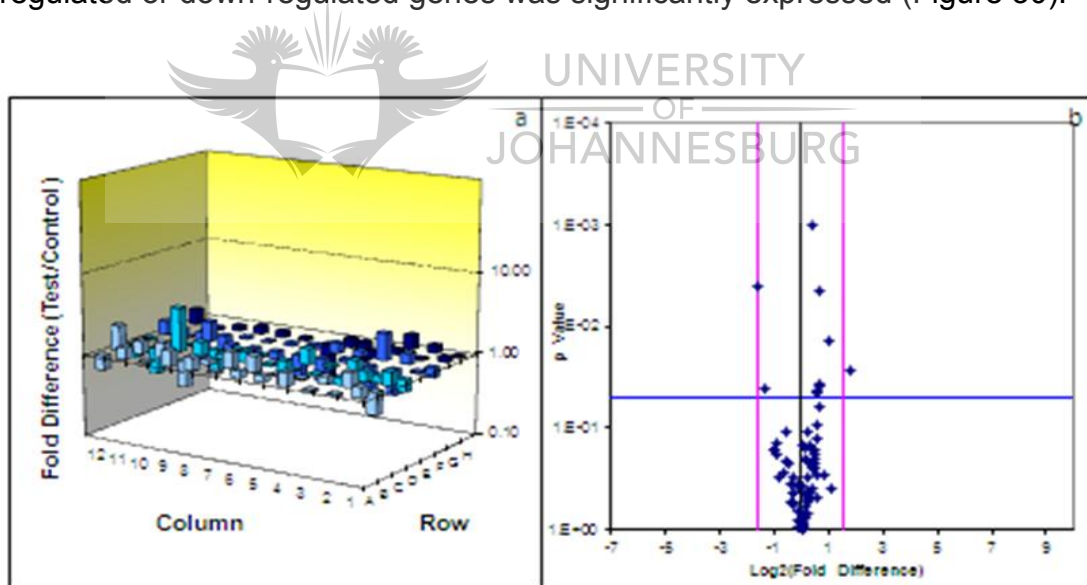


Figure 30

Gene expression profile of ZnPcS_{mix} treated cells was analysed using the Human Cell Death Pathway Finder Profiler™ PCR Array System. Treatment did not have an effect on the gene expression and none of the genes were significantly regulated as represented in the 3D Profile (fold-difference, a) and volcano plot (b). In the volcano plot, the horizontal line designates the target threshold (p=0.05) and vertical lines, the fold change (central) and target fold change threshold (peripheral) in gene expression.

Gene expression profiles of PDT treated MCF-7 cells

The gene expression analysis of PDT treated MCF-7 cells was performed after RNA was isolated and cDNA synthesised for real-time RT-PCR. Results showed that BCL-2 ($p < 0.05$), DFFA-1 ($p < 0.05$) and CASP-2 ($p < 0.001$) were significantly up-regulated when compared to the untreated control cells. None of the down-regulated genes was found to be significant (Figure 31).

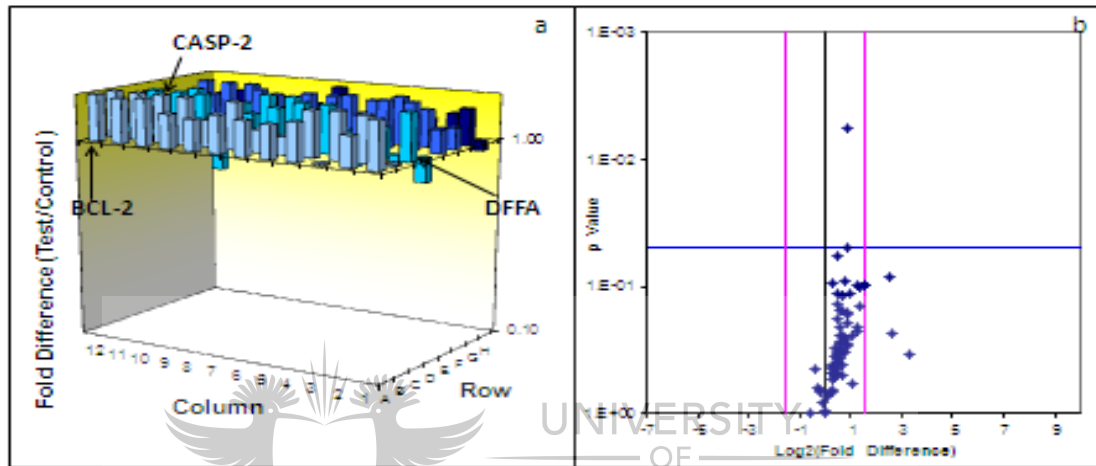


Figure 31

Gene expression profiles of PDT treated MCF-7 cells with $0.5 \mu\text{M}$ $\text{ZnPcS}_{\text{mix}}$ and 10 J/cm^2 was analysed using the Human Cell Death Pathway Finder Profiler™ PCR Array System. $\text{ZnPcS}_{\text{mix}}$ mediated PDT induced changes in gene expression and DFFA-1, BCL-2 and CASP-2 genes were significantly up-regulated as represented in the 3D Profile (a) and the volcano plot (b).

CHAPTER FIVE

DISCUSSION AND CONCLUSION

Although recent reports indicate a decrease in cancer death rates mainly due to improved treatment modalities, cancer remains a major health problem and cause of mortality worldwide, accounting for 7.6 million deaths (around 13% of all deaths) in 2008 (WHO, 2012). About 30% of deaths due to cancer can be prevented and is as a result of high body mass, low fruit and vegetable intake, lack of physical activity, and tobacco and alcohol use (WHO, 2012; Jemal *et al.*, 2010). Cancer of the breast is malignant with metastatic ability and remains resistant to many treatment modalities (Tan *et al.*, 2010, Glas *et al.*, 2006). In South Africa, 1 in 29 women is being diagnosed with breast cancer each year, and 1 in 4 will be diagnosed with the condition in their lifetime (CANSAs, 2011). Breast cancer is the leading cancer in women (CANSAs, 2011). Many cancer therapies are non-specific, killing both normal and cancer cells (Zea and Halaby, 2001). Research to develop novel cancer therapy is under evaluation and PDT is one of the current studied treatments. It is a target therapy for cancer cells and combines three non-toxic elements, namely the PS, laser irradiation and molecular oxygen (Manifold and Anderson, 2011).

Activated by light at a specific wavelength, the PS is the principal inducer of cell damage and interacts with molecular oxygen to produce ROS, which causes cancer cell death (Rao *et al.*, 2008; Plaetzer *et al.*, 2008). The development of photosensitisers is therefore a critical research area in PDT, which focuses on the ability of photosensitisers to enter dense tumour tissues and to be activated within these tissues (Wilson, 2006). Other researches

investigate the development of devices and improvement of the delivery of light activated PS in tissues (Dolmans *et al.*, 2003; Dickson *et al.*, 2002).

In this project, the photosensitising characteristic of a Zinc metallated phthalocyanine (ZnPcS_{mix}) in MCF-7 breast cancer cells was investigated. The MCF-7 cell line is a suitable *in vitro* model cell line to study human breast cancer as they mimic well the problems seen with tumour resistance to treatment (Louie *et al.*, 2010; Dumitrescu and Cotarla, 2005).

In the first study, the subcellular localisation of ZnPcS_{mix} was examined. ZnPcS_{mix} autofluoresces in the red spectrum and fluorescent microscopy was performed to determine its primary sites of localisation. ZnPcS_{mix} did not localise in the nuclei, but examination of the merged image revealed that it localised in the perinuclear area, which corresponds to the Golgi apparatus. However, it was revealed that both mitochondria and lysosomes are the primary sites of ZnPcS_{mix} as shown by the overlap in red (ZnPcS_{mix}) and green (mitochondria and lysosomes) fluorescence. Research conducted by other research groups used similar Zinc-phthalocyanines and reported that those PSs localised in the Golgi apparatus, mitochondria and lysosomes (Wood *et al.*, 1997; Fabrics *et al.*, 2001). Phthalocyanine delivery to the lysosomes is via endocytosis. Furthermore, these lysosome localised phthalocyanines accumulate in microzomes and in the mitochondria (Wood *et al.*, 1997; Fabrics *et al.*, 2001, Kessel and Luo, 1997). Lysosomes, despite their biological activity, are critical primary targets for PSs (Lin, 1991; Geze *et al.*, 1993). ZnPcS_{mix} was used in similar *in vitro* studies in lung and colorectal cancer cells, and it was reported that this PS localised in both mitochondria and lysosomes and its activated form led to good curative effects (Manoto *et al.*, 2012).

Uncoupled mitochondrial permeability transition pores (MPTP) can inhibit the synthesis of energy leading to necrotic cell death. Release of mitochondrial proteins (cytochrome C, AIF, Diablo) activates cascades responsible for the changes to cell structure and function, resulting in apoptosis. Like any phthalocyanine, ZnPcS_{mix} has a strong tendency to aggregate and has decreased water solubility. When in contact with tumour cells, which have a greater affinity for lipoproteins, ZnPcS_{mix} is taken up and retained in the organelles of tumour cells, and upon light activation induces cell death. ZnPcS_{mix} successfully entered the cells and had the ability in the presence of light, to induce cell death as it is localised in or near critical cellular organelles. After laser irradiation, the photodamaging effects of ZnPcS_{mix} on cell morphology, cell viability, cell proliferation and cytotoxicity were noted.

The dose response study revealed that the untreated control cells maintained normal cell morphology and showed the highest level of cell viability and proliferation and the lowest degree of cytotoxicity. Results indicated that ZnPcS_{mix}, when used alone on cells, appeared to have no therapeutic value as the cells remained alive and morphologically identical to the untreated cells. Similar observations were made when only irradiated cells were examined. However, PDT treated cells showed morphological changes, which depended on the ZnPcS_{mix} concentration and laser fluence used. At 0.05 and 0.1 μ M, PDT treated cells showed no major morphological changes. Morphological changes were seen with all PDT treated cells with 0.5 and 1 μ M; cells rounded up as their shape changed and detached from the plate to finally appear as free floating structures in the cell suspension, a process known as anoikis.

Anoikis is a programmed cell death event that takes place when cells lose contact with the extracellular matrix, in our case with the surface of the culture plastic dishes. These changes correspond to those of PDT treated cells undergoing cell death as described by Tesniere and coworkers (2008). Earlier work by Seotsanyana-Makhosi and colleagues (2006) examined the effects of Ge, Si and Sn phthalocyanine PSs and reported no changes in cell morphology on human esophageal carcinoma (SNO) cells and an increase in cell viability and proliferation in the untreated controls and PS controls. Those phthalocyanine PSs did not induce changes in morphology like ZnPcS_{mix}, which remains inactive and unable to affect cell viability and proliferation in the absence of light.

One of the greatest indicators of morphologically damaged/dying cells is their ability to take up certain dyes. Major changes in the Trypan blue exclusion assay were obtained with cells that received 0.5 μM and irradiated with 10 and 15 J/cm^2 ($p < 0.01$), and 1 μM of ZnPcS_{mix} and irradiated with 5, 10 and 15 J/cm^2 ($p < 0.05$, $p < 0.01$ and $p < 0.01$, respectively) in PDT. At these concentrations, cells suffered severe membrane damage following PDT and the Trypan blue dye entered cells through these damaged membranes. All cells require energy to perform their metabolic functions and ATP is the immediate source of energy that drives cellular metabolism. Significant decreases in ATP levels were noted with all PDT treated cells with 0.1 ($p < 0.05$, $p < 0.05$ and $p < 0.01$), 0.5 ($p < 0.01$, < 0.01 and $p < 0.001$) and 1 μM ($p < 0.01$, $p < 0.001$ and $p < 0.001$), except for those that received 0.05 μM of ZnPcS_{mix}.

At higher concentrations, the toxic derivatives from the activated ZnPcS_{mix} (ROS) can affect the activities of the energy metabolic enzymes and therefore

result in a decrease in ATP levels. ZnPcS_{mix} localised in mitochondria and probably Golgi apparatus and can therefore inhibit both protein and energy synthesis. Fagone and Jackowski (2009) proved that PSs that localise in the Golgi apparatus and mitochondria were able to inhibit both protein and energy production, respectively. ZnPcS_{mix} was used in a similar study in PDT and a decrease in both percentage viability and ATP levels was observed in A549 human lung cancer cells (Manoto and Abrahamse, 2011).

An effective treatment on cells with a high rate of proliferation like cancer cells would either prevent or decrease their proliferation. A significant decrease in proliferation was noted with PDT treated cells that received 0.1 μM and irradiated with 15 J/cm^2 ($p < 0.05$), 0.5 μM and irradiated with 10 and 15 J/cm^2 ($p < 0.05$), and 1 μM ZnPcS_{mix} irradiated with 5, 10 and 15 J/cm^2 ($p < 0.05$, $p < 0.01$ and $p < 0.01$, respectively). Wong *et al.*, (2003) also reported a decrease in cell proliferation in FaDu hypopharyngeal carcinoma cells 24 h after PDT. The decrease induced by ZnPcS_{mix} mediated PDT in this study might have been caused by the inability of PDT treated cells to respond to cell stimulating factors and the reduction in ATP as seen in the proliferation assays, or a combination of both. This decrease might also correspond to the decrease in metabolic and mitochondrial enzymatic activity such as the one of diaphorases, which might have become unable to catalyse and reduce alamarblue® reagent as a result of damaged suffered by mitochondria.

Cancer cells are high energy consuming cells and the ATP depletion might have induced a decrease in proliferation. ATP is mainly produced during glycolysis and oxidative phosphorylation through the electron transport chain in mitochondria. During PDT, mitochondrial localised PSs can damage these organelles and induce the inhibition of oxidative phosphorylation and

therefore reduction in ATP levels (Shulok *et al.*, 1998). Growth factors are signalling proteins capable of interacting and instructing cells which lead to specific cellular responses, including cell survival, differentiation and proliferation. These interactions are through binding to specific transmembrane receptors on the target cells (Lee *et al.*, 2010). A study on human K562 myelogenous leukemia cells treated with Calixarenes mediated PDT showed that surviving cells after irradiation lost membrane integrity and mitochondrial function (Neagu *et al.*, 2010).

In the final assay of this dose dependent study, MCF-7 cell membrane integrity after PDT was assessed. PDT aims to kill cancer cells and therefore it should be toxic to those cells. LDH leakage is one of the signs of cytotoxicity and evidence of LDH leakage into the culture media as a result of the damage suffered by the cellular components (membranes, DNA, fatty acids, proteins) due to PDT has been established before (Broker *et al.*, 2005; Manoto and Abrahamse, 2011). Photofrin (II) mediated-PDT has been reported to have induced a high level of LDH release and damage to both HeLa and Cask cell membranes (Das *et al.*, 2000).

After 24 h incubation, PDT treatment induced an increase in cell membrane damage. A significant increase in the level of LDH was detected in PDT treated cells with 0.05, 0.1, 0.5 and 1 μM ZnPcS_{mix} ($p < 0.05$, $p < 0.01$, $p < 0.01$ and $p < 0.01$ respectively). With this assay, the PDT treatment showed cytotoxic effects, which indicated increased damage in cell structure and were associated with the significant decrease in vital cell activity (ATP production and proliferation rate). As seen with the Trypan blue exclusion assay, which is also based on membrane damage, ZnPcS_{mix} mediated PDT induced damage in cell membranes and a decrease in cell viability, and showed similar

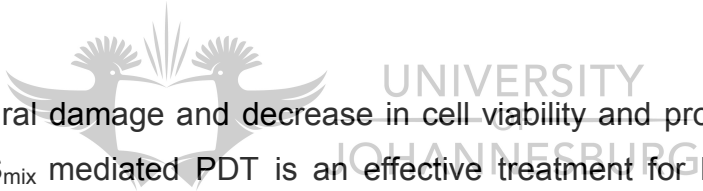
cytotoxic effects to those of Photofrin (II) (Das *et al.*, 2000). Activated ZnPcS_{mix} led to an effective antitumor activity that relies on the generation of ROS during PDT. Additionally, ZnPcS_{mix} localised in critical organelles, which have been shown in previous studies to be accumulation sites for PSs during PDT.

After the ZnPcS_{mix} dose dependent study, different samples of MCF-7 cells were treated with both a defined concentration of Hypericin (0, 0.5, 1, 1.5, 2, 4 and 6 μM) and laser irradiation (0, 5, 10, and 15 J/cm^2). Thereafter, the Trypan blue exclusion assay was performed. A cell viability decrease around 50% was obtained when cells were treated with 4 μM and 10 J/cm^2 . At a similar laser fluence, the same percentage in cell viability was obtained with 0.5 μM ZnPcS_{mix} after PDT. The newly synthesised ZnPcS_{mix} was therefore 8 times stronger than the naturally occurring Hypericin. Hypericin is a naturally occurring PS and its characteristics include photodynamic oxidising potential, tumour localisation ability, high singlet oxygen quantum yield upon illumination and minimal dark toxicity (Head *et al.*, 2006). Hypericin has the ability to induce PDT in cancer cells both *in vivo* and *in vitro* (Head *et al.*, 2006; Chen *et al.*, 2001; Assefa *et al.*, 1999). Based on its relatively low effectiveness, it was decided not to continue with Hypericin.

The characteristics of the natural occurring sensitisers (Hypericin) were thoroughly studied and the first generation sensitisers (porphyrins) were developed. The latter ones were further studied and second generation sensitisers (Phthalocyanines) were developed. ZnPcS_{mix} absorbs light near the infrared region of the electromagnetic spectrum, which confers a better light penetration into tumour tissues. Additionally, Phthalocyanine PSs are lipophilic compounds with a better chemical structure for better retention by

tumour tissues. They have sulphate groups attached to their periphery to increase their solubility in biological solvents.

When compared to other second generation PSs, Phthalocyanines have central metal atoms which enhance significant singlet oxygen quantum yield. Moreover, the accumulation of Hypericin into neoplastic cells decreased with time as the PS was released from lipoprotein complexes and showed low fluorescence intensity in tumour tissues (Van de Putte *et al.*, 2005). Therefore more Hypericin is needed to induce the same effects of a newly synthesised PS with better solubility characteristics, improved penetration properties, better retention index into tumour cells, and higher absorption of light and enhanced singlet oxygen quantum yield.



The structural damage and decrease in cell viability and proliferation proved that ZnPcS_{mix} mediated PDT is an effective treatment for breast cancer *in vitro*. Cell death mechanisms were studied to determine which mode of cell death mode was induced by this treatment. As previously mentioned, the change in both cell viability and morphology was similar to those of apoptotic cells. Flow cytometric analysis revealed that before PDT, most cells remained viable and stained negative for Annexin V-FITC and PI. After PDT or treatment with Actinomycin D, most cells stained positive for these dyes and apoptotic cells predominated over necrotic and normal cells, with more than 65% of cells stained positive for Annexin V-FITC. This finding was consistent with the work of Chiu and colleagues (2003), which found that apoptotic events were identified after PDT using a Silicon phthalocyanine. Apoptosis was also reported to be the induced cell death mode after PDT and the intrinsic pathway was largely dependent on the caspase activation cascade after the release of cytochrome and other apoptogenic factors such as AIF

(Wei *et al.*, 2001; Chen *et al.*, 2001; Buytaert *et al.*, 2005). Apoptosis is induced either through the receptor (extrinsic) or mitochondrial (intrinsic) pathway (Fulda, 2009). In normal cells, the phospholipid phosphatidylserines are localised in the cytosolic leaflet of the plasma membrane (Koopman *et al.*, 1994). Due to damage suffered by cells that resulted in structural changes, the phospholipid phosphatidylserines relocated to the outer leaflet or nucleic acids become accessible. Annexin V binds to phospholipid phosphatidylserines of apoptotic cells and PI to nucleic acid of necrotic cells (Martin *et al.*, 1995; Lecoecur, 2002).

Apoptotic cells demonstrate dynamic structural changes, such as chromatin condensation and nucleosomal DNA fragmentation. Hoechst staining and fluorescent microscopy was reported to be efficient techniques to detect apoptotic events such as nuclear condensation and DNA fragmentation (Allen *et al.*, 2001). Hoechst staining and fluorescent microscopy was performed to determine the occurrence of apoptotic nuclear condensation over a period of 15 h after irradiation. The longer the cells were incubated before Hoechst staining, the smaller the nuclei radius was. The presence of smearing seen after 3 h is an indication of nuclear degradation and the identified nuclei had a reduced diameter when compared to the control. Nuclear condensation became evident from 3 h after PDT. This time coincides with other works, where the identification of apoptotic morphological changes such as chromatin condensation and nuclear fragmentation started to be evident 3 h after PDT (Fabrics *et al.*, 2001; Allen *et al.*, 2001). It has been shown that during apoptosis, AIF and Cyclophilin A (Cyp A) mediate chromatin condensation into degradation by associating the nuclear content with proteins into apoptotic bodies (Galluzzi *et al.*, 2009). The entire nuclear content collapses outward against their periphery (Tone *et al.*, 2007).

Nuclear fragmentation was reported to occur before the chromatin condenses when a cleft in the nuclear sap forms at the periphery or by budding. Budding involves chromatin condensation resulting in clumps that press against the nuclear envelope, and protruding and budding from the nuclear membrane (Coleman *et al.*, 2003). Chromatin is composed of nucleosomes and each nucleosome consists of four kinds of core histones (H2A, H2B, H3, and H4). Histones interact with roughly 200 base pair long segments of DNA (Ajiro, 2000). An ELISA was performed to detect and quantify the nucleosomal fragmented DNA bound to anti-histone antibodies (mono- and oligonucleosomes) subsequent to the induction of apoptosis. DNA fragmentation is a well-established marker of apoptosis and ZnPcS_{mix} mediated PDT led to a significant level of DNA fragmentation in MCF-7 cells. Other studies also reported similar high levels of DNA fragmentation with 88% DNA fragmentation seen 24 h after 5 ALA mediated PDT of Jurkat cells (Gad *et al.*, 2001). Kessel and Luo (1996) observed apoptotic DNA fragmentation 1 h after PDT in murine leukemia cells, using two PSs that localised in lysosomes. During apoptosis, the effector caspase-3 cleaves the inhibitor of caspase activated DNase (ICAD) and releases the caspase activated DNase (CAD). CAD cleaves DNA at the internucleosomal linker sites between the nucleosomes. DNA fragmentation is a secondary event of apoptosis as a result of the initial action of caspase-3 on ICAD. Furthermore, most mammalian apoptotic cells demonstrate unique phosphorylation of H2B, which is associated with apoptosis specific nucleosomal DNA fragmentation and chromatin condensation. This unique phosphorylation of H2B is a useful biochemical hallmark of apoptotic cells (Ajiro, 2000).

Real-time RT-PCR was performed to evaluate the gene expression after ZnPcS_{mix} treatment alone and ZnPcS_{mix} mediated PDT on MCF-7 cells. The Human Cell Death PathwayFinderTM PCR Array was used to determine the

expression of 84 genes involved in the different cell death pathways. The normalisation, fold change and statistics were automatically performed by the PCR Array data analysis software. The student's t-test was used to calculate the P values from the replicate $2^{\Delta\text{Ct}}$ values or fold change for each gene of the untreated cells (control), ZnPcS_{mix} treated cells and PDT treated cells. None of the genes in ZnPcS_{mix} treated cells was found to be significantly regulated, but three genes were significantly up-regulated after PDT. B-cell lymphoma 2 (BCL-2, Gene bank ID: NM 000633), caspase 2 (casp-2, Gene bank ID: NM 032982) and DNA fragmentation factor alpha (DFFA, Gene bank ID: NM 004401) and all their respective gene products are involved in the apoptotic cell death pathway.

Alpha (α) DNA fragmentation factor is a 45 kD subunit of the heterodimer protein that catalyses both DNA fragmentation and chromatid condensation downstream of caspase-3. Caspase-3 activates DNA fragmentation factor (β -subunit) by proteolytic cleavage of α subunit and its dissociation from the rest of the protein. The activated form of the DNA fragmentation factor modulates the apoptotic events, which include DNA fragmentation into nucleosomal units and chromatid condensation. Published reports state that apoptosis is the mechanism that removes toxic, cell debris and often followed by shrinkage and cell fragmentation (Lui *et al.*, 1997). It was established that DNA fragmentation factor is required for genomic stability in mammalian cells and the protein is an important suppressor for cancer (Yan *et al.*, 2006).

Caspase-2 belongs to a family of cysteine proteases that are involved in cell death and inflammatory pathways (Alnamri *et al.*, 1996). Caspase-2 proteolytically cleaves proteins and associates with other proteins involved in apoptosis. In response to DNA damage, this enzyme also interacts with other

proteins to form an activation platform for proteases, known as a PIDDosome, a multiprotein complex constituted of the p53-induced protein with a death domain (PIDD) (Manzl *et al.*, 2012). Caspase-2 also induces the release of cytochrome C and other mitochondrial apoptogenic proteins including AIF and smac (secondary mitochondria derived activator caspase) into the cell cytoplasm. This release is enough to activate other mitochondrial apoptosome *in vitro* (Bouchier-Hayes, 2010). Caspase is therefore a direct effector of the mitochondrial apoptotic pathway.

In response to the high level of mitochondrial apoptogenic proteins in the cytosol such as cytochrome C, BCL-2 is overexpressed. BCL-2 is a member of a family of apoptotic regulated proteins and it is located on the outer membrane of the mitochondria. It was shown that high levels of cytosolic cytochrome C induced the overexpression of BCL-2 (Yang *et al.*, 1997). One of the main roles of the BCL-2 protein is to prevent apoptosis by reducing the release of cytochrome C.

This cell death study had shown that Annexin V stained cells were the most abundant and underwent both nuclear condensation and DNA fragmentation after PDT. The observed nuclear condensation and fragmentation degraded nucleic acids into their bases and nucleotides. ZnPcS_{mix} primarily localises in mitochondria and could have induced mitochondrial damage after irradiation. Such damage was evident with the release of mitochondrial proteins including AIF that mediates nuclear condensation, cytochrome C and other apoptogenic factors. Such proteins trigger further cell degradation after the formation of apoptosomes in the cytosol. The apoptosomes activate more proteins including caspase-3, which is the main effector of apoptosis. Caspase-3 causes DNA damage and other caspase activation. The

overexpressed caspase-2 induced stress and apoptosis by the release of cytochrome C, AIF and smac proteins. The release of cytochrome C as a response to the overexpression of caspase-2 confirmed the action of apoptotic proteins and the induction of the mitochondrial apoptotic pathway following PDT.

The uptake and retention of ZnPcS_{mix} in MCF-7 human breast cancer cells was studied and the PS localised in lysosomes, mitochondria and around the nuclei (the Golgi apparatus). These sites are common targets of photosensitisation. Diffusion across the cell membrane was the most likely mode of entry. PSs may undergo relocalisation after irradiation and these sites are therefore identified as the primary sites. Besides effective subcellular uptake, the PS had no or minimal effect in the dark. Both cells treated with ZnPcS_{mix} alone or irradiation alone did not present any significant change compared to the untreated control cells. However, when ZnPcS_{mix} and irradiation were associated during PDT, cell damage occurred in a dose dependent manner. At lower concentrations, ZnPcS_{mix} did not induce significant changes, but as the concentration increased the phototoxic effects became more pronounced. ZnPcS_{mix} is an effective inducer of singlet oxygen with improved photo-oxidising abilities. The PS displayed appreciable photosensitivity at a low concentration when compared to Hypericin. ZnPcS_{mix} was able to induce cell damage at a concentration 8 times lower than that of Hypericin. Our study demonstrated that apoptotic cells are the most abundant and also favoured by ZnPcS_{mix} which is localised in mitochondria. Disruption of mitochondrial membrane function may be responsible for apoptotic events such nuclear condensation and fragmentation. Furthermore, three genes that are involved in the apoptotic cell death pathway were found to be up-regulated. Apoptosis is a cell death mechanism that removes toxins and DNA fragmentation ensures the genetic stability and removal of damaged cells.

Additionally, caspase-2 triggered the release of apoptogenic proteins, which lead to more damage. ZnPcS_{mix} mediated PDT effects led to an efficient cell death response in the MCF-7 cell line. The opportunity of controlling the mechanism of cell death has a great importance in the clinical context and the mitochondrial apoptotic pathway can be regulated, therefore it is a suitable mode of cell death for clinical studies.

In conclusion, ZnPcS_{mix} was successfully taken up and retained in the mitochondria, lysosomes and around the nuclei of MCF-7 human breast cancer cells. The activated PS exhibited good photosensitising characteristics and induced a decrease in cell viability and proliferation, and an increase in cytotoxicity. At a concentration 8 times lower than that of Hypericin and when used in conjunction with irradiation at 10 J/cm², the PS led to 50% decrease in viability and the combination was used to study the cell death. An increase in apoptotic cell population, nuclear degradation and an increase in expression of three apoptotic genes were observed 24 h post PDT. Apoptosis was identified as the induced cell death pathway. However, the retention of ZnPcS_{mix} on normal cells and effects on blood vessels, inflammation and immune response *in situ* neoplasia need to be studied and if they are found to be limited, future work would be advised to determine whether the results obtained in this *in vitro* study, could be applied in a clinical situation.

REFERENCES

Abrahamse H., Kresfelder T., Horne T., Cronje M. and Nyokong T. (2006) Apoptotic inducing ability of a novel photosensitizing agent, GE sulfophthalocyanine, on oesophageal and breast cancer cell lines, *SPIE International Optics and Photonics-Mechanisms of Photodynamic Therapy* **6139**:17-29.

Ajiro K. (2000) Histone H2B phosphorylation in mammalian apoptotic cells. An association with DNA fragmentation, *Journal of Biology and Chemistry* **275**:439-443.

Alberts B., Johnson A., Lewis J., Raff M., Roberts K. and Walter P., Cell movements and the shaping of the vertebrate body In: *Molecular Biology of the Cell*, 4th ed. New York: Garland Science, 2002, pp. 813-849.

Allen S., Sotos J., Sylte M.J., and Czuprynski C.J. (2001) Use of Hoechst 33342 staining to detect apoptotic changes in bovine mononuclear phagocytes infected with *Mycobacterium avium* subsp. *Paratuberculosis*, *Clinical and Diagnostic Laboratory Immunology* **8(2)**:460–464.

Alnamri E.S., Livingston D.J., Nicholson D.W., Salvesen G., Thornberry N.A., Wong W.W. and Yuang J. (1996) Human ICE/CED-3 protease nomenclature, *Cell* **87(2)**:171-176.

American Cancer Society (2004) The History of Cancer www.cancer.org/docroot/CRI/content/CRI, Retrieved 2010-10-09.

American Cancer society (2010) Cancer facts and figures 2010, www.cancer.org/acs/, Retrieved 2010-04-15.

American Cancer Society (2013) Cancer facts and figures 2013, Atlanta: America Cancer Society 2013, www.cancer.org/acs/, Retrieved 2013-01-25.

Assefa Z., Vantighem A., Declercq W., Vandenneele P., Vandenneede J.R., Merlevede W., de Witte P.A.M. and Agostinis P. (1999) Activation of the C-Jun N-terminal kinase and P38 mitogen-activated protein kinase signalling pathway protects Hela cells from apoptosis following PDT with Hypericin, *Journal of Biology Chemistry* **274**:8788-8796.

Atossa Genetics (2010) The role of NAF cytology in the identification of atypical ductal hyperplasia, www.atossagenetics.com, Retrieved 2011-02-17.

Benn C.A. (2009) Breast cancer rise alarming, www.health24.com, Retrieved 2010-03-31.

Botto M. (2004) Phosphatidylserine receptor and apoptosis: consequences of a non-ingested meal, *Arthritis Research and Therapy* **6(4)**:147-150.

Bouchier-Hayes L. (2010) the role of caspase-2 in stress induced apoptosis. *Journal of Cellular and Molecular Medicine* **14(6A)**:1212-1224.

Boyle P. and Levin B., World Cancer Report 2008, International Agency for Research on Cancer; Boyle and Levin ed., IARC Scientific Publication, Lyon IARC, 2008, pp 1-260, www.iarc.fr/en/publications/pdfs-online/wcr/2008, Retrieved 2012-04-23.

Brasseur N. Sensitizers for Photodynamic therapy: phthalocyanines In: Comprehensive series in photochemical and photobiological sciences, T.

Patrice ed., the Royal Society of Chemistry, Thomas Graham house, Cambridge, UK, 2003, volume 2, pp. 109-116.

Bray F. Ren J.S., Masuyer E. and Ferlay J (2013) Global estimates of cancer prevalence for 27 sites in the adult populations in 2008, *International Journal of Cancer* **132(5)**:1133-1145.

Breast Cancer Organization (2009) Treatment and side effects of breast cancer, www.breastcancer.org, Retrieved 2010-10-12.

Broker L.E., Kruyt F.A.E and Giaccone G. (2005) Cell death independent of caspase: Review, *Clinical Cancer Research* **11**:3155-31561.

Buchholz J., Kaser-Hotz B. and Khan T. (2005) Optimizing PDT: In vivo pharmacokinetics of liposomal meta-(tetrahydroxyphenyl) chlorin in feline squamous cell carcinoma, *Clinical Cancer Research* **11(20)**:7538-7544.

Bustin S.A., Benes V., Nolan T. and Pfaffl M.W. (2005) Quantitative real-time RT-PCR: a perspective, *Journal of Molecular Endocrinology* **34**:597-601.

Buytaert W., Sevink J. and Leeuw B.D. (2005) Clay mineralogy of the soils in the south Ecuadorian páramo region, *Geoderma* **127**:114-129.

Calin M.A. and Parasca S.V. (2006) Photodynamic therapy in oncology, *Journal of Optoelectronics and Advanced Materials* **8(3)**:1173-1179.

CancerNet (2012) Breast cancer, www.cancer.net, Retrieved 2012-03-26.

CANSA (2011) Research: breast cancer type, www.cansa.org.za, Retrieved 2012-02-10.

Castano A.P., Demidova T.N., and Hamblin M.R. (2005) Mechanisms in photodynamic therapy: part two—cellular signaling, cell metabolism and modes of cell death, *Photodiagnosis and Photodynamic Therapy* **2**:1–23.

Chemistry About (2009) Porphyrin chemical structure, www.chemistry.about.com, Retrieved 2009-09-17.

Chen B., Xu Y., Roskams T., Delarey E., Agostinis P. Vandenheede J.R and de Witte P.A.M. (2001) Efficacy of antitumoral PDT with Hypericin: Relationship between biodistribution and photodynamic effects in the RIF-1 mouse tumor model, *International Journal of Cancer* **93**:275-282.

Chen C.H., Hung H.S. and Hsu S. H. (2008) Low energy laser irradiation increases endothelial cell proliferation, migration and eNOS gene expression possible via PI3k signal pathway, *Laser in Medical surgery* **40** 46-59.

Chipuk J.E. and Green D.R. (2005) Mitochondrial regulators of caspase-independent cell death, *Nature Reviews Molecular Cell Biology* **6**:268-275.

Chiu S.M, Xue L.Y, Usuda J., Azizuddin K. And Oleinick N.L. (2003) Bax is essential for mitochondrion-mediated apoptosis but not for cell death caused by PDT, *British Journal of Cancer* **89**:1590-1597.

Clark R.A., Snedeker S. and Devine C. (2002) Estrogen and breast cancer risk: factors of exposure; breast cancer and environmental risk factors in New York State; Sprecher Institute for comparative cancer research, Cornell University, www.envirocancer.cornell.edu, Retrieved 2010-07-20.

Coleman C.A., Barbara E. H., McDougal J.N. and Rogers J.V. (2003) The effect of m-xylene on cytotoxicity and cellular antioxidant status in rat dermal equivalents, *Toxicology Letters* **142**:133-142.

Das H., Koizumi T., Sugimoto T., Yamaguchi S., Hasegawa K., Tenjin Y., and Nishimura R. (2000) Induction of apoptosis and manganese superoxide dismutase gene by Photodynamic therapy in cervical carcinoma cell lines, *International Journal of Clinical Oncology* **5**:97-103.

Davey H.M. and Kell D.B. (1996) Flow cytometry and cell sorting of heterogeneous microbial populations: the importance of single-cell analyses, *Microbiological Reviews* **60(4)**:641-696.

Decreau R., Richard M.J., Verrando P., Chanon M. and Julliard M. (1999) Photodynamic activities of silicon phthalocyanines against achromic M6 melanoma cells and healthy human melanocytes and keratinocytes, *Journal of Photochemistry and Photobiology* **48**:48-56

Dickson G.E.F., Goyan R.L. and Pottier R.H. (2002) New direction in PDT, *Cellular and Molecular Biology* **48(8)**:939-954.

Dolmans D.E., Fukumura D. and Jain R.K. (2003) PDTY for cancer, *Nature Review Cancer* **3(5)**:380-387.

Dougherty T.J., Gomer C.J., Henderson B.W., Jori G., Kessel D., Korblik M., Moan J. and Peng Q. (1998) Photodynamic Therapy, *Journal National Cancer Institute* **90**:889-905.

Drabsch Y., Hugo H., Zhang R., Dowhan D.H., Miao Y.R., Gewirtz A.M., Barry S.C., Ramsay R.G. and Gonda T.J. (2007) Mechanism and requirement

for estrogen-regulated MYB expression in estrogen-receptor-positive breast cancer cells, *National Academy of Sciences of the USA* **104(34)**:13762-13767.

Dumitrescu R.G. and Cotarla I. (2005) Understanding breast cancer risk, *Journal Cellular and Molecular Medicine* **9(1)**:208-21.

EMedicine (2006) Breast Cancer Evaluation, www.emedicine.com/med/TOPIC3287.HTM, Retrieved 2010-02-05.

Engelberg K.H., Amitai S., Kolodkin-gal I. and Hazm R. (2006) Bacterial programmed cell death and multicellular behaviour bacteria, *Plos Genetic* **2(10)**:135-142.

Fabrics C., Valduga G., Miotto G., Borsetto L., Jori G., Garbisa G. and Reddi E. (2001) Photosensitization with Zinc(II) phthalocyanine as a switch in the decision between apoptosis and necrosis, *Cancer Research* **61(20)**:7495-7500.

Fagone P. and Jackowski S. (2009) Membrane phospholipid synthesis and endoplasmic reticulum function, *Journal of Lipid Research* **53**:311-316.

Fayed L. (2009) The history of cancer, www.cancer.about.com, Retrieved 2010-10-25.

Fearon E.R. and Vogelstein B. (1990) A genetic model for colorectal tumorigenesis, *Cell* **61(5)**:759-67.

Fonseca E.J.S., Monkeu C.H. and Padua S. (1999) Measurement of the de Broglie wavelength of a multiphoton wave packet, *Physic Revue Letters* **82(14)**:2868-2871.

Foster T.H., Pearson B.D., Mitra S. and Bigelow C.E. (2005) Fluorescence anisotropy imaging reveals localization of meso-tetrahydroxyphenyl chlorin in the nuclear envelope, *Photochemistry and Photobiology* **81(6)**:1544–1547.

Frankish H. (2003) 15 million new cancer cases per year by 2020 says WHO, *Lancet* **361**:1278.

Freshney R.I. Culture of animal cells In: A manual of basic technique, 5th ed. New York: John Wiley & Sons, 2005 doi: 10.1002/9780471747598.

Fulda S. (2009) Caspase 8 in cancer biology and therapy, *Cancer Letters* **28**:128-133.

Gad F., Viaug G., Boushira M., Bertrand R. And Bissonnette R. (2001) PDT with 5-Aminolevulinic acid induces apoptosis and caspase activation in malignant T cells, *Journal of Cutaneous Medicine and Surgery* **5(1)**:8-13.

Galluzzi L., Kepp O. and Kroemer G. (2009) RIP Kinases Initiate Programmed Necrosis, *Journal of Molecular Cell Biology* **1**:8–10.

Gewies A. (2003) Introduction to apoptosis, www.celldeath.de/encyclo/aporev Retrieved 2011-04-12.

Geze M., Morliere P., Maziere J.C., Smith K.M. and Sautus R. (1993) Lysosome, atarget of hydrophobic photosensitizers proposed for

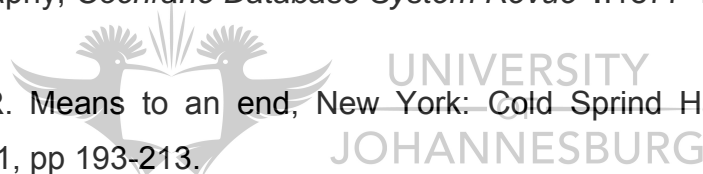
photochemotherapeutic applications, *Journal of Photochemistry and Photobiology Biology* **20(1)**:23-35.

Glas A. M., Floore A., Delahaye L. J. M. J., Witteveen A. T., Pover R. C. F., Bakx N., Lahti-Domenici J., Bruinsma T. J., Warmoes M. O., Bernards R., Lodewyk F. A. and Van der Veer L. J. (2006) Converting a breast cancer microarray signature into a high-throughput diagnostic test, *BMC Genomics* **7**: 278-287.

Gomer C.J., Rucker N., Ferrario A. and Wong S. (1989) Properties and applications of PDT, *Radiation Research Society* **120**:1-18.

Gotzsche P.C. and Nielsen M. (2009) Screening for breast cancer with mammography, *Cochrane Database System Review* **4**:1877-1883.

Green D.R. Means to an end, New York: Cold Spring Harbor Laboratory Press, 2011, pp 193-213.



Grossweiner L.I. (1992) Singlet oxygen: generation and properties, www.photobiology.com/educational, Retrieved 2011-03-05.

Gustafsson A.B. and Gottlieb R.A. (2007) Bcl-2 family members and apoptosis, taken to heart, *American Journal of Cell Physiology* **292**:45-51.

Guyton K.Z., Kyle A.D., Aubrecht J., Cogliano V.J., Eastmond D.A., Jackson M., Keshava N., Sandy M.S., Sonawane B., Zhang L., Waters M.D. and Smith M.T. (2009) Improving prediction of chemical carcinogenicity by considering multiple mechanisms and applying toxicogenomic approaches, *Mutation Research* **681(3)**:230-240.

Head S.C, Lun Q., Sercarz J., and Soxton R. (2006) PDT and tumor imaging of Hypericin-treated squamous cell carcinoma, *World Journal of Surgical Oncology* **4**:87-97.

Hernandez C. (2010) A new way to kill cancer cells, www.smartplanet.com, Retrieved 2010-10-07.

Ho A., Hua K.L., Mooi L.Y. and Weng S.M. (2008) Cancer research: Cancer biology and therapeutics, www.utar.edu.my, Retrieved 2011-02-10.

Hockenbery D.M., Zutter M., Hickey W., Nahm M. and Korsmeyer S.J. (1991) Bcl2 protein is topographically restricted in tissues characterized by apoptotic cell death, *Proceedings of the National Academy of Sciences USA* **88**:6961-6965.

Hu Y. (2009) Hormone and tissue specific tumour suppression, *International Journal of Biological Sciences* **5(1)**:20-27.

International Agency for Research on Cancer (WHO), Cancer Incidence in Five continents (volume VIII) In: Cancer Incidence in Five continents (volume IX), Curado M.P., Edwards B., Shin H.R., Storm H., Ferlay J., Heanue M and Boyle P ed., IARC Scientific Publication No 160, Lyon IARC, 2007, pp 956-961.

Jagtap P. and Szabo C. (2005) Poly (ADP-ribose) polymerase and the therapeutic effects of its inhibitors, *Nature Reviews Drug Discovery* **4**:421-440.

Jemal A., Bray F., Center M.M., Ferlay J., Ward E. and Forman D. (2011) Global cancer statistics, *Cancer Journal for Clinicians* **61(2)**:69-90.

Jemal A., Ward E. and Thun M. (2010) Declining death rates reflect progress against cancer, *Plos One* **5(3)**:9584-9594.

Josefsen L.B. and Boyle R.W. (2007) PDT and the development of metal-based photosensitizers, *Metal Based Drugs* **8**:1-24.

Kantari C. and Walczak H. (2011) Caspase-8 and Bid: caught in the act between death receptors and mitochondria, *Biochimica et Biophysica Acta* **1813**:558-563.

Karpozilos A. and Pavlidis N. (2004) The treatment of cancer in Greek antiquity, *European Journal of Cancer* **40(14)**:2033–2040.

Kaufmann T., Tai L. and Ekert P.G. (2007) The BH3-only protein bid is dispensable for DNA damage- and replicative stress-induced apoptosis or cell-cycle arrest, *Cell* **129**:423-433.

Keller D.K., Bastian J., Thews O. and Vaupe P. (2003) Enhanced effects of ALA-based PDT through local hyperthermia in rat tumours, *British Journal of Cancer* **89**:405-411.

Kessel D. and Luo Y. (1996) Delayed oxidative photodamage induced by PDT, *Photochemistry and Photobiology* **64(3)**:601-604.

Kessel D. and Luo Y. (1997) Initiation of apoptosis versus necrosis by PDT with chloroaluminium phthalocyanine, *Photochemistry and Photobiology* **66(4)**:479-483.

Kessel D. and Oleinick N.L. (2010) Photodynamic therapy and cell death pathways, *Methods in Molecular Biology* **635**:35-46.

Kirste M., Cox R., Vernon D., Griffiths J. and Brown S. (2002) In Vitro photodynamic activity of a series of methylene blue analogues, *Photochemistry and Photobiology* **75(4)**:392–397.

Klionsky D.J. (2007) Autophagy: from phenomenology to molecular understanding in less than a decade, *Nature Reviews Molecular Cell Biology* **8**:931-937.

Konopka K. and Goslinski T. (2007) Photodynamic Therapy in Dentistry, *Journal of Dental Research* **86(8)**:694-707.

Koopman G., Reutelingsperger C.P., Kuijten G.A., Keehnen R.M., Pals S.T. and van Oers M.H. (1994) Annexin V for Flow Cytometric Detection of Phosphatidylserine Expression on B Cells Undergoing Apoptosis, *Blood* **84**:1415-1420.

Korbelik M. and Cecic I. (1998) Contribution of myeloid and lymphoid host cells to the curative outcome of mouse sarcoma treatment by PDT, *Cancer Letters* **137**:91-98.

Kroemer G., Galluzzi L. and Vandenabeele P. (2009) Classification of cell death: recommendations of the Nomenclature Committee on Cell Death 2009, *Cell Death Differentiation* **16**:3-11.

Lacroix M. (2006) Significance, detection and markers of disseminated breast cancer cells, *Endocrine-Related Cancer* **13(4)**:1033–1067.

Lai Y.L., Chung Y.K., Tan H.C., Yap H.F., Yap G., Ooi E.E., Ng L.C. (2007) Cost-effective real-time reverse transcriptase PCR (RT-PCR) to screen for Dengue virus followed by rapid single-tube multiplex RT-PCR for serotyping of the virus, *Journal of Clinical Microbiology* **45(3)**:935-941.

Lamkanfi M., Festjens N., Declercq W., Berghe T.V. and Vandenabeele P. (2007) Caspases in cell survival, proliferation and differentiation, *Cell Death and Differentiation* **14**:44-55.

Lecoeur H. (2002) Nuclear apoptosis detection by flow cytometry: influence of endogenous endonucleases, *Experimental Cell Research* **277(1)**:1-14.

Lee K., Silva E.A. and Mooney D.J. (2010) Growth factor delivery-based tissue engineering general approaches and a review of recent development, *Journal of the Royal Society Interface* **6(55)**:153-170.

Lemasters J.J. (2005) Dying a thousand deaths: redundant pathways from different organelles to apoptosis and necrosis, *Gastroenterology* **129**:351-360.

Levine B. and Deretic V. (2007) Unveiling the roles of autophagy in innate and adaptive immunity, *Nature Reviews Immunology* **7**:767-777.

Levine B., Mizushima N. and Virgin H.W. (2011) Autophagy in immunity and inflammation, *Nature* **469(7330)**:323-335.

Lin C.W. (1991) Photodynamic therapy of malignant tumours recent developments, *Cancer Cells* **3**:437-444.

Louie M.C., McClellan A., Siewil C. and Kawabatal L. (2010) The estrogen receptor regulates E2F1 expression to mediate tamoxifen resistance, *Molecular Cancer Research* **8**:343-352.

Lui X., Zou H., Shangter C. and Wang X. (1997). DFF, a heterodimeric protein that functions downstream of caspase-3 to trigger DNA fragmentation during apoptosis, *Cell Death Differentiation* **8**:124-128.

Luke C.J., Pak S.C. and Askew Y.S. (2007) An intracellular serpin regulates necrosis by inhibiting the induction and sequelae of lysosomal injury, *Cell* **130**:1108-1119.

Luksiene Z. (2003) PDT: mechanism of action and ways to improve the efficiency of treatment, *Medicina* **39**:12-17.

Majno G. and Joris I. (1995) Apoptosis, oncosis, and necrosis: an overview of cell death, *American Journal of Pathology* **146**:3-15.

Manifold R.N. and Anderson C.D. (2011) Increase cutaneous oxygen availability by topical application of hydrogen peroxide cream enhances the PDT reaction to topical 5ALA-methyl ester, www.springerlink.com, Retrieved 2011-09-18.

Manoto S.L. and Abrahamse H. (2011) Effect of a newly synthesized Zn sulfophthalocyanine derivative on cell morphology, viability, proliferation, and cytotoxicity in a human lung cancer cell line (A549), *Lasers Medical Sciences* **43**:333-342.

Manoto S.L., Sekhejane P.R., Houreld N.N., Abrahamse H. (2012) Localization and phototoxic effect of zinc sulfophthalocyanine photosensitizer

in human colon (DLD-1) and lung (A549) carcinoma cells (in vitro), *Photodiagnosis and Photodynamic Therapy* **9(1)**:52-59.

Manzl C., Peintner L., Krumschnabel G., Bock F., Labi V., Drach M., Newbold A., Johristone R and Vilunger A. (2012) PIDDosome independent tumor suppressor by caspase-2, *Cell Death Differentiation* **19(10)**:1722-1732.

Martin S.J., O'Brien G.A., Nishioka W.K., McGahon A.J., Mahboubi A., Saido T.C. and Green D.R. (1995) Proteolysis of fodrin (non-erythroid spectrin) during apoptosis, *Journal of Biological chemistry* **270(12)**:6425-6428.

McNaught A.D. and Wilkinson A., Photophysical proces UIPAC In: Compendium of chemical terminology, 2nd ed. Oxford UK, Gold Book, Blackwell Scientific Publications, 1997, pp. 2240-2264.

Melino G. (2001) The Sirens' song, *Nature* **412**:23-28.



Merck Manual of Diagnosis and Therapy (2003) Breast Disorders: Cancer, www.merck.com, Retrieved 2010-02-05.

Mitra A. and Stables G.I. (2006) Topical photodynamic therapy for non-cancerous skin conditions, *Photodiagnosis and Photodynamic Therapy* **3(2)**:116-127.

Molete M. (2009) Position statement on breast cancer, www.cansa.org.za, Retrieved 2009-04-01.

Moor A.C.E, Ortel B. and Tayyaba H. Mechanism of Photodynamic Therapy In: Comprehensive series in photochemical and photobiological sciences, T.

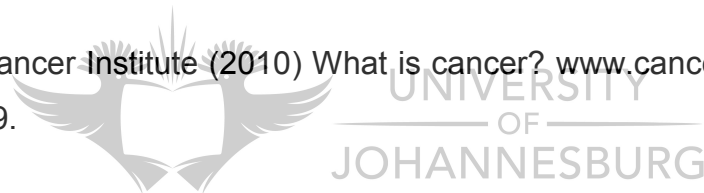
Patrice ed., the Royal Society of Chemistry, Thomas Graham house, Cambridge, UK, 2003, volume 2, pp. 22-57.

Mroz P., Szokalska A., Wu M.X. and Hamblin M.R. (2010) Photodynamic therapy of tumours can lead to development of systemic antigen-specific immune response, *PLoS One* **5**:15194-1599.

National Cancer Institute (2004) Metastatic Cancer: Questions and Answers. www.cancer.gov/cancertopics/factsheet/Sites-Types/metastatic, Retrieved 2010-02-06.

National Cancer Institute (2005) Paget's disease of the Nipple: Questions and Answers, www.cancer.gov/cancertopics, Retrieved 2010-02-06.

National Cancer Institute (2010) What is cancer? www.cancer.gov, Retrieved 2011-01-09.



National Cancer Registry (2008) Statistics, www.cansa.org, Retrieved 2009-04-12.

National Institutes of Health (2007) SEER training modules, www.cancer.gov Retrieved 2012-04-12.

Neagu M, Ion R.M., Manda G., Constantin C., Radu E. and Cristu Z. (2010) Antitumoral effect of calixarenes in experimental photodynamic therapy with K56 with tumour cell line, *Romanian Journal of Biochemistry* **47(1)**:17–35.

Netting R. and Fisher D. (2011) What is a laser? www.spaceplace.nasa.gov Retrieved 2011-05-02.

Newby J.A. and Howard C.V. (2005) Environmental influences in cancer oncology. *Journal of Nutritional & Environmental Medicine* **15(3)**:56-114.

Ning S.B., Wang L. and Song Y.C. (2000) An ELISA Assay for detection of apoptosis in plant cells, *Development and Reproductive Biology* **9(2)**:61-68.

O'Malley S., Schazmann B., Diamond D. and Nolan K. (2007) Preparation and sensor evaluation of a Pacman phthalocyanine, *Tetrahedron Letters* **48**:9003-9007.

Ogunsipe A., Chen J.Y. and Nyokong T. (2004) Photophysical and photochemical studies of Zinc (II) phthalocyanine derivatives – effects of substituents and solvents, *New Journal of Chemistry* **28**:822-827.

Osborne K.M.J. (2007) What does LASER stand for? www.suite101.com, Retrieved 2010-11-26.

Parkin D.M., Bray F., Ferlay J. and Pisani P. (2005) Global Cancer Statistics, *CA Cancer Journal of Clinicians* **55**:74-108.

Parkin D.M. and Fernandez L.M. (2006) Use of statistics to assess the global burden of breast cancer, *Breast Journal* **12(1)**:70-80.

Philippi C., Loretz B., Schaefer U.F. and Lehr C.M. (2010) Telomerase as an emerging target to fight cancer - Opportunities and challenges for nanomedicine, *Journal of Controlled Releases* **146(2)**:228–240.

Plaetzer K., Krammer B., Berlanda J., Berr F. and Kiesslich T. (2008) Photophysics and photochemistry of PDT fundamental aspects, *Laser Medical Sciences* **1**:1-5.

Pratt S.E. and Pollak M.N. (1993) Estrogen and antiestrogen modulation of MCF7 human breast cancer cell proliferation is associated with specific alterations in accumulation of insulin-like growth factor-binding proteins in conditioned media, *Cancer Research* **53**:5193-5198.

Rabinowitz J.D. and White E. (2010) Autophagy and metabolism, *Sciences Magazine* **330(6009)**:1344-1348.

Rada B. and Leto T.L. (2008) Oxidative innate immune defenses by Nox/Duox family NADPH oxidases, *Contribution to Microbiology* **15**:164–187.

Ramsay D.T., Kent J.C., Owens R.A. and Hartmann P.E. (2004) Ultrasound of milk ejection in the breast of lactating women, *Pediatrics* **113**:361–367.

Rao J., Bissonnette R., Suthamjariya K. and Taylor C.R. (2008) Photodynamic Therapy for the Dermatologist (www.emedicine.com/derm/topic636), Retrieved 2010-09-15.

Ray A. and Mittra A.B. (2003) Estrogen and breast cancer, *ICMB Bulletin* **33(2)**:13-19.

Reape T.J., Molony E.M. and McCabe P.F. (2008) Programmed cell death in plant: distinguishing between different modes, *Journal of Experimental Botany* **59(3)**:435-444.

Rosen E.M., Fan S. and Issacs C. (2008) BRCA1 in hormonal carcinogenesis: basic and clinical research, *Endocrine-Related Cancer* **12(3)**: 533-548.

Rousset N., Bourre L. and Thibaud S. Sensitizers in Photodynamic Therapy In: Comprehensive series in photochemical and photobiological sciences, T. Patrice ed., the Royal Society of Chemistry, Thomas Graham house, Cambridge, UK, 2003, volume 2, pp. 61-76.

Ryer A. (1997) Light measurement handbook, www.intl.light.com/handbook, Retrieved 2010-08-02.

Salas C.E., Gomes M.T.R, Hernandes M. and Lopes M.T.P. (2008) Plant cysteine proteinase: Evaluation of the pharmacological activity, *Phytochemistry* **68(12)**:2263-2269.

Sazgarnia A., Bahreyni M.A., Layegh P., Rajabi O. and Ghodsunia R.M. (2010) Liposomal zinc phthalocyanine as a potential agent for PDT of Leishmaniasis, *Indian Journal of Dermatology, Venereology and Leprology* **76(4)**:417-422.

Seotsanyana-Makhosi I., Kresfelder T., Abrahamse H. and Nyokong T. (2006) The effect of Ge, Si and Sn phthalocyanine photosensitizers on cell proliferation and viability of human oesophageal carcinoma cells, *Journal of Photochemistry and Photobiology B. Biology* **83**:55-62.

Shulok R., Klaunig J.E., Selman S.H., Schafer P.J. and Goldblatt P.J. (1998) Cellular effects of hematoporphyrin derivative photodynamic therapy on normal and neoplastic rat bladder cells, *The American Journal of Pathology* **122(2)**:277-283.

Siegel R., Naishadadham D. and Jemal A. (2012) Cancer statistics 2012, *CA Cancer Journal for Clinicians* **62(1)**:10-29.

Sieron A. and Kwiatek S. (2006) Twenty years of experience with PDD and PDT in Poland-Review, *Photodiagnosis and Photodynamic Therapy* **6(2)**:73-78.

Smith C.C.T. and Yellon D.M. (2011) Necroptosis, necrostatins and tissue injury, *Journal of Cellular and Molecular Medicine* **15(8)**:45-49.

Soule H.D., Vazquez J., Long A., Albert S. and Brennan M. (1973) A human cell line from a pleural effusion derived from a breast carcinoma, *Journal of the National Cancer Institute* **51**:1409-1416.

Tan W.S.D., Gerlinger M., Teh B.T. and Swanton C. (2010) Anti-cancer drug resistance: Understanding the mechanisms through the use of integrative genomics and functional RNA interference, *European Journal of Cancer* **46(2)**:166–217.

Taylor R.C., Cullen S.P. and Martin S.J. (2008) Apoptosis: controlled demolition at cellular level, *Nature Reviews Molecular Cell Biology* **9**:231-241.

Tayyaba H., Moore A.C.E. and Ortel B. Holland-Frei Cancer Medicine, 5th ed., Hamilton (ON): BC Decker; 2000, www.ncbi.nlm.nih.gov, Retrieved 2011-05-10.

Tesniere A., Apetoh L., Ghiringhelli F., Joza N., Panaretakis T., Kepp O., Schlemmer F., Zitvogel L. and Kroemer G. (2008) Molecular characteristics of immunogenic cancer cell death, *Cell Death Differentiation* **15**:3-12.

Tone S., Sugimoto K., Tanda K., Suda T., Uchira K., Kanouchi H., Samejima K., Minatogawa Y. and Earnshaw W.C. (2007) Three distinct stages of apoptotic nuclear condensation revealed by time lapse imaging, biochemical

and electron microscopy analysis of cell free apoptosis, *Experimental Cell Research* **313(16)**:3635-3644.

Tromberg B.J., Shah N., Lauming R., Cerussi A., Espinoza J., Pham T., Svaasand L. and Butler J. (2000) Noninvasive *in vivo* characterization of breast tumours using photon migration spectroscopy, *Neoplasia* **2**:26-40.

Tsai Y.C., Hong C.Y., Liu L.F. and Kao C.H. (2004) Relative importance of Na⁺ and Cl⁻ in NaCl-induced antioxidant systems in roots of rice seedlings. *Physiologia Plantarum* **122**: 86-94.

Turro N.J., Ramamurthy V. and Scaiano J.C., Principle of molecular photochemistry: An introduction In: Transition states between photophysical processes, International ed., New York: University Sciences Publishers, Angewandte Chemie, 2008, pp. 240-264.

Tynga I. and Abrahamse H., Caspase-8 properties, functions and regulation during Photodynamic Therapy. In: Advances in Genetics Research, K.V. Urbano ed., Nova Sciences Publishers, 2012, volume 9, chapter 4, pp.107-119.

UNAids organisation (2010) Global report, unaids report on the global aids epidemic, [www.unaids.org/documents, 20101123](http://www.unaids.org/documents/20101123), Retrieved 2013-01-04

Usuda J., Kato H., Okunaka T., Furukawa K., Tsutsui H., Yamada K., Suga Y., Honda H., Nagatsuka Y., Ohira T., Tsuboi M., and Hirano T. (2006) Photodynamic therapy for Lung cancer, *Journal of Thoracic Oncology* **1(5)**:489-493.

Van de Putte M., Roskams T. Vandenheede J.R., Agostinis P. and de Wiite P.A.M. (2005) Elucidation of tumorigenic principle of Hypericin, *British Journal of Cancer* **92**:1406-1413.

Van Loo G., Saelens X., Matthijssens F., Schotte F., Bayaert R., Declercq W. and Vandenabeele P. (2002) Caspases are not localized in mitochondria during life or death, *Cell Death and Differentiation* **9**:1207-1211.

Van Zyl C., Lottering M.L., Steffens F. and Joubert D. (2008) In vitro effect of 2-MEM on MCF-7 and MCF-12A cell growth, morphology and mitotic spindle formation, *Cell Biochemistry* **26**:632-642.

Vanlangenakker N., Berghe T.V., Krysko D.V., Festjens N. and Vandenabeele P. (2008) Molecular mechanisms and pathophysiology of necrotic cell death, *Current Molecular Medicine* **8**:207-220.

Varricchio C.G., American Cancer Society. In: A cancer source book for nurses, 8th ed., Canada, Jones and Bartlett Publishers, 2004, pp 1-580.

Vogelstein B. and Kinzler K.W. (2004) Cancer genes and the pathways they control, *Nature Medicine* **10(8)**:789-799.

Vorobiof D.A. and Ruff P. (2011) Cancer in South Africa and the role of the national cancer registry, www.ascopost.com, Retrieved 2011-09-28.

Vorobiof D.A., Sitas F. and Vorobiof G. (2001) Breast cancer incidence in South Africa, *Journal of Clinical Oncology* **18(19)**:125-127.

Wang L., Zhang Z.G., Zhang R.L., Jiao Z.X., Wang Y., Pourabdollah-Nejad D.S., Letourneau Y., Gregg S.R. and Chopp M. (2006) Neurogenin 1

mediates erythropoietin enhanced differentiation of adult neural progenitor cells, *Journal of Cerebral Blood Flow and Metabolism* **26**:556–564.

Watanabe E., Muenzer J.T. and Hawkins W.G. (2009) Sepsis induces extensive autophagic vacuolization in hepatocytes: a clinical and laboratory-based study, *Laboratory Investor* **89**:549-561.

Wei M.C., Zong W.X., Cheng E.H., Lindsten T., Panoutsakopoulou V., Ross A.J., Roth K.A., MacGregor G.R., Thompson C.B. and Korsmeyer S.J. (2001) Proapoptotic BAX and BAK: a requisite gateway to mitochondrial dysfunction and death, *Science* **292(5517)**:727-730.

Willeit P., Willeit J., Mayr A., Weger S., Oberhollenzer F., Brandstätter A., Kronenberg F. and Kiechl S. (2010) Telomere length and risk of incident cancer and cancer mortality, *JAMA* **304(1)**:69–75.

Wilson B.C. (2006) Photonic and non-photonic based nanoparticles in cancer imaging and therapeutics, *Photon-based Nano-science and Nano-Biotechnology* **239**:121-157.

Wilson J.D., Bigelow C.E., Calkins D.J. and Foster T.H. (2005) Light scattering from intact cells reports oxidative-stress induced mitochondrial swelling, *Biophysical Journal* **88(4)**:2929–2938.

Wong T.W., Tracey E., Oseroff A.R. and Baumann H. (2003) Photodynamic Therapy Mediates Immediate Loss of Cellular Responsiveness to Cytokines and Growth Factors, *Cancer Research* **63**:3812-3818.

Wood S.R., Holroyd J.A. and Brown S.B. (1997) The subcellular localization of Zn (II) phthalocyanines and their redistribution on exposure to light, *Journal of Photochemistry and Photobiology B.Biology* **65(3)**:397-402.

World Health Organisation (2006) World Cancer Day: Global action to avert 8 million cancer-related deaths by 2015, www.who.int/mediacentre, Retrieved 2009-03-26.

World Health Organisation (2010) Global status report on noncommunicable diseases 2010, www.who.int/nmh/publications/ncd, Retrieved 2011-03-26.

World Health Organisation (2012), Cancer, Glocan 2008, www.who.int/mediacentre, Retrieved 2013-01-26.

Yager J.D. (2000) Endogenous estrogen as carcinogens through metabolic activation, *Journal of National Institute* **27**:67-73.

Yan B., Wang H., Peng Y., Hu Y., Wang H., Zhang X., Chen Q., Bedford J.S., Dewhirst M.W. and Li C.Y. (2006) A unique role of DNA fragmentation factor in maintaining genomic stability, *PNAS* **103(5)**:1504-1509.

Yang J., Liu X., Bhalla K., Kim C.N., Ibrado A.M., Cai J., Peng T.I., Jone D.P. and Wang X. (1997) Preventing of apoptosis by Bcl-2: release of cytochrome C from mitochondria blocked, *Science* **275(5303)**:1129-1132.

Youle R.J. and Strasser A. (2008) The Bcl-2 protein family: opposing activities that mediated cell death, *Nature Reviews Molecular Cell Biology* **9**:41-59.

Zea M. and Halaby R. (2001) Lysosomal and mitochondrial changes detected during TNF- α induced apoptosis in MCF-7 human breast cancer cells, *Journal of Young Investigators* **5(1)**:32-47.

Zebu.uoregon.edu, www.zebu.uoregon.edu, Retrieved 2010-09-10.

Zong W.X. and Thompson C.B. (2006) Necrotic death as a cell fate, *Genes & Development* **20**:1-15.



APPENDIX A

LIST OF CONSUMABLES

Table A1: List of consumables used throughout the study.

Items	Catalogue Number	Company
AE buffer	19077	Qiagen
Amphotericin- β	P11-001	PAA Laboratories GmbH
AnnexinV-FITC/PI apoptosis detection kit for apoptosis and necrosis (for flow cytometry): alamarBlue®	A2214	Sigma Aldrich
Biofreezing medium	F2270	Biochrom
CellTiter-Glo® Luminescent Cell Viability kit	G7570	Promega
Centrifuge tube, 50 ml, PP flat top, sterile, bulk	CR430829	Corning Products
Clear nail varnish	NY11553	Sally Hansen®DIV. DIST
Cryogenic vial, Int-thread, 2 ml, round	CR430489	Corning Products
Culture dishes	430165	Adcock Ingram
Coverslips	CG88	Lasec
Cyto Tox96® non-radiative cytotoxicity	G1780	Promega
4'6-diamidine-2-phenylindole (DAPI)	AP402-0010	Sigma Aldrich
1 ml Disposable pipette	BD357522	Beckson Dickinson
2 ml Disposable pipette	BD357507	Beckson Dickinson
5 ml Disposable pipette	BD357543	Beckson Dickinson
10 ml Disposable pipette	BD357551	Beckson Dickinson
25 ml Disposable pipette	BD357525	Beckson Dickinson
Dulbecco's Modified Eagle Medium	INV41966-029	Gibco Invitrogen Corporation
ELISA cell death detection kit	11774425001	Roche
Eppendorf®, Microtubes	Z666521	Sigma Aldrich
Eppendorf®, Microtubes	Z666505	Sigma Aldrich
Eppendorf®, Microtubes	Z666515	Sigma Aldrich
Ethanol absolute	32221	Sigma Aldrich

Falcon (5ml) Polystyrene round bottom tube	BD352054	Beckson Dickinson
Foetal bovine serum	A15-101	PAA Laboratories GmbH
37% Formaldehyde solution	F8775	Sigma Aldrich
Glass slides	MG42	Lasec
Hanks balanced salt solution	INV14170088	Gibco Invitrogen Corporation
Heavy Tin foil	6001007162603	Pick n' Pay
Hoechst 33258	H6024	Sigma Aldrich
Human malignant breast cancer cell line MCF-7	ATCC: HTB 22	Sigma Aldrich
Latex Gloves, medium, powder free	EV40511	Scientific Group
Microscope slides, frosted one side	CLS294875	Corning Products
Penicillin-streptomycin	P11-010	PAA Laboratories GmbH
Phosphate buffered saline	P3744	Sigma Aldrich
Propyl gallate, Fluka	02370	Sigma Aldrich
Quant-IT™ RNA assay	Q32852	Gibco Invitrogen Corporation
QuantiTect Reverse transcription kit	205311	Qiagen
RNeasy kit	74104	Qiagen
RT ² profiler PCR array human cell death	330231-A-12 PAHS-212A	SABiosciences
RT ² qPCR SYBR Gree/ROX	330522	SABiosciences
Tissue culture dish 3.3 cm ² diameter	BD/353001	Beckson Dickson
Tissue culture flask 25 cm ² , angled neck, vent, sterile	CR/423052	Corning Products
Tissue culture flask 75 cm ² , canted neck, anti-tip, vent, sterile	CR/430641	Corning Products
Tissue culture flask 175 cm ² , canted neck, vent, sterile	CR/431080	Corning Products
Triton X-100	T9284	Sigma Aldrich
Trypan Blue powder	T6146	Sigma Aldrich
TrypIExpress	INV12605028	Gibco Invitrogen Corporation
Universal fit pipette tips, 1-	CR4798	Corning Products

200 μ l, Natural, Bulk
Universal fit pipette CR4868
tips, 100-1000 μ l, Bulk
ZnPcS_{mix} powder, molar
mass: 883g/mol

Corning Products

Synthesised and donated
by Prof Tebello Nyokong



APPENDIX B

LIST OF CHEMICALS, SOLUTIONS AND MEDIA

Table B1: List chemicals, solutions and media used during the study.

MCF-7 Cell culture				
Complete DMEM for		DMEM		44.5 ml
cell growth with 10%		FBS		5 ml
FBS		Penicillin-streptomycin		0.25 ml
		Amphotericin		0.25 ml
Complete DMEM for		DMEM		39.5 ml
cell growth with 20%		FBS		10 ml
FBS		Penicillin-streptomycin		0.25 ml
		Amphotericin		0.25 ml
Photosensitisers				
0.0005 M ZnPcS _{mix}		ZnPcS _{mix} powder		0.0005 g
(stock)		0.01 M PBS		1.25 ml
0.0005 M Hypericin		Hypericin powder		1 mg
(stock)		DMSO		4 ml
Sterilisation				
70% Ethanol		Absolute ethanol		70 ml
		Autoclaved distilled water		30 ml
Experiments				
1 µg/ml Actinomycin D		Powdered Actinomycin D		1 mg
		DMSO		0.8 ml
1x Annexin V-FITC/PI		10x binding buffer		1.7 ml
		Autoclaved distilled water		17 ml
		Powdered Propidium Iodide		250 mg
		1x binding buffer		1 ml
ATP Cell Titre-Glo		ATP Cell Titre-Glo buffer		1 ml

reagent	ATP Cell Titre-Glo substrate	0.007 mg
0.01 M PBS	Phosphate buffered dry saline powder	1 packet
	Autoclaved distilled water	1 l
0.1 mg DAPI	5 mg/ml DAPI (stock)	0.2 ml
	Autoclaved distilled water	9.8 ml
3.5% Formalin solution	37% Formaldehyde solution	9.5 ml
	Autoclaved distilled water	90.5 ml
10 mg/ml Hoechst stock	Powdered Hoechst	0.001 g
	Autoclaved distilled water	1 ml
LDH reconstitute substrate	LDH assay buffer	1.2 ml
	LDH substrate mix	0.012 g
0.1 M Propyl gallate in solution with glycerol and PBS	Powdered Propyl gallate	0.212 g
	Concentrated glycerol	9 ml
	0.01 M PBS	1 ml
0.5% Triton-100	Triton-100	0.5 ml
	Autoclaved distilled water	99.5 ml
0.4% Trypan blue	Powdered Trypan blue	0.4 g
	HBSS	100 ml

APPENDIX C

CALCULATIONS

C1. Calculation of cell viability

- For cell viability assays the percentage of viable cells was determined after using the Trypan blue exclusion assay.
- Once 100 µl of cellular suspensions were stained with 0.4% (w/v) Trypan blue in HBSS, and transferred to the hemocytometer slide which was placed under a light microscope they were counted using the 10 x objective .
- The number of viable cells which remained unstained and so were clear in colour were noted and the number of non viable cells which stained blue was noted.
- All five squares of both chambers of the hemocytometer were counted.
- An average count of viable cells which per square was determined by adding up the total number of viable cells per all the squares counted on the hemocytometer and dividing this total number by 10 (the total number of square counted on the hemocytometer).
- An average count of non viable cells per square was determined by up the total number of non viable cells per the entire square counted on the hemocytometer and dividing this total number by 10 (the total number of squares counted on the hemocytometer).
- The average number of total cells per square was determined by adding the average count of viable cells per square to the average count of non viable cells per square.
- The percentage of viable cells per an experimental or control group calculated using the following formula:

$$\% \text{ cell viability} = \frac{(\text{average count of viable cells per square}) \times 100}{(\text{average number of total cells per square})}$$

C2. Calculation of cell seeding for culturing of cell in flasks

- The number of viable cells obtained during cell viability calculation (C1) was multiplied by the total resuspension volume of cell media.
- Once the total number of viable cells contained within the total resuspension volume of cell media was determined, the seeding ratio of cells per a cm^2 was divided by this number, in order to obtain the volume of cells required to cover a cm^2 surface area of the flask.
- This number was then multiplied by the total surface area of the actual culture flask and the volume of the cells from the cell suspension that had to be added to the culture flask in order to obtain the correct seeding ratio of cells would be acquired.
- Example calculation: if the average count of viable cells per a square after performing a Trypan blue was 180, and the cell pellet was resuspended in 5 ml of complete culture media and you wanted to produce a 75 cm^2 cell culture flask with a seeding ratio of 5×10^5 cells/ cm^2 the following would perform calculation:
 - Viable cells = $(180 \text{ viable cell / square}) (10) (10^4)$
 - $= 1.8 \times 10^7 \text{ cells / ml}$
 - $1.8 \times 10^7 \text{ cells} \times 5 \text{ ml} = 9 \times 10^7 \text{ cells / 5 ml}$
 - $(5 \times 10^5 \text{ cells / cm}^2) / (9 \times 10^7 \text{ cells / 5ml}) = 0.005 \text{ ml/cm}^2$
 - $(0.028 \text{ ml/cm}^2) (75 \text{ cm}^2) = 0.375 \text{ ml}$
 - Therefore from the 5 ml cell suspension you would remove 0.375 ml and pipette it into a 75 cm^2 cell flask containing complete cell culture medium in order to seed the flask at a ratio of 5×10^5 cells/ cm^2

C3. Calculation of cell seeding for cryopreservation

- The number of viable cells obtained during cell viability calculation (C1) and was divided by the required cryopreservation seeding ratio of cells (4×10^6) in order to obtain the volume of freezing media to be added.

- After centrifugation, the determined volume of freezing media was added to resuspend the cells and then 2 ml was allocated to each cryovial, in order to acquire the correct seeding ratio.

Example calculation: if the average count of visible cells per a square after performing a Trypan blue was 160, and the cell pellet was suspended in 5 ml of HBSS and you wanted to cryopreserve cells with a seeding ratio of 4×10^6 cells/ml.

Calculation:

- Viable cells / ml = (160 viable cells/ square)(10) (10^4)
- $= 1.6 \times 10^7$ cells /ml
- 1.6×10^7 cells / ml x 5 ml = 8×10^7 cells / 5 ml
- $(8 \times 10^7 \text{ cells}) / (4 \times 10^6 \text{ cells}) = 20$ ml cryovials
- $20 \text{ ml} / (2 \text{ ml of cell suspension per vial}) = 10$ cryovials

C4. Calculation for seeding of cell culture plates

- To calculate the cell seeding ratio into a culture plate, the number of viable cells (C1) per ml, was multiplied by the total suspension volume cell media.
- Once the total number of viable cells contained within the total suspension volume of the cell media was determined, this number was divided by the required culture plate seeding ratio of cells, in order to obtain the number of cell culture plates the cell suspension could produce.
- The total suspension volume of cell media was then divided by the total of culture plate the cellular suspension could produce, obtaining the volume of cellular suspension to be added to each culture plate in order to acquire the correct seeding ratio.
- The volume of cellular suspension to added to each culture plate was then subtracted from the volume of complete cell culture medium to be

contained within the culture plate in order to obtain the correct volume of complete cell culture medium to be added to each culture plate, before adding the calculated volume of cell suspension so each culture plate contained the exact same volume of culture media.

Example calculation: if the average count of viable cell per cells per square after performing a Trypan blue was 80, and the cell pellet was resuspension in 2 ml of complete culture media and you wanted to calculate how many 3.3 cm³ in diameter culture plates containing 3 ml of complete culture medium could be produced with a seeding ratio of 5 x 10⁵ cells / 3.3 cm³, then would perform the following calculation:

- Viable cells / ml = (80 viable cells / square)(10)(10⁴)
= 8 x 10⁷ cells / ml
- 8 x 10⁷ cells / ml x 2 ml = 1.6 x 10⁸ cells / 2 ml
- (1.6 x 10⁸ cells / 2ml) / (5 x 10⁵ cells / 3.3 cm²) = 320 plate
- (2 ml)/(320 culture plates)= 0.00625 ml of cell resuspension per culture plate
- (3 ml volume of complete culture medium) – (0.00625 ml of cell resuspension per culture plate) = 2.99375 ml of complete cell culture medium to be added to the culture plate.
- Therefore from 2 ml cellular resuspension you would remove 0.00625 ml and pipette it into a 3.3 cm³ in diameter culture plate containing 2.99375 ml of complete cell culture medium, in order to obtain a culture plate which contains a total volume of 3 ml of complete culture medium and seeding ratio of 5 x 10⁵ cells / 3.3 cm³.

C5. Calculation of working concentration of 0.5 μM Hypericin

- A stock solution of 0.5 mM Hypericin was made.
- The culture plate contained 1 ml of relevant complete medium. Thus if you wanted to add working concentration of 0.5 μM Hypericin which is equivalent to 0.0005 mM Hypericin to this culture plate the stock concentration of 0.5 mM Hypericin would have to be diluted
- The following calculation was done:
$$C_1 V_1 = C_2 V_2$$
$$(0.5 \text{ mM Hypericin}) V_1 = (0.0005 \text{ mM Hypericin}) (1 \text{ ml of medium})$$
$$V_1 = 0.001 \times 1 \text{ ml} = 1 \mu\text{l}$$
- Therefore 1 μl of the stock solution of 0.5 mM Hypericin photosensitiser was added to the culture plate which contained 1 ml of relevant complete growth culture medium in order to acquire a working concentration of 0.5 μM Hypericin.
- Similar calculations were performed for the other working concentrations of Hypericin used and for the $\text{ZnPcS}_{\text{mix}}$.

Table C1: Calculation of Hypericin (stock) volumes that were added for different concentrations.

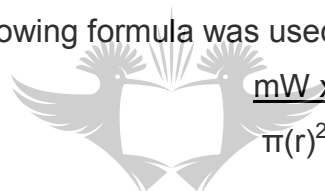
0.5 mM Hypericin	
Working concentration tested in human melanoma dose response essay	Calculated volume of Hypericin added to culture plate of cells containing 1ml of media
0.5 μM Hypericin	1 μl
1 μM Hypericin	2 μl
1.5 μM Hypericin	3 μl
2 μM Hypericin	4 μl
4 μM Hypericin	8 μl
6 μM Hypericin	12 μl

Table C2: Calculation of ZnPcS_{mix} (stock) volumes that were added for different concentrations.

0.5 mM ZnPcS_{mix}	
Working concentration tested in human melanoma dose response essay	Calculated ZnPcS _{mix} volume of Hypericin added to plate of cells containing 1ml of media
0.05 μM ZnPcS _{mix}	0.1 μl
0.1 μM ZnPcS _{mix}	0.5 μl
0.5 μM ZnPcS _{mix}	1 μl
1 μM ZnPcS _{mix}	2 μl

C6. Calculation average laser irradiation times for the diode lasers

- The output power of the 594 nm diode laser was 99 mW
- The following formula was used to calculate all laser irradiation times:



$$\frac{\text{mW} \times 4}{\pi(r)^2} = \text{mW/cm}^2$$

$$\frac{\text{mW/cm}^2}{1.000} = \text{W/cm}^2$$

$$\frac{\text{Energy fluence (J/cm}^2\text{)}}{\text{Work (W/cm}^2\text{)}} = \text{Time (s)}$$

$$\frac{\text{Time (s)}}{60} = \text{Time (X min)}$$

60

$$\text{X min} \times 60 = \text{Y}$$

$$\text{Time (s)} - \text{Y} = \text{Seconds to add to X min}$$

C7. Purity of nucleic acid

Table C3: Absorbance ratios of samples used for gene expression analysis.

	A_{260/280} ratio	
	RNA	cDNA
Untreated control samples	1.84	1.86
	1.90	1.91
	1.85	1.83
	1.89	1.92
ZnPcS_{mix} treated samples	1.89	1.88
	1.90	1.87
	1.84	1.85
	1.88	1.91
PDT treated samples	1.92	1.93
	1.89	1.87
	1.94	1.86
	1.87	1.88

**APPENDIX D
ETHICAL APPROVAL**



**FACULTY OF HEALTH SCIENCES
ACADEMIC ETHICS COMMITTEE**

AEC58/01-2010

23 July 2010

TITLE OF RESEARCH PROPOSAL: Effectiveness of zinc-phthalocyanine and hypericin in inducing cell death in human breast cancer cells (MCF-7) using low intensity laser irradiation (LILI)

DEPARTMENT OR PROGRAMME: M.TECH : BIOMEDICAL TECHNOLOGY

RESEARCHER: MFOUC-TYNGA, IDS **STUDENT NO.** 200504361

SUPERVISOR: Prof H Abrahamse

CO-SUPERVISOR: Dr N Houreid

The Faculty Academic Ethics Committee has scrutinised your research proposal and confirm that it complies with the approved ethical standards of the University of Johannesburg.

The AEC would like to extend their good wishes to you in your endeavour of your research project.

Yours sincerely,

Prof. Karien Jooste

Chair: Faculty of Health Sciences: Academic Ethics Committee

APPENDIX E
RT-PCR RESULTS

Gene expression profiling (p-values)

Table E1: The p-values of genes analysed during the RT-PCR array.

Position	Symbols	p-value (comparing to control group)	
		ZnPcS _{mix} treated	PDT treated
A01	ABL1	0.220	0.280
A02	AKT1	0.823	0.137
A03	APAF1	0.365	0.999
A04	APP	0.221	0.323
A05	ATG12	0.310	0.304
A06	ATG16L1	0.482	0.247
A07	ATG3	0.859	0.240
A08	ATG5	0.159	0.398
A09	ATG7	0.204	0.274
A10	ATP6V1G2	0.982	0.208
A11	BAX	0.249	0.089
A12	BCL2	0.106	0.049
B01	BCL2A1	0.142	0.963
B02	BCL2L1	0.094	0.258
B03	BCL2L11	0.144	0.160
B04	BECN1	0.915	0.251
B05	BIRC2	0.888	0.534
B06	BIRC3	0.062	0.348
B07	BMF	0.238	0.243
B08	C1orf159	0.435	0.341
B09	CASP1	0.166	0.096
B10	CASP2	0.129	0.005
B11	CASP3	0.184	0.114
B12	CASP6	0.213	0.100
C01	CASP7	0.293	0.291
C02	CASP9	0.225	0.444
C03	CCDC103	0.563	0.653
C04	CD40	0.353	0.590
C05	CD40LG	0.861	0.142
C06	CFLAR	0.746	0.119
C07	COMMD4	0.243	0.178
C08	CTSB	0.594	0.489
C09	CTSS	0.490	0.228
C10	CYLD	0.227	0.082
C11	DEFB1	0.166	0.337

C12	DENND4A	0.215	0.646
D01	DFFA	0.223	0.043
D02	DPYSL4	0.425	0.829
D03	EIF5B	0.197	0.370
D04	ESR1	0.736	0.415
D05	FAS	0.237	0.375
D06	FASLG	0.166	0.096
D07	FOXI1	0.768	0.096
D08	GAA	0.200	0.287
D09	GADD45A	0.301	0.996
D10	GALNT5	0.934	0.237
D11	GRB2	0.442	0.668
D12	HSPBAP1	0.972	0.415
E01	HTT	0.982	0.504
E02	IFNG	0.122	0.096
E03	IGF1	0.166	0.098
E04	IGF1R	0.761	0.325
E05	INS	0.181	0.096
E06	IRGM	0.166	0.096
E07	JPH3	0.544	0.631
E08	KCNIP1	0.166	0.096
E09	MAG	0.267	0.673
E10	MAP1LC3A	0.288	0.491
E11	MAPK8	0.921	0.391
E12	MCL1	0.242	0.452
F01	NFKB1	0.346	0.484
F02	NOL3	0.200	0.206
F03	OR10J3	0.396	0.096
F04	PARP1	0.211	0.117
F05	PARP2	0.391	0.331
F06	PIK3C3	0.442	0.484
F07	PVR	0.460	0.478
F08	RAB25	0.379	0.156
F09	RPS6KB1	0.146	0.167
F10	S100A7A	0.166	0.096
F11	SNCA	0.241	0.099
F12	SPATA2	0.297	0.430
G01	SQSTM1	0.530	0.312
G02	SYCP2	0.662	0.669
G03	TMEM57	0.679	0.522
G04	TNF	0.529	0.741
G05	TNFRSF10A	0.163	0.428
G06	TNFRSF11B	0.203	0.191
G07	TNFRSF1A	0.154	0.112

G08	TP53	0.107	0.301
G09	TRAF2	0.441	0.485
G10	TXNL4B	0.509	0.155
G11	ULK1	0.929	0.057
G12	XIAP	0.245	0.094



APPENDIX F

LIST OF PUBLICATIONS



The primary subcellular localization of Zinc phthalocyanine and its cellular impact on viability, proliferation and structure of breast cancer cells (MCF-7)

I.M. Tynga, N.N. Houreld, H. Abrahamse*

Laser Research Centre, Faculty of Health Sciences, University of Johannesburg, P.O. Box 17011, Doornfontein 2028, South Africa

ARTICLE INFO

Article history:
Received 15 October 2012
Received in revised form 20 November 2012
Accepted 25 November 2012
Available online xxxxx

Keywords:
Breast cancer
Zinc phthalocyanine
Photodynamic therapy

ABSTRACT

The development of curative techniques which are selective for neoplasms is one of the main focal areas in cancer research. The mechanism of cell damage due to Zinc phthalocyanine (ZnPc_{mix})-mediated photodynamic therapy (PDT) in a breast cancer cell line (MCF-7) was assessed by inverted light microscopy for morphology, the Trypan blue exclusion assay and adenosine triphosphate (ATP) luminescence assay for cell viability, alamarBlue for proliferation, Lactate Dehydrogenase (LHD) membrane integrity for cytotoxicity and fluorescent microscopy for ZnPc_{mix} localization. Fluorescent microscopy revealed that ZnPc_{mix} was localized in both mitochondria and lysosomes, and PDT treated cells showed damaging structural changes and decreased cell viability and proliferation. The light-dependent ZnPc_{mix} displayed appreciable photosensitivity and the intensity of damage was directly related to its concentration. © 2012 Elsevier B.V. All rights reserved.

1. Introduction

Cancer refers to a group of diseases characterized by uncontrolled cell growth and the spread of these abnormal cells can lead to death [1]. Cancer is the second major cause of death worldwide after heart-related diseases. The effects of cancer are seen by the high death rate and the increasing number of people affected [2]. Breast cancer is regarded as the most common and deadliest cancer among females [3,4]. Anyone can develop cancer since the risk of developing cancer increases with age and about 78% of all cancers are diagnosed in individuals that are 55 years old and older. Cancer is caused by both external and internal factors which may act together or in a sequential manner to promote carcinogenesis [5]. Although deaths related to cancer decrease with early detection and treatment such as surgery, radiotherapy and chemotherapy, most treatments are more palliative and present more side effects than the beneficial therapeutic value. Cancer therapy research aims to develop new and effective means of dealing with cancer.

Photodynamic therapy (PDT) is an emerging light dependent chemotherapy used for the control of a variety of cancers. It is a synchronized process which first requires the exposure of cancer tissue to a photosensitizer (PS), administered either by a topical, oral or intravenous route depending on the location of the targeted tissues [6,7]. The activation of a PS is done through laser irradiation at a wavelength specific to the PS. An activated PS is excited and promoted from the ground state to a higher level of energy known

as the singlet state. This state of the PS has a very short lifespan and can lose its energy by fluorescence or internal conversion into heat. However in PDT, the spin of an excited electron can be reversed, leaving the PS in an excited triplet state; this is called intersystem crossing. The excited triplet state is a lower electronic energy than the excited singlet state of the PS. Photosensitizer in the excited triplet state reacts with molecular oxygen and gives rise to free radical species that can destroy tissue [8,9]. PDT achieves selective cell destruction and minimizes damage to adjacent healthy structures as a PS largely accumulates in cancer cells [10,11]. The growing interest of PDT in cancer research is highly dependent on the characteristics of the PS used, which includes the ability of the PS to accumulate in neoplastic tissues, to remain inactive in the dark and to absorb light at long wavelengths [8].

Phthalocyanines are second generation sensitizers that are used in phototherapeutic applications. These sensitizers contain a central atom, which determines not only the high triplet state quantum yields, but also the prolonged lifespan of this excited state of the molecule [12,13]. Lysosomes, mitochondria, plasma membranes, the nucleus and vasculature of the cancer cells are reported to be the primary sites for the accumulation of the sensitizers [14,15]. Current Zinc phthalocyanines (ZnPcs) used in PDT, are insoluble or less soluble in water and research which aims to develop better PSs is an on-going process [16–18].

In this study, we investigated the potential photosensitizing characteristics of a phthalocyanine which contains various sulfonated groups and a central Zinc atom (ZnPc_{mix}). These various sulphated groups increase the solubility of ZnPc_{mix} and the effects of this sulfonated ZnPc in the absence and presence of laser irradiation were studied on a breast cancer cell line *in vitro*. A dose

* Corresponding author. Tel.: +27 11 559 6406; fax: +27 11 559 6884.
E-mail address: habrahams@uj.ac.za (H. Abrahamse).

1011-1344/\$ - see front matter © 2012 Elsevier B.V. All rights reserved.
<http://dx.doi.org/10.1016/j.jphotobiol.2012.11.009>

Please cite this article in press as: I.M. Tynga et al., The primary subcellular localization of Zinc phthalocyanine and its cellular impact on viability, proliferation and structure of breast cancer cells (MCF-7), J. Photochem. Photobiol. B: Biol. (2012), <http://dx.doi.org/10.1016/j.jphotobiol.2012.11.009>

dependent study was performed to identify the appropriate laser fluence and sensitizer concentration to be used in a cell death study using a breast cancer cell line (MCF-7).

2. Materials and methods

2.1. Cell culture

A breast cancer cell line, MCF-7 (ATCC HTB-22), was used for this study. Cells were cultured in Dulbecco's Modified Eagle's Medium supplemented with 10% fetal bovine serum (FBS; Gibco 306.00301), 5% penicillin/streptomycin (PAA Laboratories GmbH, P11-010) and 1 µg/ml Amphotericin B (PAA Laboratories GmbH, P11-001) in an 85% humidified atmosphere at 37 °C and 5% CO₂. Cells were subcultured two to three times weekly. When confluent, cells were washed twice with Hank's Balanced Salt Solution (HBSS, Invitrogen, 10-543F) and trypsinized using 1 ml/25 cm² of TrypLE Express (Gibco, 12604). Cells were seeded at a final concentration of 5×10^5 cells and cultured in 3.4 cm² diameter culture dishes and incubated for 4 h to allow the cells to attach.

2.2. Photosensitizer

A mixed isomer of ZnPc_{mix} was used in this study. It is a mixture of several sulfophthalocyanines and was synthesized from (OH)₂ZnPC and fuming sulfuric acid (30% SO₃) [19] at Rhodes University in South Africa and donated by Prof Tebello Nyokong. The ZnPc_{mix} has a peak absorbance at 680 nm and four concentrations of this PS were used (0.05, 0.1, 0.5 and 1 µM) to determine which would be the most suitable to monitor and induce cell toxicity and death using PDT.

2.3. Laser irradiation

A 680 nm diode laser (Oriol Corporation, USA, LREB00-R07H1) provided by the National Laser Center of South Africa was used to irradiate the cells. Before exposure, output power was measured using the FieldMate Laser Power Meter and the value was used to calculate the exposure time. An output power of 52 mW and power density of 5.73 mW/cm² was obtained. Cells were irradiated for 14 min 33 sec, 29 min 05 sec and 43 min 37 s to deliver an energy density of 5, 10 and 15 J/cm² respectively. The laser spot size covered the entire area of the culture dish (9.1 cm²); this was achieved by irradiating culture dishes via a fiber optic set at 8 cm above the cell monolayer. Cells were irradiated without the culture dish lid at room temperature. In order to eliminate light interference, all irradiation protocols were performed in the dark. Dosage was calculated as follows: Irradiance (J/cm²) = time (s) × [power (W)/surface (cm²)] [20].

Cell cultures were divided into 4 study groups. Group 1 was an unirradiated control with no ZnPc_{mix}, group 2 contained ZnPc_{mix} but was not irradiated and group 3 was irradiated but no ZnPc_{mix} was added. Group 4 was treated with ZnPc_{mix} and was irradiated. All samples were incubated for 24 h after treatment and the dose response determined.

2.4. Subcellular localization of ZnPc_{mix}

MCF-7 cells were grown on glass coverslips in 35 mm culture dishes. An hour prior to observation, cells that received 1 µM of ZnPc_{mix} were washed (3x with HBSS) and stained with 50 µl of 35 nM Mitotracker (Invitrogen M7514) for mitochondria or Lyso-tracker (Invitrogen L7526) for lysosomes, then incubated at room temperature for 15 min. Cells were fixed with 200 µl of 3.5% (v/v) Formaldehyde (Sigma–Aldrich P3744) in DMEM and permeabi-

lized with 200 µl of 0.5% (v/v) TritonX-100 (Sigma–Aldrich T9284) in distilled water, then washed with HBSS. Fifty microliters of 1 µg/ml 4'-6-Diamidino-2-phenylindole (DAPI, Invitrogen, D1306) was used to stain the nuclei. After 5 min of incubation, the samples were rinsed with HBSS and the coverslips were inverted onto glass microscope slides onto which a 30 µl of 20% mounting media (Propyl Gallate, Fluka, Sigma–Aldrich, 02370) in distilled water had been added. Coverslip borders were sealed with nail polish and slides were examined using the Carl Zeiss Axio Z1 Observer. The following filters were used for each fluorescent compound: 490_{Ex}/516_{Em} for Mitotracker, 380_{Ex}/576_{Em} for Lyso-tracker, 359_{Ex}/461_{Em} for DAPI and 594_{Ex}/615_{Em} for ZnPc_{mix}.

2.5. Changes in cell morphology

An inverted light microscope (Wirsam, Olympus CKX41) was used to observe and study the morphological changes that occurred in different treated groups of MCF-7 cells 24 h after addition of ZnPc_{mix}, laser irradiation or PDT. Morphological pictures were taken with the SC30 Olympus camera.

2.6. Cell viability

The Trypan blue assay (Sigma–Aldrich T8154) is a quantitative assay and was used to determine the percentage viability of various treated MCF-7 cells. In this assay, viable cells with an intact cellular membrane do not take up the dye and maintain a clear appearance under the microscope while damaged non-viable cells are stained blue as they take up dye. The cell suspension was carefully mixed with 0.4% Trypan blue reagent in a 1:9 ratio before the mixture was transferred to a Neubauer hemocytometer counting chamber to determine the number of viable and non-viable cells. Cells were counted in the 1 mm central square and four 1 mm corner squares. Percentage viability was determined by multiplying the viable cell number by 100 then dividing the obtained number by the total cell number (clear and blue).

The adenosine triphosphate (ATP) cell viability assay was used to evaluate mitochondrial activity in each type of treatment. For this purpose the cell Titer-Glo[®] luminescent cell viability assay (Anatech, Promega G7573), was used. Equal volumes of cell suspension and reconstituted reagent were added together and mixed to induce cell lysis. The mixture was allowed to stabilize at room temperature for 10 min. ATP present in each sample was quantified and luminescence was recorded using the Perkin–Elmer, VICTOR3[™] Multilabel Counter (model 1420) in relative light units (RLUs).

2.7. Cell proliferation

Cells normally maintain a reducing state within their cytosolic environment. MCF-7 cells were treated with 10% alamarBlue (Invitrogen, DAL 1025). The reducing potential of MCF-7 cells converted alamarBlue into a fluorescent and colorimetric indicator. The fluorescent indicator generated from this assay was proportional to the cell proliferation rate. In the assay, 1/10th volume of alamarBlue was added to resuspended cells. The reaction mixture was incubated at 37 °C and 5% CO₂ for 2 h. The indicator was detected at 550 nm using 620 nm as a reference wavelength (Perkin–Elmer, VICTOR3[™]).

2.8. Cytotoxicity

Membrane integrity was assessed by estimating the amount of Lactate Dehydrogenase (LDH) present in the culture media. LDH is a cytosolic enzyme released due to membrane damage. The Cytotoxicity assay (Anatech, Promega G400) was used to measure the

Please cite this article in press as: I.M. Tynga et al., The primary subcellular localization of Zinc phthalocyanine and its cellular impact on viability, proliferation and structure of breast cancer cells (MCF-7), J. Photochem. Photobiol. B: Biol. (2012), <http://dx.doi.org/10.1016/j.jphotobiol.2012.11.009>

released LDH. Fifty microliters of reconstituted reagent was added to an equal volume of cell culture medium and incubated in the dark at room temperature for 30 min. The colorimetric compound was measured spectrophotometrically at 490 nm (Perkin-Elmer, VICTOR3™).

2.9. Statistics

A breast cancer cell line was used with passages between 10 and 15. Each set of experiments was repeated six times ($n = 6$) while each assay was performed in duplicate, with the results being averaged. Untreated cells were included throughout the course of the study and all treated samples were compared to those cells by means of one-way ANOVA to determine the statistical difference. Statistical analysis was performed using SigmaPlot version 11.0 and the mean, standard deviation and standard error were obtained. Statistical significances between untreated control cells and treated cells are shown in the graphs as $P < 0.05$ (*), $P < 0.01$ (**) and $P < 0.001$ (***). Significant differences were considered at the 95th percentile.

3. Results and discussion

Although recent reports indicate a decrease in cancer death rate mainly due to improved treatment modalities, it remains a major health problem and cause of mortality worldwide, as cancer claims more than 7.6 million deaths per annum. Breast cancer is one of the deadliest forms of cancer in women and is a malignant cancer that remains resistant to many treatments [21,22]. Many therapeutic interventions are non-specific and kill both healthy and cancerous cells [23]. However, PDT is an emerging therapy that targets cancer cells and combines three elements; PS, laser irradiation and molecular oxygen [24]. Once activated by light, the PS is the principal inducer of damage by activating reactive oxygen species that induce death in cancer cells [25]. In this study the photosensitizing characteristics of ZnPc_{mix} were examined.

3.1. Photosensitizer localization

Cell staining showed the successful uptake of ZnPc_{mix} as well as its initial sites of localization in MCF-7 cells after less than 1 h

incubation. In the merged picture of ZnPc_{mix} (red) and Lyso-/Mito-tracker (green), there is an overlap in color giving rise to an intermediate yellowish tint (Fig. 1). There is no evidence of overlap between ZnPc_{mix} and DAPI, which was used to stain the nuclei. However it is evident that ZnPc_{mix} localizes in the perinuclear area, which corresponds to the Golgi apparatus and this still needs to be confirmed.

Fluorescent microscopy revealed that mitochondria and lysosomes are the primary sites of ZnPc_{mix} localization, as red and green fluorescence overlapped producing an intermediate yellow fluorescence due to the co-localization of ZnPc_{mix} in both mitochondria and lysosomes. Wood et al. and Fabrics et al. [15,26], used similar Zinc-phthalocyanines and reported that these sensitizers localized in Golgi apparatus, mitochondria and lysosomes. Lysosomes, despite their biological activity, are critical primary targets for photosensitizers [27,28]. It has been shown that a Zinc (II) phthalocyanine localizes in the lysosomes and phthalocyanine delivery to the lysosomes is via endocytosis [15]. Furthermore, these lysosome localized phthalocyanines accumulate in microzomes and in the mitochondria [26,29]. Uncoupled mitochondrial permeability transition pores (MPTP) can inhibit the synthesis of energy leading to necrotic death. Releases of mitochondrial proteins (cytochrome C, AIF, Diablo) activate cascades responsible for changes in cell structure and function, resulting in apoptosis. Like any phthalocyanine, ZnPc_{mix} has a strong tendency to aggregate and has decreased water solubility. When in contact with tumor cells, which have a greater affinity for lipoproteins, ZnPc_{mix} is taken up and retained in the organelles of tumor cells, and upon light activation induces cell death [4]. ZnPc_{mix} did not only successfully enter the cells but also had the ability, in the presence of light, to induce cell death as it is localized in or near critical cellular organelles. After laser irradiation, the photodamaging effects of ZnPc_{mix} on cell morphology, cell viability, cell proliferation and cytotoxicity were noted.

3.2. Cell morphology

After culture, MCF-7 cells treated with either laser irradiation or non-activated ZnPc_{mix} did not present any morphological changes when compared to untreated control cells (not shown). However, ZnPc_{mix} in conjunction with the PDT laser brought about cellular

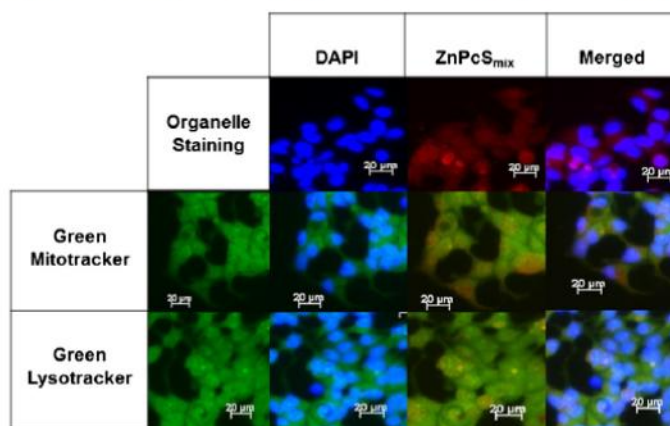


Fig. 1. Subcellular localization of ZnPc_{mix} in MCF-7 cells. DAPI stained nuclei (blue), Mito- and Lyso-tracker stained mitochondria and lysosomes, respectively (both green). ZnPc_{mix} localized in both mitochondria and lysosomes (red). Distinct red and blue fluorescence were seen (merged image) as ZnPc_{mix} does not localize in the nuclei but in the perinuclear area. (For interpretation of the references to color in this figure legend, the reader is referred to the web version of this article.)

Please cite this article in press as: I.M. Tynga et al., The primary subcellular localization of Zinc phthalocyanine and its cellular impact on viability, proliferation and structure of breast cancer cells (MCF-7), J. Photochem. Photobiol. B: Biol. (2012), <http://dx.doi.org/10.1016/j.jphotobiol.2012.11.009>

changes that appeared to be dose dependent. At very low ZnPc_{mix} concentrations, it was difficult to distinguish any change, but as the concentration increased, cells began to lose their characteristic shape; they became rounded up and detached and appeared as free-floating structures in the culture medium (Fig. 2). Untreated control cells maintained normal cell morphology and showed the highest level of cell viability and proliferation, and the lowest degree of cytotoxicity. Results indicated that ZnPc_{mix}, when used alone, appeared to have no therapeutic value as the cells remained alive and morphologically identical to the untreated cells. However, morphological changes were seen with all concentrations of PDT treated cells; cells rounded up as their shape changed and detached from the plate to finally appear as free floating structures in the cell suspension. These changes correspond to those of PDT treated cells undergoing cell death as described by Tesmiere et al. [30]. Seotsanyana and colleagues [19] examined the effect of Ge, Si and Sn phthalocyanine sensitizers and reported no changes in cell morphology on human esophageal carcinoma (SNO) cells. They also reported an increase in cell viability and proliferation in the untreated controls and PS-controls.

3.3. Cell viability

One of the greatest indicators of dying cells is their ability to take up certain dyes. The Trypan blue exclusion assay was performed to determine the proportion of viable and damaged/dead cells in different treated cell populations. Results for the Trypan blue exclusion assay and ATP luminescence are presented in Table 1. Cells treated with either laser irradiation or ZnPc_{mix} alone maintained a high percentage viability and did not differ much from the untreated control cells. However, a decrease in percent-

age viability was observed in PDT treated cells. The change in percentage viability became significant with 0.5 and 1 μM of ZnPc_{mix} ($P < 0.05$ and $P < 0.01$ respectively) when used in combination with a fluence of 10 or 15 J/cm^2 .

At a very low ZnPc_{mix} concentration of 0.05 μM , ATP luminescence did not vary when compared to the untreated control cells and a similar observation was made for cells treated with ZnPc_{mix} alone or laser alone. PDT treated cells with 0.1 ($P < 0.05$, $P < 0.05$ and $P < 0.01$), 0.5 ($P < 0.01$, $P < 0.01$ and $P < 0.001$) and 1 μM ($P < 0.01$, $P < 0.001$ and $P < 0.001$) ZnPc_{mix} showed major ATP depletion in a dose dependent pattern when irradiated at 5, 10 and 15 J/cm^2 respectively. With both viability assays, it was observed that the decrease in viability correlated with the concentration of ZnPc_{mix}; under similar irradiation conditions, an increase in ZnPc_{mix} concentration resulted in a further decrease in cell viability. In a similar manner, the efficacy of the ZnPc_{mix}-mediated PDT indicated important irradiation dependence; the viability decreased with an increase in laser irradiation. Major changes in Trypan blue cell viability were observed with cells that received 0.5 and 1 μM of ZnPc_{mix}. At these concentrations, cells suffered severe membrane damage following PDT and the Trypan blue dye entered cells through these damaged membranes. All cells require energy to perform their metabolic functions and ATP is the immediate source of energy that drives cellular metabolism. Significant decreases in ATP levels were observed with all PDT treated cells, except for those that received 0.05 μM of ZnPc_{mix}. At these higher concentrations, the toxic derivatives from the activated ZnPc_{mix} inhibit the activities of the energy metabolic enzymes and therefore decrease ATP levels. ZnPc_{mix} localized in mitochondria and probably in Golgi apparatus, inhibits both protein and energy synthesis [31]. In a similar study, a decrease in both percentage viability

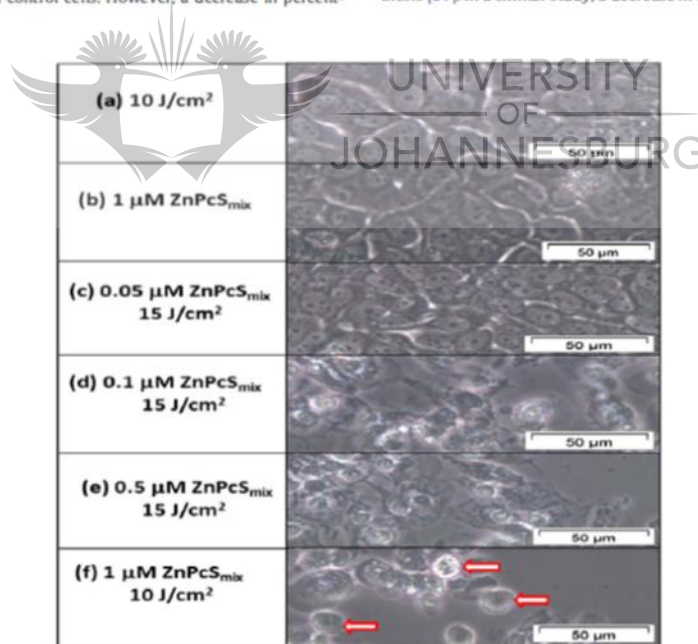


Fig. 2. Morphology of MCF-7 cells after treatment. No morphological change was noted when cells were treated with laser alone (a), ZnPc_{mix} alone (b) or a low concentration of ZnPc_{mix} in PDT (c). As the ZnPc_{mix} concentration increased in PDT, cells started to round up (d and e) and appeared as free floating structures (arrows) at 1 μM of ZnPc_{mix} (f) (200 \times magnification).

Please cite this article in press as: I.M. Tynga et al., The primary subcellular localization of Zinc phthalocyanine and its cellular impact on viability, proliferation and structure of breast cancer cells (MCF-7), J. Photochem. Photobiol. B: Biol. (2012), <http://dx.doi.org/10.1016/j.jphotobiol.2012.11.009>

Table 1

Trypan blue exclusion (percentage) and ATP luminescence (relative light units, RLU) assays were performed to assess cellular viability of different treatments. Statistical significances as compared to untreated control (0 μM and 0 J/cm^2) are shown as * $P < 0.05$, ** $P < 0.01$ and *** $P < 0.001$ respectively. Cells treated with the highest concentration of ZnPC_{mix} (1 μM) and irradiated at 680 nm showed the lowest cellular viability.

	Concentration of ZnPC_{mix}				
	0 μM	0.05 μM	0.1 μM	0.5 μM	1 μM
<i>Trypan blue</i>					
0 J/cm^2	99 \pm 0.62 ^a	98 \pm 0.36	98 \pm 0.26	94 \pm 0.57	93 \pm 0.62
5 J/cm^2	99 \pm 0.89	95 \pm 0.61	90 \pm 0.84	81 \pm 1.51	71 \pm 2.76*
10 J/cm^2	100 \pm 1.26	95 \pm 0.72	90 \pm 0.88	54 \pm 1.38**	42 \pm 1.45**
15 J/cm^2	101 \pm 0.77	94 \pm 0.68	88 \pm 1.29	44 \pm 1.77**	42 \pm 1.15**
<i>ATP (RLU)</i>					
0 J/cm^2	215361 \pm 686	215958 \pm 461	216029 \pm 817	220598 \pm 1941	205059 \pm 2019
5 J/cm^2	203548 \pm 1436	202885 \pm 793	138753 \pm 1233*	86578 \pm 353**	82396 \pm 87**
10 J/cm^2	196836 \pm 2376	195260 \pm 1971	126301 \pm 581*	81790 \pm 256**	49604 \pm 28***
15 J/cm^2	196568 \pm 2380	194825 \pm 2484	103920 \pm 2647**	52913 \pm 250***	48652 \pm 34***

^a \pm SE

ity and ATP levels were observed with A549 human lung cancer cells after PDT [10].

3.4. Cell proliferation

An effective treatment on cancer cells, which have a high rate of multiplication, would either prevent or decrease their proliferation. The alamarBlue assay was performed to determine the degree of cell proliferation. Decreased cell proliferation was observed with all PDT treated cells and no statistical significance was noted with cells that received either laser irradiation alone or ZnPC_{mix} alone. Important changes in cell proliferation were observed when high concentrations of ZnPC_{mix} (0.5 and 1 μM) used in PDT treated cells were compared to untreated control cells (* $P < 0.05$ and $P < 0.01$ respectively) (Fig. 3). Wong et al. [32] reported that 24 h after PDT, a decrease in cell proliferation was also seen with FaDu hypopharyngeal carcinoma cells. This decrease might have been due to the inability of PDT treated cells to react to cell stimulating factors. Cancer cells are high energy consuming cells and the ATP depletion might have induced a decrease in proliferation. ATP is mainly produced during glycolysis and oxidative phosphorylation through the electron transport chain in mitochondria. During PDT, mitochondrial-localized photosensitizers can damage these organelles and induce the inhibition of oxidative phosphorylation and therefore reduction in ATP levels [33].

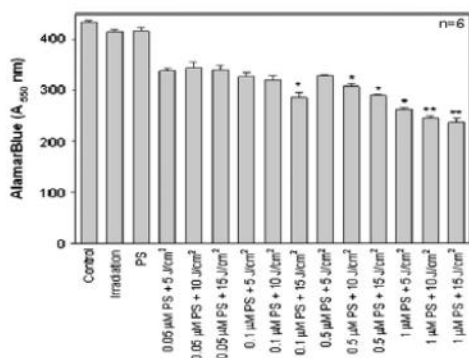


Fig. 3. alamarBlue proliferation assay of treated MCF-7 cells. PDT treated cells had a slow proliferation rate as less absorbance was detected when compared to the untreated control ($P < 0.05^*$ and $P < 0.01^{**}$). No significant change was noted with cells treated with laser alone or PS alone.

3.5. Cytotoxicity

PDT aims to kill cancer cells; therefore it should be dangerous or toxic to those cells. The CytoTox96[®] assay was performed and the level of LDH released into the culture media was measured to determine the level of cellular damage, in particular cellular membrane damage subsequent to MCF-7 cells being treated with ZnPC_{mix} -mediated PDT.

After 24 h incubation, PDT treatment induced an increase in cell membrane damage, as noted by the significant increase in the level of LDH detected with 0.05 μM ($P < 0.05$), 0.1 μM ($P < 0.01$), 0.5 μM ($P < 0.01$) or 1 μM ($P < 0.01$) ZnPC_{mix} when compared to the untreated control (Fig. 4). ZnPC_{mix} showed similar cytotoxic effects to those of Photofrin (II). Photofrin (II) mediated-PDT has been reported to have induced a high level of LDH release and damage to both HeLa and Cask cell membranes [34]. LDH leakage is one of the signs of cytotoxicity and evidence of LDH leakage into the cell suspension was noted with all PDT samples as a result of the damage suffered by the cellular components [35].

The cytotoxic effects of ZnPC_{mix} -mediated PDT were dependent on the concentration of PS used. These effects were noted with a

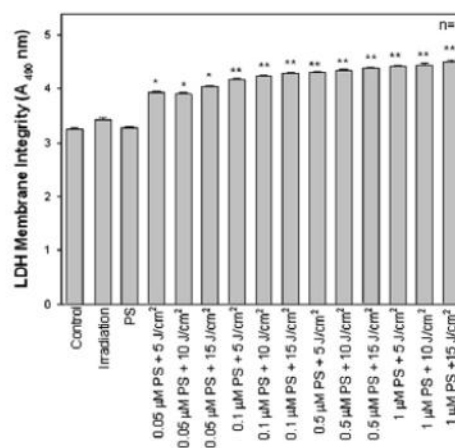


Fig. 4. LDH membrane integrity cytotoxicity assay. The cytodamage was significant in all PDT samples ($P < 0.05^*$ and $P < 0.01^{**}$) as indicated by the amount of LDH released when compared to the untreated control. No significant change was noted when cells were treated with irradiation alone or with PS alone.

Please cite this article in press as: I.M. Tynga et al., The primary subcellular localization of Zinc phthalocyanine and its cellular impact on viability, proliferation and structure of breast cancer cells (MCF-7), J. Photochem. Photobiol. B: Biol. (2012), <http://dx.doi.org/10.1016/j.jphotobiol.2012.11.009>

significant decrease in vital cell activity such as ATP production and proliferation rate, and increased damage in cell structure. The active ZnPcS_{mix} led to an effective antitumor activity that relies on the generation of reactive oxygen species in PDT. Additionally, ZnPcS_{mix} localized in critical organelles, which have been shown to be accumulation sites for PSs during PDT.

In summary, the results presented in this paper demonstrate that PDT using ZnPcS_{mix} and irradiation at 680 nm induced cell damage to breast cancer cells. The effectiveness of this mixture of sulfonated Phthalocyanines was found to correlate with both its concentration and laser fluence; an increase in either laser fluence or PS concentration led to a subsequent decrease in cell viability and proliferation and increased cytotoxicity. Thus, ZnPcS_{mix} is an effective photodynamic agent *in vitro* and localizes in the mitochondria, lysosomes and probably Golgi apparatus. In its inactive form, ZnPcS_{mix} showed no apparent destructive effects. However, irradiation of MCF-7 cells treated with a minimum concentration of 0.1 μM ZnPcS_{mix} led to increased cell membrane damage and a decrease in both cell viability and proliferation.

This photosensitizer displayed toxic effects on breast cancer cells post-PDT but did not induce cell damage in its initial non-activated state in the absence of irradiation. It would be interesting to monitor the effects of ZnPcS_{mix} in an *in vivo* model as a potential breast cancer treatment modality.

Acknowledgments

This work was conducted at the Laser Research Centre of the University of Johannesburg and supported by the University of Johannesburg, African Laser Centre and National Research Foundation of South Africa. We thank Prof. Tebello Nyokong (Department of chemistry, Rhodes University, South Africa) for the synthesis and supply of the PS and the National Laser Centre of South Africa is acknowledged for the supply and maintenance of lasers.

References

- [1] I.F. Tannock, R.P. Hill, *The Basic Science of Oncology*, third ed., McGraw Hill, Singapore, 1998.
- [2] M.A. Calin, S.V. Parasca, Photodynamic therapy in oncology, *J. Optoelectron. Adv. M* 8 (3) (2006) 1173–1179.
- [3] C. Albrecht, Overview of oncology research in South Africa, 2006. <<http://www.sahelthinfo.org/cancer/overviewdocument.pdf>> (accessed 04.12.11)
- [4] M. Ochsner, Photochemical and photobiological processes in the photodynamic therapy of tumours, *J. Photochem. Photobiol. B* 39 (1997) 1–18.
- [5] D.A. Vorobiof, P. Ruff, Cancer in South Africa and the role of the national cancer registry, *Ascopost* 2 (7) (2011) 12–19.
- [6] A. Juzeniene, J. Moan, The history of PDT in Norway part one: identification of basic mechanisms of general PDT, *Photodiagn. Photodyn. Ther.* 4 (2007) 3–11.
- [7] J. Rao, R. Bissonnette, K. Suthamjaraya, C. R. Taylor, Photodynamic Therapy for the Dermatologist, 2008. <<http://www.emedicine.com/derm/topic636>> (accessed 15.09.10).
- [8] A.P. Castano, T.N. Demidova, M.R. Hamblin, Mechanisms in photodynamic therapy: part one-photosensitizers, photochemistry and cellular localization, *Photodiagn. Photodyn. Ther.* 1 (2004) 279–293.
- [9] P. Mroz, A. Szokalska, M.X. Wu, M.R. Hamblin, Cell death pathways in PDT of cancer, *J. Pone* 5 (12) (2010) 15194–15201.
- [10] S.L. Manoto, H. Abrahams, Effect of a newly synthesized Zn sulfophthalocyanine derivative on cell morphology, viability, proliferation, and cytotoxicity in a human lung cancer cell line (A549), *Lasers Med. Sci.* 43 (2011) 333–342.
- [11] L. Dini, V. Inguscio, B. Tenuzzo, E. Panzarini, Rose bengal acetate photodynamic therapy-induced autophagy, *Cancer Biol. Ther.* 10 (10) (2010) 1048–1055.
- [12] A. Ogunsipe, J.Y. Chen, T. Nyokong, Photophysical and photochemical studies of Zinc(II) phthalocyanine derivatives – effects of substituents and solvents, *New J. Chem.* 28 (2004) 822–827.
- [13] D. Kessel, N.L. Oleinick, Photodynamic therapy and cell death pathways, *Methods Mol. Cell Biol.* 635 (2010) 35–46.
- [14] L.J. Dougherty, C.J. Gomer, B.W. Henderson, G. Jori, D. Kessel, M. Korbelik, J. Moan, Q. Peng, Photodynamic therapy, *J. Nat. Cancer Inst.* 90 (12) (1998) 889–905.
- [15] S.R. Wood, J.A. Holroyd, S.B. Brown, The subcellular localization of Zn (II) phthalocyanines and their redistribution on exposure to light, *J. Photochem. Photobiol. B* 65 (3) (1997) 397–402.
- [16] L. Yang, L. Guo, Q. Chen, H. Sun, H. Yan, Q. Zeng, X. Zhang, X. Pan, S. Dai, Substituents effects of Zinc phthalocyanine derivatives: a theoretical calculation and screening of sensitizer candidates for dyes-sensitized solar cells, *J. Mol. Graph Model* 38 (2012) 82–89.
- [17] L. Li, Z. Luo, Z. Chen, J. Chen, S. Zhou, P. Xu, P. Hu, J. Wang, N. Cheng, J. Huang, M. Huang, Enhanced photodynamic efficacy of Zinc phthalocyanine by conjugating to Heptahistine, *Bioconjugate Chem.* (2012). <http://www.ncbi.nlm.nih.gov/pubmed/2305765> (accessed 10–11.09.12).
- [18] S. Tuncel, F. Dumonlin, J. Gailer, M. Soorigaarachchi, D. Atilla, M. Durmus, D. Bouchu, H. Savoie, R.W. Boyle, V. Ahsen, A set of highly water soluble tetraethyleneglycol-substituted Zn(II) phthalocyanine synthesis, photochemical and photophysical properties, interaction with plasma proteins and *in vitro* phototoxicity, *Dalton Trans.* 40 (16) (2011) 4067–4079.
- [19] I. Seotsanyana-Makhosi, T. Kresfelder, H. Abrahams, T. Nyokong, The Effect of Ge, Si and Sn phthalocyanine photosensitizers on cell proliferation and viability of human oesophageal carcinoma cells, *J. Photochem. Photobiol. B* 83 (1) (2006) 55–62.
- [20] C.H. Chen, H.S. Hung, S.H. Hsu, Low energy laser irradiation increases endothelial cell proliferation, migration and eNOS gene expression possible via PI3k signal pathway, *Laser Surg. Med.* 40 (2008) 46–59.
- [21] A.M. Glas, A. Floore, L.J.M.J. Delahaye, A.T. Witteveen, R.C.F. Pover, N. Balox, J. Lahti-Domenici, T.J. Bruinsma, M.O. Warmoes, R. Bernards, F.A. Lodewyk, L.J. Van der Veer, Converting a breast cancer microarray signature into a high-throughput diagnostic test, *BMC Genom.* 7 (2006) 278–287.
- [22] A.D.V.M. Jemal, F. Bray, M.M. Center, J.M.E. Ferlay, E. Ward, D. Forman, Global cancer statistics, *J. Clin. Oncol.* 61 (2011) 69–90.
- [23] M. Zea, P. Halabiy, Lysosomal and mitochondrial changes detected during TNF- α induced apoptosis in MCF-7 human breast cancer cells, *JYI* 5 (1) (2001) 32–47.
- [24] R.N. Manifold, C.D. Anderson, Increased cutaneous oxygen availability by topical application of hydrogen peroxide cream enhances the photodynamic reaction to topical 5-aminolevulinic acid-methyl ester, *Arch. Dermatol. Res.* 303 (4) (2011) 285–292.
- [25] B.C. Wilson, Photodynamic therapy for cancer: principles, *Gastroenterol* 16 (6) (2002) 393–396.
- [26] C. Fabrics, G. Valdivia, G. Miotto, L. Borsetto, G. Jori, J. Garbisa, E. Reddi, Photosensitization with Zinc(II) phthalocyanine as switch in the decision between apoptosis and necrosis, *Cancer Res.* 61 (20) (2001) 7495–7502.
- [27] C.W. Lin, Photodynamic therapy of malignant tumors recent developments, *Cancer Cells* 3 (1991) 437–444.
- [28] M. Geze, P. Morliere, J.C. Maziere, K.M. Smith, R. Santus, Lysosomes, a key target of hydrophobic photosensitizers proposed for photochemotherapeutic applications, *J. Photochem. Photobiol. B* 20 (1993) 23–35.
- [29] D. Kessel, Y. Luo, Y. Deng, C.K. Chang, The role of subcellular localization in initiation of apoptosis by photodynamic therapy, *J. Photochem. Photobiol. B* 65 (3) (1997) 422–426.
- [30] A. Tesniere, L. Apetoh, F. Ghiringhelli, N. Joza, T. Panaretakis, O. Kepp, F. Schlemmer, L. Zitvogel, G. Kroemer, Molecular characteristics of immunogenic cancer cell death, *Cell Death Differ* 15 (2008) 3–12.
- [31] P. Fagone, S. Jackowski, Membrane phospholipid synthesis and endoplasmic reticulum function, *J. Lipid Res.* 5 (2009) 311–316.
- [32] T.W. Wong, E. Tracey, A.R. Oseroff, H. Baumann, Photodynamic therapy mediates immediate loss of cellular responsiveness to cytokines and growth factors, *Cancer Res.* 63 (2003) 3812–3818.
- [33] J.R. Shulok, J.E. Klauing, S.H. Selman, P.J. Schafer, P.J. Goldblatt, Cellular effects of hematoporphyrin derivative photodynamic therapy on normal and neoplastic rat bladder cells, *Am. J. Pathol.* 122 (2) (1986) 277–283.
- [34] H. Das, T. Koizumi, T. Sugimoto, S. Yamauchi, K. Hasegawa, Y. Tenjin, R. Nishimura, Induction of apoptosis and manganese superoxide dismutase gene by photodynamic therapy in cervical carcinoma cell lines, *Int. J. Clin. Oncol.* 5 (2000) 97–103.
- [35] R.J. Brooker, *Genetics: Analysis and Principles*, fourth ed., McGraw, Hill, USA, 2012.

ADVANCES IN GENETICS RESEARCH

ADVANCES IN GENETICS RESEARCH

VOLUME 9



nova
publishers
New York

CONTENTS

Preface		vii
Chapter 1	A Prioritized Panel of Candidate Genes to Be Explored for Associations with the Blood Pressure Response to Exercise <i>Garrett I. Ash, Amanda L. Augeri, John D. Eicher, Michael L. Bruneau, Jr. and Linda S. Pescatello</i>	1
Chapter 2	Caspase-8 Roles in Cancer and Development – Lessons in Multitasking <i>Tal Teitz, Manrong Jiang, Devin Twitchell and Jill M. Lahti</i>	55
Chapter 3	Self-Fertility in Scots Pine as a System for Regulating Close Relationships and the Species Survival in an Adverse Environment <i>N. F. Kuznetsova</i>	83
Chapter 4	Caspase-8 Properties, Function and Regulation during Photodynamic Therapy <i>I. M. Tynga and H. Abrahamse</i>	107
Chapter 5	Reproductive Performances of Holsteins under Tropical Conditions <i>R. Bouraoui, A. Ben Gara, B. Jemmali and B. Rekik</i>	121
Chapter 6	Caspase-8: Properties, Functions and Regulation <i>Daisuke Fujikura and Tadaaki Miyazaki</i>	135
Chapter 7	Role of Caspase-8 in Neuropathic Pain Syndrome <i>Dario Siniscalco, Francesco Rossi and Sabatino Maione</i>	143
Index		149

Chapter 4

CASPASE-8 PROPERTIES, FUNCTION AND REGULATION DURING PHOTODYNAMIC THERAPY

*I. M. Tynga and H. Abrahamse**

Laser Research Centre, Faculty of Health Sciences,
University of Johannesburg, Doornfontein, South Africa

ABSTRACT

Caspases are cysteine proteases that play critical roles in apoptosis, necrosis and inflammatory reactions. Within the caspase family, caspase-8 (Cas-8) is an initiator apoptotic protease, activated at the cytosolic face of the cell membrane [1]. Upon activation, Cas-8 can either cleave downstream effector caspases including caspase-3 (Cas-3), or promote effector caspase-9 (Cas-9) via the cleavage of Bid (Bcl-2 Interacting Domain) [2]. Upon activation, an active Cas-8 forms a heterotetramer, consisting of two large and two small subunits. Cas-8 is also involved in several non-apoptotic processes including proliferation, differentiation, nuclear factor kappa-light-chain-enhancer of activated B cell (NF- κ B) activation, adhesion and migration. In spite of its numerous functions, Cas-8 is well characterized for its dominant role in the transmission of signals in the extrinsic apoptotic pathway by coupling the stimulating receptors to the activation of the intracellular signalling cascade that lead to cell death². Cas-8 is a crucial regulatory protein for apoptosis and impaired expression or function of this protein may contribute to the formation and progression of cancer. Impaired expression is usually due to epigenetic silencing and post-translational alteration. Demethylating agents and Interferon-gamma (IFN- γ), which is a glycoprotein, can both up-regulate Cas-8 in various human tumour cases [2]. Caspases have been identified as potential therapeutic targets. Photodynamic therapy (PDT) is a light induced chemotherapy process which is used for cancer treatment. Reactive oxygen species (ROS) are very small toxic molecules that are abundantly produced during the course of PDT. ROS can cause severe damage to DNA, proteins and lipids, which lead to cell death via either apoptotic or necrotic mechanisms. ROS plays an important role in Cas-8 mediated apoptosis. In PDT-induced Cas-8 activation, cell death occurs by intrinsic mitochondrial apoptosis [3- 5]. In this chapter we

* Tel. +27 11 559 6406, Fax. +27 11 559 6558 / 0866956973, Email. habrahamse@uj.ac.za, Website [http:// www.uj.ac.za/lrg](http://www.uj.ac.za/lrg).

explore the basic function and properties of Cas-8 focusing on the role and mechanism of function during PDT when used as a photochemotherapeutic intervention for the treatment of cancer. The induction of apoptotic cell death during PDT is the preferred mechanism of introducing cancer cell death and we investigate the possible contribution that Cas-8 may make to PDT induced cancer cell death.

INTRODUCTION

1. Properties of Cysteine Proteases

Cysteine proteases belong to a family of degrading enzymes that have various functions within an organism. They play important roles in plant development, senescence, cell death, storage and mobilization of germinal proteins. In humans, they have pharmacological roles in wound healing, immunomodulation, digestive and neoplastic conditions [6]. Among the members of this family; caspases are critical proteins as they are directly involved in cell death pathways and have non-cell death functions, including red blood cell maturation and skeletal muscle myoblast proliferation [7]. According to the Hugo Gene Nomenclature Committee, different caspases had been identified in humans and subdivided into initiator and effector caspases. Initiator caspases activate effector caspases, which then cleave other protein substrates within the cell to induce specific mechanism like apoptotic processes [8, 9]. Cas-8 is the most significant of these initiators as it plays a critical part in the regulation of programmed cell death and is required for proper signalling via the extrinsic pathway of apoptosis. Improper expression of Cas-8, may contribute to carcinogenesis and its progression [2].

2. Structure of Caspase 8

Cas-8 is an evolutionary and greatly conserved protein. There is roughly 20% resemblance between mammalian Cas-8 and its nematode *C. elegans* homologue, the ced-3 protein. The human Cas-8 gene maps to chromosome 2q33. The inactive Cas-8 is a 55 kDa protein, composed of 480 amino acids with its proteolytic domain at the C-terminus with specificity to a tetra-peptide. At the other end of this peptide, two N-terminal death effector domains (DED) are involved in protein-protein interactions [2]. The N-terminal prodomains of this cysteine protease are used for the recruitment to macromolecular activation platforms for death-inducing signalling complex (DISC) or the inflammasome. Inhibition studies revealed that binding of a substrate to the active site of cas-8 is done by an induced-fit model mechanism [10]. According to their substrate specificity, caspases had been sub-classified into three groups. Group I, includes Cas-1, Cas-4 and Cas-5 with a preference for Trp-Glu-His-Asp, group 2 consist of Cas-2, Cas-3 and Cas-7 with a preference for Asp-Glu-X-Asp and the final group, group 3, Cas-6, Cas-8, Cas-9 and Cas-10, which favours (Leu/Val)-Glu-X-Asp (where X is any amino acid). Among the caspases, the initiator Cas-8 is undoubtedly the best-studied of this family [8, 10].

Cas-8 plays many important roles within an organism, and its specificity and relationship to structure are critical for cell death. Upon activation, the nascent procas-8 zymogen is



proteolytically processed into a large (~20 kDa) and small (~12 kDa) polypeptide, forming a heterodimeric structure, consisting of two subunits known as P18 and P12. Each subunit consists of six beta (β) strands, five parallels (a, b, c, d, e) and one anti-parallel (f) that together form a twisted β -sheet structure with two alpha (α) helices (H2, H3) on one side and three α helices (H1, H4 and H5) on the other running parallel to the β strand (Figure 1) [8, 11-12].

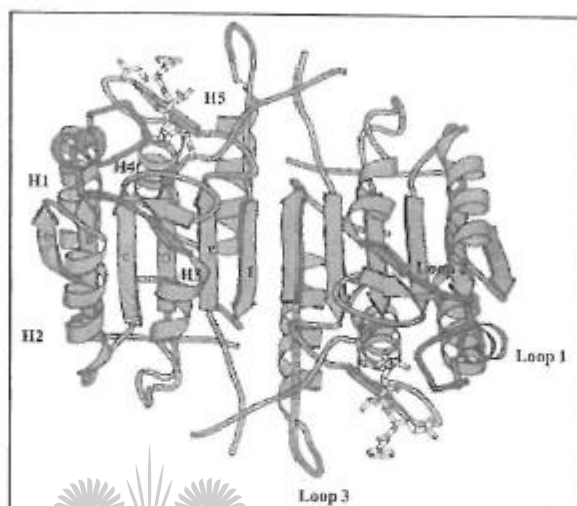


Figure 1. Cas-8 dimer structure is represented as a ribbon diagram; the p18 subpart is coloured in red while the p12 is in green. The yellow ball and stick structure of the inhibitor are covalently attached to the active site Cys-285 and the loops around the active site are in navy blue [12].

The active site is located at the C-terminal end of the parallel β strand within each P18-P12 unit. The P18-P12 dimer forms a twofold non-crystallographic symmetry (NCS) axis. The architecture of Cas-8 resembles that of Cas-1 and Cas-3 but the significant differences are observed at the active site. An important feature of Cas-8 when compared to its counter-family members is a larger loop one, having seven and ten more amino acids than Cas-3 and Cas-1 respectively. A short section of this loop one, presents an α -helical structure (residues 173-175) which is absent from the other two caspases. The fundamental structural alternations between these three phenotypes are localised in the sub-sites S3 and S4, which mostly initiate from the different determining surfaces loop sizes forming these parts of the active sites. The Cas-8 S4 has preference for hydrophobic substrates, while S3 shows a strict preference for glutamic acid [12].

3. Functions of Caspase 8

3.1. Mechanism of Cas-8 Activation

Cas-8 is a zymogen initiator caspase that become activated prior to the induction of apoptosis via oligomerization in a complex at activated death receptors [13]. Mechanisms of

Cas-8 activation occur through its recruitment into the intracellular membrane complexes associated death receptors.

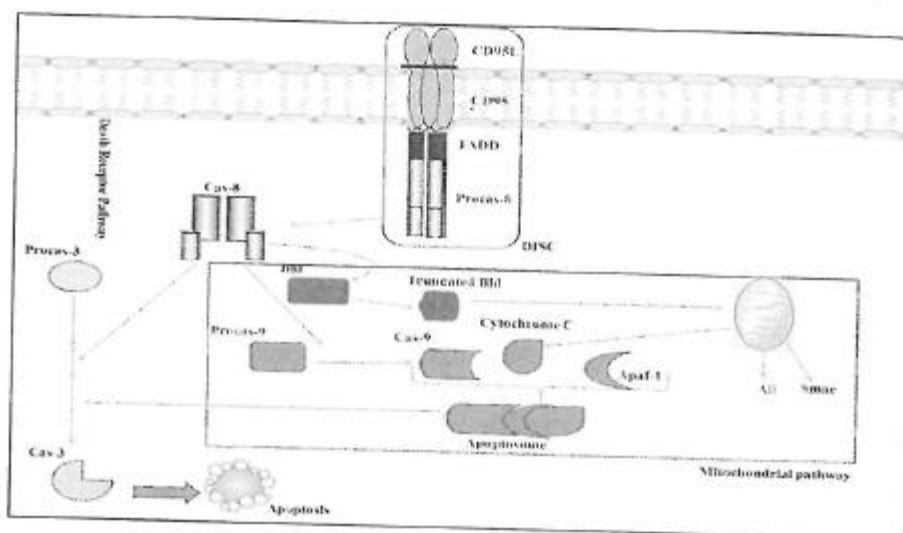


Figure 2. Apoptosis signalling pathways. The death receptor pathway is stimulated by the binding of death receptor ligand (CD95/TNFR/ TRAIL ligands) to death receptors (CD95/TNFR/ TRAILRs). The ligation triggers receptor trimerization, recruitment of the adaptor Fas associated death domain protein (FADD) and ProCas-8 to form the death inducing signalling complex (DISC) and activation of Cas-8 through induced proximity at this complex. The cross talk between the extrinsic and intrinsic pathway is initiated by a pro-apoptotic truncated Bid (tBid), processed by Cas-8. tBid translocates to mitochondria and favours Smac, AIF and Cytochrome C release from mitochondria into the cytosol. Cytochrome C together with Cas-9 and Apaf-1, forms the apoptosome, triggers Cas-3 activation, while AIF and Smac promotes apoptosis, the latter by neutralizing "Inhibitor of Apoptosis Proteins" (IAPs).

Fas/tumour necrosis factor receptor (TNFR/CD95) family are trans-membrane proteins that are categorized as death receptors due to their cytoplasmic death domain (DD). These receptors ligate with their corresponding ligands to form trimeric structures with aggregated intracellular DDs and promote apoptosis. This begins a subsequent protein interaction with the C-terminus of an adaptor molecule Fas-associated DD (FADD), the N-terminal death effector domain (DED) of recruits which recruits procas-8 by interaction with DED in the Cas-8 prodomain and the resulting structure is known as DISC (Figure 2). When bound to DISC and due to induced-proximity effect, procas-8 undergoes autoproteolytic cleavage [2]. Upon oligomerization, single zymogen Cas-8 interacts with each others dimers leading to cross-cleavage which involve two events.

The fully active Cas-8 is obtained after the separation of the large and small subunit followed by the separation of the large subunit from the prodomain [8].

3.2. Caspases as Central Initiators and Executioners of Apoptosis

Apoptosis is critical for normal tissue homeostasis and also beneficial as a natural anti-cancer mechanism; as cells become damaged, they can undergo apoptosis thereby preserving the healthy state of the organism. Apoptosis is a cell death regulated biochemical process,

which is a vital mechanism for removal of unnecessary, aberrant, infected and damaged cells without damaging normal ones [14]. Characteristic features of apoptosis consist of DNA fragmentation, disruption of mitochondrial membrane potential, cell shrinkage and phosphatidylserine externalization at the cell surface, nuclear/cytoplasmic condensation, and dilation of the endoplasmic reticulum. These morphological differences are allegedly attributed to caspases, which are derived from Cysteine-dependent Aspartate specific proteases [13]. Two standard apoptotic pathways occur in mammalian cells; the receptor (extrinsic) and mitochondrial (intrinsic) pathway. Depending on the stimulus, caspases can be activated through either the extrinsic death receptor or intrinsic pathways (Figure 2). Among the caspase family, Cas-8 is the most upstream and plays a determinant role in cell death induction, particularly via the death receptor pathway [2]. The apoptotic extrinsic pathway is initiated by precise ligands (Fas and CD95/TNFR/TRAIL), each binding to their respective death receptor and forming a trimeric death receptor (Figure 2). This trimeric death receptor recruits adaptor molecules via its cytoplasmic DDs. Besides having DDs, the adaptor contains a DED which recruits procas-8 by allowing a DISC assemblage and by autoproteolytic cleavage; procas-8 is activated in the cytoplasm. The active initiator Cas-8 cleaves and activates effector caspases (cas-3/-9) for the execution of apoptosis.

The intrinsic pathway is triggered by cellular changes caused by the mitochondria that play a dominant role in the cellular lifespan of the cell but is also a crucial mediator for cell death with the disruption and permeabilisation of the outer mitochondrial membrane, and the release of pro-apoptotic proteins, cytochrome C and a repressor of (IAP) as well as the release of second mitochondria derived activator of caspases (Smac) into the cytosol⁸. The death signals in this part of the apoptotic pathway are attributed to the effects of Cas-8 and Bid. Bid is a member of the Bcl2 family of proteins belonging to the subfamily BH-3 which contain pro-apoptotic activity. Proteins from the BH-3 subfamily are responsible for cross-linking to death receptors in the mitochondrial cell membrane to activate apoptosis. The uncleaved form of Bid is non-functional but upon Cas-8 cleavage, the truncated Bid (tBid) translocates to the mitochondria and, there induces the pro-apoptosis changes that release cytochrome c and further activates other effector caspases (Figure 2). Hence the association between death receptor stimulation and mitochondrial apoptotic events [8].

According to the type of cells, Cas-8 stimulates executioner caspases independent of the mitochondria and cleaves the Bid protein to generate the pro-apoptotic t-Bid. After translocation, the t-Bid protein induces cytochrome C release from the mitochondria and further induces activation of other caspases through formation of an apoptosome, which then result in cell death [13]. However the mitochondrial apoptotic pathway is also initiated in response to both external and internal cues such as DNA damages.

3.3. Non Apoptotic Functions

Caspases or Aspartate specific cysteine proteases are mainly known and well identified for their roles in programmed cell death signalling. Cas-8 had been mostly considered as a significant initiator caspase in death receptor induced signalling and its CD95 induced cell death. Recent observations on Cas-8 activities coupled with interaction with other substrates in the absence of death, suggested the involvement of this initiator protein in other processes such as in cell proliferation, activation and cellular differentiation. In addition to its key part in the regulation of apoptosis, Cas-8 also has non-apoptotic properties, e.g. in the regulation of T cell homeostasis via control of Interleukin-2 generation; in the control of differentiation

and proliferation in the hematopoietic system and in the transduction of signals via the T cell receptor, B cell receptor, and Toll-like receptors and roles in cell migration and adhesion [15].

3.3.1. Proliferation

In addition to its role in apoptosis, Cas-8 has also been shown to be essential for T-cell proliferation in response to antigenic or mitogenic stimuli. Studies showed that a functional Cas-8 has an indispensable role in the maintenance of the immune system where a mutated Cas-8 will lead to impaired proliferation of the immune cells namely T-, B- and natural killer cells. In summary, an individual with an altered Cas-8 will experience a decreased interleukin-2 (IL-2) production; a type of cytokine immune system signalling molecule, which is a leukocytotropic hormone that is involved in the body's natural response to microbial infection and identification of foreign molecules. Humans with a germline point mutation in the Cas-8 gene, manifest a condition associated with autoimmunity like lymphadenopathy and splenomegaly. While a prolonged effect of a T-cell specific deletion of the Cas-8 gene in mice lead to an age-dependent condition known as lethal lymphoproliferation and lymphoinfiltrative phenotype resembling the human autoimmune condition of the lungs, liver and kidneys followed by tissue damage [7]. Cas-8 is required in regulating lymphocyte homeostasis, thus loss of Cas-8 leads to a complex immune condition manifesting features of immunodeficiency and autoimmunity.

3.3.2. Differentiation

Either, deletion of the Cas-8 gene using Cre/loxP recombinant in monocytes obtained after a recombinase catalyzes site specific recombination of DNA between the lox P site (Known as Cre/Lox system), or blocking caspase activation through the use of caspase inhibitors (eg. baculovirus p35 or cowpox virus) prevents their differentiation into macrophages. Exposing monocytes to macrophage colony stimulating factor (M-CSF), promotes the formation of a complex containing Cas-8 and receptor interacting protein-1 (RIP-1) thereby limiting its full capacity for inducing apoptosis and stimulating differentiation potential. Cas-8, Cas-9 and Cas-3 activity are influenced in this manner. These changes lead to a death receptor independent, non-apoptotic role of Cas-8 in monocyte differentiation into macrophages and down regulation of NF- κ B activity [16]. Macrophage maturation involves changes in the cell state such as in the cytoskeleton, in cell adhesion and differential transcription regulation. All these processes require proteins that have to be partially cleaved by caspases without causing cell death. Optimal activity of Cas-8 is required to activate Cas-9 and Cas-3, which allows greater processing capacity of a larger number of substrates. Upon M-CSF stimulation, Cas-8 cleaves RIP-1, which favors proper macrophages and NF- κ B inactivation [17]. Cas-8 activity has also been required for differentiation of human placental villous trophoblasts. Activated Cas-8 is highly present in differentiated cytotrophoblasts where it is not directly involved in fusion but it primes mononucleated cytotrophoblasts for syncytial fusion [7, 18].

3.3.3. B-Cell Activation

Toll like receptors (TLRs) are regulatory proteins of the innate immune system that identify specific microbial constituents to generate the induction of an inflammatory response. TLRs are not only innate immune receptors but have also been reported to require Cas-8 for

NF- κ B activation. Cas-8 contribute to the TLR induced NF- κ B activation cascade [17]. At first the molecular mechanism of Cas 8-mediated NF- κ B activation, involves the catalytic activity of the large domain of Cas-8, which may be required for NF- κ B activation in response to specific subset of NF- κ B activating agents. The dissociation of FADD from the TRAIL-R and subsequent formation of a second complex requires Cas-8 enzymatic activity. Following TNF-R triggering, Cas-8 forms a complex with TRAF2 and FLASH (FLICE (FADD-like interleukin-1 beta converting enzyme) associated huge protein) to initiate the NF- κ B activation pathway. TNF-induced NF- κ B activation in fibroblast and epithelia cell lines depend on Cas-8 but Cas-8 enzymatic activity is not indispensable for TNF-induced NF- κ B activation to take place in these cells [7].

3.3.4. Adhesion and Migration

Cell migration influences tumor invasion and metastasis. Phosphatidylinositol 3 kinase (PI3K) belongs to a family of enzymes involved in cell growth, proliferation, differentiation and motility. PI3K is an essential component of the cell migration apparatus and consists of a p110 catalytic subunit and a p85 regulatory subunit. The regulatory subunit controls the basal activity of this enzyme, the stability of the catalytic subunit and the activation of the enzyme by tyrosine residues. In non-apoptotic cells, caspase autoproteolytic processes does not take place; Cas-8 exists as a zymogen (proCas-8) and is able to restore cell migration/adhesion. Cas-8 enhances cell migration through interaction with the p85 subunit of PI3K, which then activates Rac, followed by cell migration. ProCas-8 is phosphorylated on Tyrosine 380 (Y380), this phosphorylation not only suppresses Cas-8 autocleavage but also facilitates its interaction with phosphotyrosine's binding domain of PI3K. When Y380 phosphorylated proCas-8 interacts with the p85 subunit of PI3K in an independent catalytic manner, cell adhesion is promoted [19].

4. Regulation of Caspase 8 Activity

The extensive pro-domain of the zymogen Cas-8 favours interactions with Cas-8 activating death receptors. However, this interaction can be prevented by several types of inhibition and alternation of Cas-8 pro-domain. Proteins such as viral FLICE inhibitory protein (FLIP) and cellular FLICE proteins contain two N-terminal DEDs that compete with proCas-8 for binding to FADD and in doing so inhibit the Cas-8 activation. Certain viral proteins (poxvirus, baculovirus p35) and IAPs inhibit Cas-8 activity in a non-competitive fashion and are also involved in cell division and suppression of apoptosis. Some IAPs directly prevent the Cas-8 catalytic functions whereas others interact with Cas-8s' pro-domain blocking the recruitment of proCas-8 into activating apoptosome complexes [11]. The inability to undergo apoptosis in response to apoptotic stimuli is one of the main features of human cancer cells. An effective way to escape apoptosis is the inactivation of Cas-8 by epigenetic mechanisms, alternative splicing or post-translational modifications. Cas-8 expression can be altered by methylation of regulatory sequences of the initiator caspase which leads to epigenetic silencing in leukemia and neuroblastoma.

Mutated Cas-8 (Cas-8-L) acts in a dominant negative manner preventing the recruitment of the wild-type Cas-8 to death receptor upon receptor ligation, and the inhibition of the extrinsic apoptotic pathway. Cas-8 pro-apoptotic activity can be suppressed by

phosphorylation of the initiator caspase on Tyrosine 380 by kinases such as Src, which is a proto-oncogenic Tyrosine kinase (Src for Sarcoma). Integrin mediated adhesion was reported to enhance Tyrosine-380 phosphorylated Cas-8 which is essential for cell migration and switches Cas-8 function [2]. The cyclin-dependent kinase-1 (Cdk1) in complex with cyclin B is one of the most important mitotic regulatory kinases, as this complex controls many aspects of the cell cycle. Serine-387 phosphorylation of proCas-8 in breast cancer and proliferating T-cells, inhibits Cas-8 processing and Cdk1/cyclin B appears to be a potent mitotic cell protection mechanism against extrinsic death stimuli [20].

5. Photodynamic Therapy

Photodynamic therapy (PDT), a light induced chemotherapeutic procedure for the management of a variety of malignancies [21] is also extensively used in dermatology due the fact that light is more easily accessible to skin structures than any other structure of the body [22]. It is a synchronized procedure which firstly requires the exposure of cells or tissues to a photosensitizing drug, a photosensitizer (PS), administered either by topical, oral or intravenous routes depending on the targeted body tissues.

The second step involves the activation of the PS in the presence of molecular oxygen, which is done by irradiation of target cells with a precise wavelength of visible light specific to the used PS. It induces the production of ROS which causes tumour destruction. With this combination of nontoxic elements (PS, light and oxygen), PDT achieves the selective destruction of abnormal tissues and minimizes damage to adjacent healthy structures [23]. This damage induces cell death by the efficient induction of apoptotic as well as non-apoptotic mechanisms, such as necrosis and autophagy, or a combination of all three mechanisms [24].

PDT merges the preferential accumulation of a non-toxic photosensitizer (PS) into damaged tissues and local irradiation of a harmless visible light at a suitable wavelength to be absorbed by the PS, to offer the selectivity of the treatment in the presence of molecular oxygen. After photons of light being absorbed by the PS, an electron in the ground state of PS is heightened to form the first excited singlet state which has of short-life span and only last a few nanoseconds. The excited singlet state PS can lose its energy by fluorescence, internal conversion into heat or may invert to form a relatively long lived (milliseconds) excited triplet state, a process known as intersystem crossing. The PS excited triplet state can undergo two different pathways also designated as type I and type II reactions [25]. In the first one, the triplet PS can exchange an electron with a neighbouring molecule. The latter is the most common type of reaction that occurs during PDT where the triplet PS can transfer its energy directly to molecular oxygen (ground state triplet) to form ROS and free radicals [26].

PDT is an essential anti-cancer process as it mediates ROS-tumor death; tumor associated vascular damage, stimulation of inflammatory responses and engages both innate and adaptive immune systems in the host response to cancer. ROS produced during the course of PDT lead to oxidative damage to mitochondrial proteins, membranes and DNA, weakening the ability of mitochondria to synthesize ATP and to carry out their metabolic functions. Mitochondrial oxidative damage increases the tendency of mitochondria to release intermembrane space proteins such as cytochrome C to the cytosol by mitochondrial outer membrane permeabilization (MOMP) and thereby activate the cell death machinery. In

addition, mitochondrial ROS leads to induction of the mitochondrial permeability transition pore (PTP), which renders the inner membrane permeable to small molecules in situations such as ischaemia/reperfusion injury. Mitochondrial ROS may act as a redox signal, reversibly affecting the activity of a range of functions in the mitochondria, cytosol and nucleus [27]. PDT plays a stimulating role in local inflammation and an even more important role in induced immunity. PDT has recently been revealed for contributing in systemic antigen-specific anti-tumor immunity [25].

5.1. Photodynamic Therapy and Cell Death

Lethal mechanisms initiated by the photosensitization process appear to encompass the three major morphologies of programmed cell death, e.g. apoptotic, necrotic and autophagic cell death. The extrinsic pathway of apoptosis is activated by the binding of a death ligand, belonging to the tumor necrosis factor- α (TNF- α) superfamily, to its receptor inducing the formation of the death inducing signaling complex (DISC), mediating the activation of the initiator procaspase-8. Cas-8 proteolytically activates effector caspases-3/7 leading to apoptosis characterized by DNA fragmentation. Initiated by the release of apoptogenic factors such as cytochrome C and apoptosis inducing factor (AIF) from the intermembrane space of the mitochondria into the cytosol, the intrinsic or mitochondrial pathway is characterized by the formation of the apoptosome, a heptameric complex that triggers the activation of the initiator Cas-9. Cas-9 in turn activates the effector caspases-3/7 which results in apoptotic cell death, including internucleosomal DNA fragmentation, membrane blebbing and cell shrinkage. Cas-8 also mediates the cleavage of the cytosolic pro-apoptotic Bcl-2 family member Bid providing a molecular link between the extrinsic and intrinsic apoptotic pathways [28].

5.2. Cell Death in Photosensitized Cells

Depending on the nature of the PS and its intracellular localization, the initial photodamage involve different molecules with consequent activation of specific death pathways ultimately leading to mitochondrial membrane permeabilization (MMP). Mitochondria-localized PS causes light-dependent photodamage to mitochondrial anti-apoptotic Bcl-2 and Bcl-xL proteins. This in turn activates the release of caspase-activating molecules, such as cytochrome C. PSs accumulating in lysosomes induce lysosomal membrane permeabilization leading to the release of lysosomal hydrolases and cleavage of the pro-apoptotic Bid, which can culminate in Bax mediated MMP and caspase activation. With endoplasmic reticulum (ER) localizing PSs, extensive photodamage leads to ER Ca^{2+} depletion, which initiates Bax dependent mitochondrial apoptosis. An increase in intracellular Ca^{2+} concentration can result in the activation of cytosolic phospholipase A₂ (cPLA₂) and generation of Arachidonic acid (AA). Mitochondrial Ca^{2+} uptake, reactive oxygen species (ROS) and AA can synergize inducing MMP (Buytaert et al., 2007). During autophagy induced by photo-oxidative damage to key organelles like the ER, mitochondria and lysosomes survival pathways may be activated as an attempt to remove the dysfunctional organelles. Photo-oxidative damage to the anti-apoptotic Bcl-2/Bcl-xL, may alter their interaction with Beclin 1 and favor the induction of autophagy [29].

6. Photodynamic Therapy and Caspase 8-Mediated Cell Death

Mitochondria are potential sources of ROS within most mammalian cells. The production of ROS is important for both mitochondrial induced damage in certain pathological conditions and in redox signalling from the organelle to the rest of the cell. Superoxide ($O_2^{\cdot-}$) is the primary synthesized species, which is produced by the one-electron reduction of oxygen (O_2) with a constant standard reduction potential of minus 160 mV at pH 7, for every 1 M O_2 . One of the most important factors to be considered for this reduction to take place is the concentration of enzyme or protein (reducing agent) and the proportion of this reducing agent present in a redox form (tBid/excited PS) that can be converted from O_2 to $O_2^{\cdot-}$ [27].

Two benzodiazepine receptors (BR) have been identified, one from the brain, referred to as the central BR and another from the adrenal, kidney or hematopoietic system referred to as the peripheral BR. Peripheral BR is an outer mitochondrial membrane receptor protein, which is associated with two other proteins; an outer voltage dependent anionic channel protein (VDAC) and an inner adenine nucleotide translocator protein (ANT). Taken together, VDAC and ANT form a multi-protein complex at the inner and outer site of the mitochondrial membrane responsible for the initiation and regulation of apoptosis by controlling mitochondrial membrane potential and the release of mitochondrial pro-apoptotic factors. Peripheral BR act as a target for hexaminolevulinate based PDT when transport occurs as a result of interaction between ANT and VDAC, which disrupts the mitochondrial transmembrane potential and release mitochondrial pro apoptotic factors [30]. As an initiator caspase, Cas 8 increases the apoptotic signal by activating downstream caspases and cleave the BH-3 domain of Bid. The truncated protein brings a conformational change in Bax and induces mitochondrial dysfunctioning and cytochrome C release.

In human leukemia cancer cells, the combined effect of iflumic acid and ciglitazone treatment induces apoptosis via the mitochondrial pathway after triggering the Cas 8/Bid/Bax pathway [31]. A similar trend is observed with dimethyl phytosphingosine (DMPS), which induces Cas-8 dependent cytochrome C release and apoptosis through loss of mitochondrial membrane potential and ROS generation in the same cell line²⁸. Targeted PDT for choroidal neovascularization (CNV) and prostate cancer leads to the induction of apoptosis after the activation of Cas-8 which appears to be the central mediator for Vertepofrin in CNV membranes [32]. Most PDT induced apoptosis occurs via the mitochondrial intrinsic pathway as the majority of PS are lipophilic and generally are localized in the intracellular membrane system, particularly in mitochondria. The subcellular location of PS in cells is an important factor for the initiation of cell death.

Following PDT, the outer mitochondria membrane becomes permeable; resulting in cytochrome C leakage into the cytosol where it interacts with apoptotic protease activating factor 1 (Apaf-1) and dATP forming the apoptosome³. High glucose in PC12 neuronal cells, induces apoptosis in a similar manner by lowering the level of pro-caspases (Cas-8, Cas-9 and Cas-3), which is followed by disturbance of mitochondrial membrane permeability, release of cytochrome C and formation of the apoptosome (Aparf-1, cytochrome C, Cas-9) [33]. In human lymphocytes, hypoxia/re-oxygenation leads to ROS production, ROS then activates the Cas-8/Bid/Bax pathway and presents as an important regulator of Cas-8 mediated apoptosis in hypoxia/re-oxygenation treated lymphocytes [14].

Although most PDT and chemotherapeutic applications lead to the activation of the intrinsic apoptotic pathway, certain treatments lead to the cytoplasmic extrinsic pathway,

initiated by death receptors such as tumor necrosis factor. Upon maturation, Cas-8 can translocate from the DISC to the cytosol, where it cleaves several substrates and effector caspases and this time initiates Fas-mediated apoptosis [20]. Dandelion Root Extract (DRE) induces apoptosis in human leukemia cells by activation of Cas-8, which subsequently activates Cas-3 showing that DRE induces apoptosis in a receptor mediated pathway [34].

CONCLUSION

Cas-8 is the main initiator apoptotic protease, in its active form; it processes effector caspases (cas-3/-9) and other cytoplasmic proteins (Bid). In addition to its major contribution to signal transmission in cell death pathways, Cas-8 promotes cellular maturation and has been identified as an effective target for certain type of treatments. PDT is an emerging cancer therapy that induces the ROS production in treated cells.

ROS causes several cellular damages, impaired cellular functions and plays a critical role in Cas-8 mediated apoptosis initiation. In PDT induced Cas-8 activation, cell death mainly occurs by intrinsic mitochondrial apoptosis.

REFERENCES

- [1] Oberst A., Pop C., Tremblay A.G., Blais V., Derault J.B., Salvesen G.s. and Gree D.R. (2010) Inducible dimerization and inducible cleavage reveal a requirement for both processes in caspase 8 activation, *Journal of Biology and Chemistry* 285:16632-16642.
- [2] Fulda S. (2009) caspase 8 in cancer biology and therapy. *Cancer letters* 28:128-133.
- [3] Liu T., Wu L.Y., Choi J.K. and Berkman C.E. (2010) Targeted PDT for prostate cancer: inducing apoptosis via activation of caspase-8/3 cascade pathway. *International Journal of Oncology* 36:777-784.
- [4] Byeong M.K., Choi Y.J., Yun Y.S. and Sung H.H. (2009) N.N. Dimethyl phytosphingosine induces caspase-8 dependent cytochrome C release and apoptosis through ROS generation in human leukemia cells, *Toxicology and Applied Pharmacology* 239:87-97.
- [5] Olivo M and Seyed M.A (2007) Apoptosis signalling mechanisms in human cancer cells induced by calphostin-PDT, *International Journal of Oncology* 30:537-548.
- [6] Salas C.E, Gomes M.T.R, Hernandez M. and Lopes M.T.P. (2008) Plant cysteine proteinase: Evaluation of the pharmacological activity. *Phytochemistry* 68(12): 2263-2269.
- [7] Lamkanfi M., Festjens n., Declercq W., Berghe T.V. and vandenabeele P. (2007) Caspases in cell survival, proliferation and differentiation. *Cell death and differentiation* 14:44-55.
- [8] Kantari C. and Walczak H. (2011), Caspase-8 and Bid: caught in the act between death receptors and mitochondria. *Biochimica et Biophysica Acta* 1813:558-563.
- [9] Gewies A., (2003). Introduction to apoptosis, *Aporev*, www.celldeath.de/encyclo/aporev (Accessed 2011-04-12).

- [10] Keller M, Grutter M.G and Zerbe O. (2010) Studies of the molecular mechanism of cas-8 activation by solution NMR, *Cell death and Differentiation* 17:710-718.
- [11] Kruidering M. and Evan G.I. (2000), Caspase-8 in apoptosis: the beginning of the end *IUBMB life* 50:85-90.
- [12] Blanchard H., Kodandapani L., Mittl P.R.E, Di-marco S., Krebs J.F. Wu J.C., Tomaselli K.J. and Grutter M.G. (1999) The three dimensional structure of cas-8: an initiator of enzyme in apoptosis, *Structure* 7(9):1125-1133.
- [13] Ren W. and Beebe S. J. (2011), Apoptosis targeted stimulus with nanosecond pulsed electric fields in E4 squamous cell carcinomas. *Apoptosis* 16:382-393.
- [14] Byeong M.K. and Chung H.W. (2007) Hypoxia/reoxygenation induces apoptosis through a ROS mediated caspase 8/Bid/Bax pathway in human lymphocytes, *Biochemical and Biophysical Research Communication* 363:745-750.
- [15] Salmena, L., B. Lemmers, A. Hakem, E. Matysiak-Zablocki, K. Murakami, P.Y. Au, D.M. Berry, L. Tamblin, A. Shehabeldin, E. Migon (2003) Essential role for caspase 8 in T-cell homeostasis and T-cell-mediated immunity. *Genes Dev.* 17:883-895.
- [16] Cullen S.P. and Martin S.J. (2009) Caspase activation pathways: some recent progress, *Cell Death and Differentiation* 16:935-938.
- [17] Maelfait J. and Beyaert R. (2008) Non apoptotic functions of Cas-8, *Biochemical Pharmacology* 76:1365-1373.
- [18] Gauster M. and Huppertz B. (2010) The Paradox of Cas-8 in human villous trophoblast fusion, *Placenta* 31:82-88.
- [19] Senft J., Helfer B. and Frisch S.M. (2007) Cas-8 interact with the p85 subunit of phosphatidylinositol - kinase to regulate cell adhesion and migration, *Cancer Research* 67(24):11505-11509.
- [20] Matthes Y., Raab M., Sanhaji M., Lavrik I.N. and Strebhardt K. (2010) Cdk1/cyclin B1 controls Fas-mediated apoptosis by regulating Cas-8 activity, *Molecular and Cellular Biology* 30(24):5726-5740.
- [21] Juzeniene A. and Moan J. (2007) The history of PDT in Norway, Part 1: Identification of basic mechanisms of General PDT. *Photo Diagnosis and PDT* 4: 3-11.
- [22] Rao J., Bissonnette R., and Taylor C.R. (2010) PDT for the dermatologist, Medscape drugs, diseases and procedures, www.emedicine.medscape.com (Accessed 2011-03-12).
- [23] Manoto S.L. and Abrahamse H. (2011) Effect of a newly synthesized Zn sulfophthalocyanine derivative on cell morphology, viability, proliferation, and cytotoxicity in a human lung cancer cell line (A549) *Lasers in Medical Science* 43:333.
- [24] Dini L., Inguscio V., Tenuzzo B. and Panzarini E. (2010) Rose Bengal acetate PDT - induced autophagy, *Cancer Biology Therapy* 10(10):1048-1055.
- [25] Mroz P., Szokalska A., Wu M.X. and Hamblin M.R. (2010) PDT of tumors can lead to development of systemic antigen specific immune response. *Journal.pone* 5(12):15194-15201.
- [26] Castano A.P., Demidova T.N. and Hamblin M.R. (2004) Mechanism in photodynamic therapy: part one - photosensitizer, photochemistry and cellular localization, *Photodyn. Ther.* 1: 279-293.
- [27] Murphy M. P. (2009) How mitochondria produce ROS, *Biochemical Journal* 417:1-13.

- [28] Buytaert E., Dewaele M. and Agostinis P. (2007) Molecular effectors of multiple cell death pathways initiated by photodynamic therapy, *Biochimica et Biophysica Acta* 1776: 86-107.
- [29] Reiners J.J. Jr, Agostinis P., Berg K., Oleinick N.L. and Kessel D. (2010) Assessing autophagy in the context of photodynamic therapy. *Autophagy* 6(1): 7-18.
- [30] Furre I.E., Shahzidi S., Luksiene Z., Moller M.T.N., Borgen E., Morgan J., Tkaczstachowska K., Nesland J.M. and Peng Q. (2005) Targeting PBR by hexaminolevulinate-mediated PDT induces apoptosis through translocation of apoptosis-inducing factor in human leukemia cells. *Cancer Research* 65 (23):11051-11060.
- [31] Byeong M.K., Kyungah M., Kee H.L. and Sung H.H. (2011) Combined treatment with the Cox-2 inhibitor niflumic acid and PPAR gamma ligand ciglitazone induces ER stress/Cas-8 mediated apoptosis in human lung cancer cells, *Cancer Letters* 300:134-144.
- [32] Matsubara A., Nakazawa T., Noda k., She H., Connolly E., Young T.A., Ogura Y., Gragoudas E.S. and Miller J.W. (2007) PDT-induces capase dependent apoptosis in rat CNV model, *Investigative Ophthalmology and Visual Science* 48:4741-4747.
- [33] Sharifi A.M., Eslami H., Larijani B. and Davoodi J. (2009) Involvement of caspase 8, 9 and 3 in high glucose induced apoptosis in PC12 cells, *Neurosciences Letters* 459:47-51.
- [34] Ovadje P., Chatterjee S., Griffin C., Tran C., Hamm C. and Pandey S. (2010) Selective induction of apoptosis through activation of cas-8 in human leukemia cells jurkat by dandelion root extract, *Journal of Ethnopharmacology* 133:86-91.

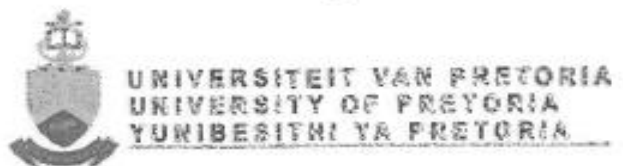


**Programme
and
Book of Abstracts**



**South African Institute of Physics
57th Annual Conference**

hosted by the



Ability of ZnPcS_{mix} phthalocyanine in inducing cellular death in human breast cancer cells (MCF-7) using laser irradiation

I.M. Tynnga, N.N Houreld and H. Abrahamse

Email: habrahamse@uj.ac.za

Abstract. Approximately 180,000 new cases of breast cancer are diagnosed yearly worldwide and is the leading cancer for women in SA and around the world. Photodynamic therapy (PDT) is a light induced chemotherapy process which is used for cancer treatment. The aims of this study were to determine the effects of ZnPcS_{mix} on MCF-7 cells and identify the mode of cell death induced by PDT using the optimum ZnPcS_{mix} concentration and laser fluency. The ability of ZnPcS_{mix} to induce cell death in MCF-7 cells was determined after the following techniques and assays were performed: subcellular localization (fluorescence microscopy), viability (trypan blue staining and adenosine triphosphate, ATP, luminescence), proliferation (AlamarBlue® assay) and cytotoxicity (Lactate Dehydrogenase, LDH). The mode of cell death was determined by flow cytometry (Annexin-V), Hoechst staining and Enzyme linked immunosorbent assay (ELISA). Mitochondrial, lysosomal and Golgi apparatus were the cellular primary localization sites of ZnPcS_{mix}. The optimal parameters were identified as 0.5 µM of ZnPcS_{mix} at 10 J/cm² and treated cells showed a 50% decrease in cell viability, low proliferation and high cytotoxicity. More than 90% of cells were apoptotic and nuclear fragmentation occurred after treatment. The treatment is an effective method to induce cell death in MCF-7 cells and apoptosis was the main mode of cell death. ZnPcS_{mix} mediated PDT may be considered for designing a more effective cancer treatment.

1. Introduction

Cancer refers to a genetic disorder that is the second cause of death worldwide after heart-related condition (Calin and Parasca, 2006). Many types of cancer exist and cancer of the breast accounts for 23% of cancer cases. Breast cancer is the most diagnosed and the leading cause of mortality among women worldwide (Van Zyl *et al.*, 2008; Benn, 2009). It is believed that cancer can be overcome through research, which aims to identify and develop anti-cancer means to deal with the condition.

Photodynamic therapy is a cancer target therapy, which uses a photochemotherapeutic agent also known as photosensitizer (PS), in conjunction with laser irradiation to induce cancer cell death. The administration of PS and its incorporation into body tissues is done in a selective manner so that cancerous tissues are mainly affected. The activation of PS is the second step which is done through laser irradiation at a wavelength specific to the PS. Activated PS is excited and promoted from the ground state to a higher level of energy known as the singlet state, which reacts with oxygen and gives rise to free radical species to destroy tissue (Castano *et al.*, 2004; Mroz *et al.*, 2010). Phthalocyanines are second generation family of PSs that contain a central atom. The atom ensures not only the high

triplet state quantum yields but also the prolonged lifespan of this state of the molecule (Ogunsipe *et al.*, 2004; Kessel, 2004).

In the study, the photosensitizing features of a Zinc-phthalocyanine (ZnPcS_{mix}) were assessed by means of a dose dependent study and the appropriate laser fluence and the concentration of the ZnPcS_{mix} to be used in a cell death study using a breast cancer cell line (MCF-7) was identified.

2. Materials and Methods

Cells were seeded into 3.3 cm² diameter culture dishes and incubated for 4 h to allow cells to attach. Cell cultures were divided into 4 groups (G): G1 was an unirradiated control with no ZnPcS_{mix}, G2 contained ZnPcS_{mix} but was not irradiated and G3 was irradiated but no ZnPcS_{mix} was added. G4 was irradiated and received ZnPcS_{mix}. Cells were treated using one of the four concentrations of ZnPcS_{mix} and one of the three laser fluences to monitor PDT. All samples were incubated for 24 h and thereafter dose response was determined. *Cell viability*: All cells were stained with Trypanblue and percentage viability was determined. *ATP present* in each sample was quantified by recording the luminescence signal. *Cell proliferation*: Cells were treated with 10% alamarBlue[®] and absorbances were detected at 550 nm. *Cytotoxicity*: Membrane integrity was assessed and LDH was measured at 490 nm (Manoto and Abrahamse, 2011). *Fluorescence staining*: G2 cells were stained with DAPI and either mitotracker or lysotracker before being examined (Manoto *et al.*, 2011). *Cell death*: PDT cells (0.5 μM ZnPcS_{mix}; 10 J/cm²) were separated treated with annexin-V and PI before cell death was measured (Van Engeland *et al.*, 1998). Significant differences were indicated as p<0.05 (*), p<0.01 (**) and p<0.001 (***) were considered at the 95th per centile.

3. Results

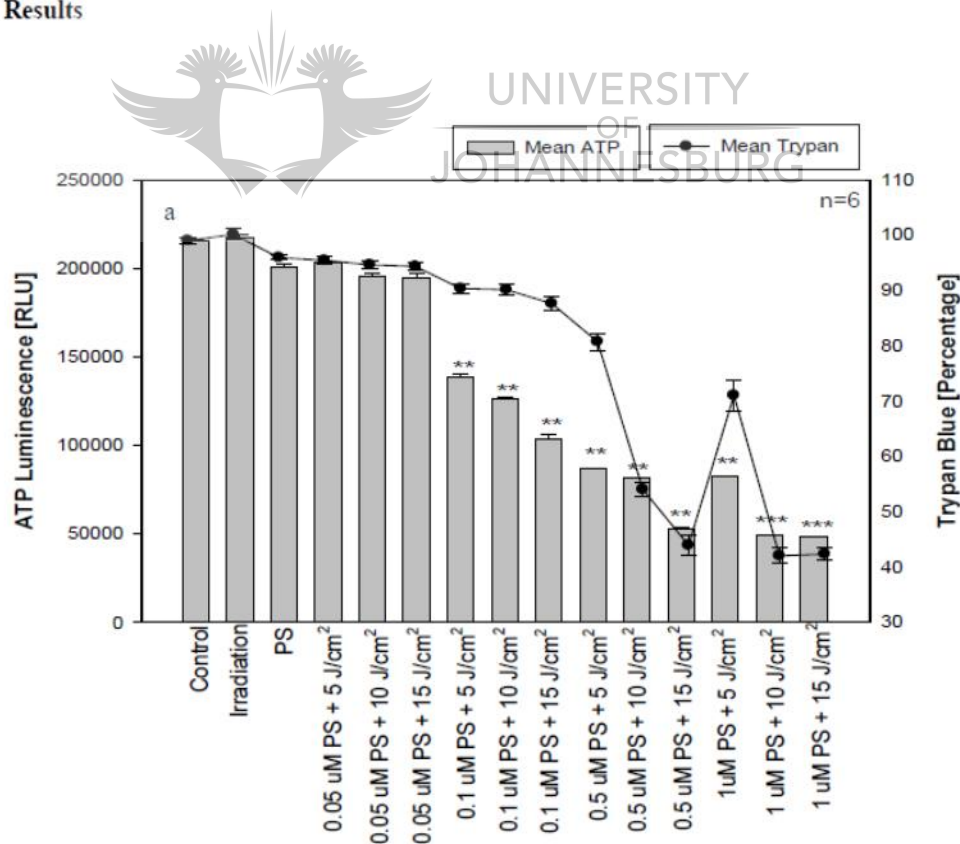


Figure 1: Decrease in ATP luminescent and percentage viability is seen with all PDT samples and no significant change was observed with Irradiation- and PS-treated samples. Statistical differences (P<0.05*) (P<0.01**) (P<0.001***) were compared to the reference control group of cells only. Results were repeated six times (n=6).

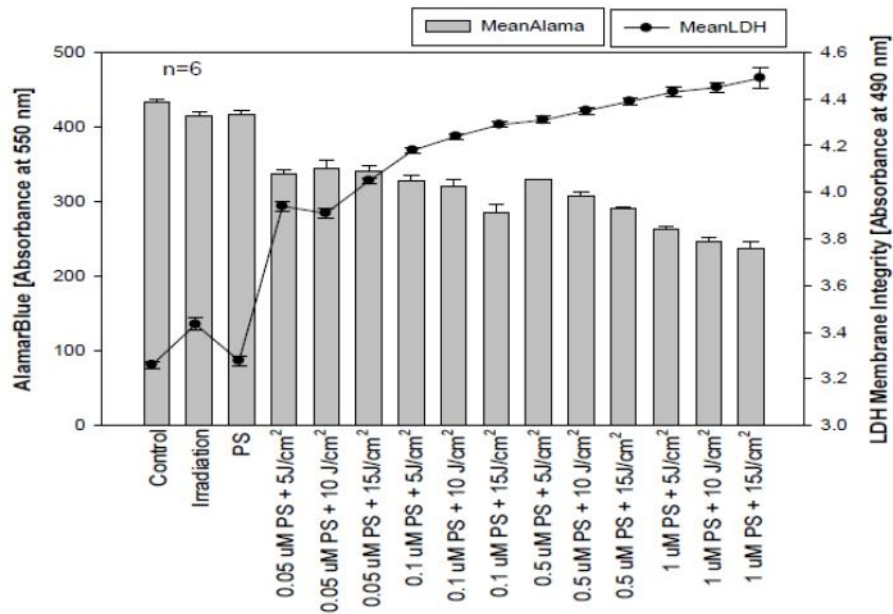


Figure 2: The cytodamages were momentous with all PDT samples (LDH) and PDT treated cells have a slow proliferation rate (alamarBlue). The statistical significances were expressed ($P < 0.05^*$) ($P < 0.01^{**}$) ($P < 0.001^{***}$) and compared to the reference control group of cells only. No major change was identified with Irradiation- and PS-treated samples. Results were repeated

JOHANNESBURG

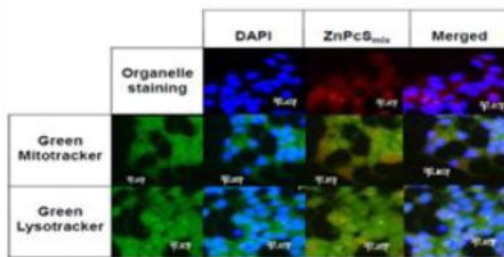


Figure 3: Blue DAPI stained the nuclei, green mito- and green lyso-tracker stained mitochondria and lysosomes, respectively. Red ZnPcS_{max} localizes in both mitochondria and lysosomes as the intermediate yellow between green and red and not in nuclei (superimposed images).

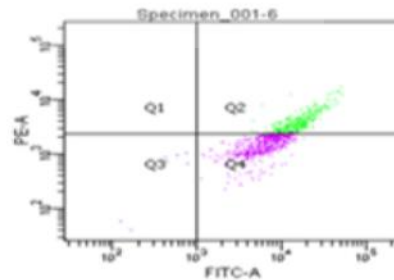


Figure 4: Flow cytometry analysis shows that 37% of cells were in the early apoptotic stage and 64.3% in the late apoptotic cells after PDT.

4. Discussion and conclusion

A subsection Fluorescence microscopy reveals that ZnPcSmix localizes at perinuclear sites, which corresponds to the Golgi apparatus and this finding concurs with the work done by Wood et al. (1997) and Fabris et al. (2001). Mitochondria and lysosomes are the primary sites of ZnPcSmix, as red and green fluorescence merged to give the observed intermediate yellow fluorescence after ZnPcSmix co-localized in both mitochondria and lysosomes. It was shown that a similar Zinc (II) phthalocyanine localizes in the lysosomes and phthalocyanine delivery to the lysosomes is done via endocytosis (Wood et al., 1997). Moreover, these lysosome localized-PSs accumulate in microzomes and in the mitochondria (Fabris et al., 2001; Kessel and Luo, 1997). Mitochondria are important organelles in cellular energy metabolism and are important role-players in cell death. Under stress, release of mitochondrial proteins triggers cascades responsible for the changes to cell structure and functions resulting in apoptosis. Like any phthalocyanine, ZnPcSmix has a strong tendency to aggregate, is taken up and retained in the organelles of tumor cells, where upon light activation they induce cell death (Ochsner, 1996). At higher of these concentrations, ZnPcSmix induces cells membrane damaged following PDT and trypan blue dye entered cells through these damaged membranes. At the same concentration, the produced toxic derivative prevents the activities of the energy metabolic enzymes and therefore decreases the ATP level. ZnPcSmix localized in Golgi apparatus and mitochondria, might affect both protein and energy synthesis. Decreases in both percentage viability and ATP level was observed with A549 human lung cancer cells after PDT using a similar PS (Manoto and Abrahamse, 2011). The drop in ATP level correlates with the decrease in the proliferation of cancer cells. Cancer cells are highly consumer of energy, less energy are available to cancer cells to perform their activities such cell division. Wong et al. (2003) reported a decrease in proliferation with FaDu hypopharyngeal carcinoma cells. These decreases might be due to the absence of sensitivity of PDT samples to cell stimulating factors.

For our study, we have identified 0.5 μM ZnPcSmix and 10J/cm² as the PDT condition that induced approximately 50% of cell death in MCF-7 cells. The quasi totality of cells was found to be apoptotic with the majority in their late apoptotic stage. Tomecka and colleagues (2005) reported that 32-65% of G361 tumor cells were undergoing apoptosis and early apoptosis occurred between 8-15 hours after PDT treatment using ZnTPPS4 as a sensitizer. Chen *et al.* (2001) also found out that PDT using motexafin Lutetium induces up to 35 % increase in the apoptosis of vascular cells. It was reported that the cell death is dependent on the cell line, photosensitising agent, and/or experimental conditions.

ZnPcSmix localizes in mitochondria, lysosomes and golgi apparatus and induced cytotoxic reactions leading to cell death. About 99 % of dead cells and nuclear fragmentation (not shown) were observed after ZnPcSmix mediated PDT treatment. This sensitizer has demonstrated to be an effective inducer of cell death.

References

- Calin MA and Parasca SV (2006). Journal of optoelectronics advanced materials 8(3):1173-1179.
- Benn CA (2009) www.Health24.com/woman/medical accessed on 31 March 2010.
- Ochsner R (1997) Journal of Photochemistry and Photobiology 39: 1-18.
- Castano AP, Demidora TN and Hamblin MR. 2004. Photodiagnostic photodynamic therapy 1:279-293.
- Mroz P, Szokalska A, Wu MX and Hamblin MR (2010) Journal pone 5(12): 15194-15201.
- Manoto SL and Abrahamse H (2011) Lasers in medical sciences 43: 333-342.
- Ogunsipe A, Chen JY and Nyokong T (2004) New journal of chemistry 28:822-827.
- Kessel D and Oleinick NL (2010) Methods in Molecular Biology 635:35-4.
- Wood SR, Holroyd JA and Brown SB (1997) Photochemistry and photobiology B 65(3):397-402.

Fabrics C, Valduga G, Miotto G, Borsetto L, Jori G, GarbisaI J and Reddi E (2001) *Cancer Research* 61(20):7495.
Kessel D, Luo Y, Deng Y and Chang CK 1997. *Photochemistry and Photobiology* 65(3): 422-426.
Wong TW, Tracey E, Oseroff AR and Baumann H (2003) *Cancer Research* 63:3812-3818.
Chen Z, Woodburn KW, Shi C et al (2001) *Arterioscler Thromb Vasc Biol* 21(5): 759-64.

